Homogeneous Catalysis by Organometallic Polynuclear Clusters

Nielsen, Mathias Thor; Padilla Paz, Rosa Maria; Nielsen, Martin

Published in:
Journal of Cluster Science

Link to article, DOI:
10.1007/s10876-019-01635-3

Publication date:
2020

Document Version
Peer reviewed version

HOMOGENEOUS CATALYSIS BY ORGANOMETALLIC POLYNUCLEAR CLUSTERS

Mathias T. Nielsen,[1] Rosa Padilla,[1] Martin Nielsen*[1]

Martin Nielsen, marnie@kemi.dtu.dk

[1]Department of Chemistry, Technical University of Denmark, DK-2800 Kgs. Lyngby, Denmark.

Abstract

Homogeneous polynuclear metal clusters constitute a broad class of coordination compounds with important applications in catalysis. The current interest of synthetic chemistry in this field demands the exploration of new strategies to develop catalytic methods that work under mild conditions and maximize atom utilization. This review covers the application of polynuclear clusters of nuclearity ≥3 in homogeneous catalytic processes, with focus on providing an array of examples of various reaction types within cluster catalysis.

Keywords: polynuclear cluster · ligand scaffold · homogeneous catalysis

LIST OF CONTENTS

1 INTRODUCTION

Polynuclear metal clusters constitute a broad class of coordination compounds with numerous applications in catalysis. As is true for traditional mononuclear organometallic catalysis, polynuclear clusters may perform complex transformations in homogeneous solution. The principal objective of both fields is the exploration of new strategies to develop novel catalytic atom-efficient transformations that work under mild conditions. The typical approach towards this goal is to employ a transition metal or -ion with specific fundamental features, and then fine-tune the catalytic behavior by proper modification of the ligand scaffold. In this regard, compared to mononuclear complexes, the study of polynuclear cluster catalysis offers the potential of tuning an entirely new dimension, namely the interaction between several transition metals.

The chemistry involved in activation of small molecules, such as alkenes, alkynes, CO, and H_2, by metal-(hydrido)carbonyl clusters is well reported [1–5]. The binding of substrate to these clusters varies from analogous to monometallic complexes, to simultaneous interactions of the substrate with multiple metal centers resulting in unique chemo-, regio- and stereoselectivities, see for example **Scheme 1** [6–8]. These scenarios provide many opportunities for novel transformations and, as such, demonstrate that the combined application of more than one metal offers appealing new opportunities for the synthetic community.

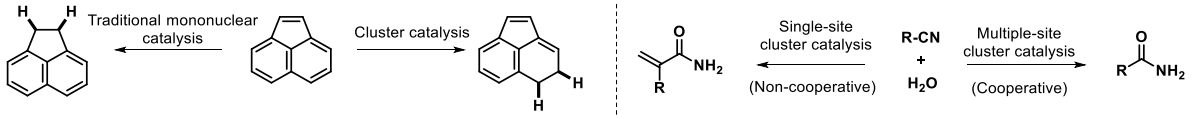

Scheme 1. Examples of unique cluster catalyzed transformations compared to traditional mononuclear catalysis (left scheme) and between different types of cluster catalysis (right scheme), [6–8].

In this review, we focus on catalysis based on homogeneous polynuclear transition metal clusters with nuclearities of three or higher. We do so because dinuclear clusters have recently been extensively discussed in excellent reviews [9, 10]. In the course of analyzing the definitions and criteria discussed below, we have sought to provide pertinent literature, which serves to deliver excellent illustrations on current state-of-the-art within cluster catalysis.

1.1 Cluster catalysis

The term *cluster* was introduced in 1964 by F. A. Cotton to designate a finite number of metal atoms held together to a certain extent, either by metal-metal interactions or metal-nonmetal bonds [11–13]. The nuclearity defines the total number of metal atoms comprising the cluster, and further classification is made with respect to the number of different metals. For example, a hexanuclear bimetallic cluster refers to a complex comprising of six metals of two different natures, such as [Ru_5Pt] [14]. In addition, it may be practical to state whether a cluster comprises metal-metal interactions [15]. The proximity between metal centers permits unique substrate transformations as multiple binding sites are available, and each metal center potentially provides additional redox-active electrons.

A given cluster's electronic properties and catalytic proficiency largely relate to three parameters, namely, (*i*) electronic properties of the parent metals, (*ii*) the combination of metal and ligand, and (*iii*) the extent of metal-metal interactions. Cluster frameworks consisting of early-transition metals predominantly comprise high valent metals combined with σ/π-donating ligands, such as halides and chalcogenides (*high valent clusters*) [16, 17]. The ligands act as a source of electrons that promote bonding interactions between the metals, as well as stabilizing the positive oxidation states. Such electropositive clusters often act as potential Lewis acidic catalysts. Contrary, late-transition metal clusters mainly comprise low valent metals combined with π-accepting ligands (*low valent clusters*) [18]. Hereof, CO represents the more common ligand albeit other examples of π-accepting ligands have been reported, such as phosphines, alkenes, alkynes, and heteroaromatics. These typically redox-active compounds may undergo oxidative addition and can catalyze reactions such as hydrogenation, hydroformylation and C-H bond activation.

The propensity to form M-M bonds increases when going from 3*d*, through 4*d*, to 5*d* metals, which reflects the increased possible *d-d* orbital overlap when going down a transition metal triad. A range of [MRu_2], M = Ni, Pd, Pt, clusters work to demonstrate the effect on catalysis when substituting one metal for another in a triad. Thus, for the

catalytic oxidation of benzylic alcohol to benzaldehyde, the activity was observed to increase up to five-fold when substituting either [$PdRu_2$] or [$PtRu_2$] with [$NiRu_2$] [19]. Interestingly, the effect of substituting Pt with Ni was also reflected in the structures of the cluster cores. As such, the $NiRu_2$ core in [$NiRu_2$] is asymmetric with Ni-Ru bond lengths of 2.90 and 3.12 Å, respectively, whereas in [$PtRu_2$] the $PtRu_2$ core is symmetric with equidistant Pt-Ru bond lengths of 3.16 Å.

Clusters containing first-row transition metals are significantly more affected by ligation than the corresponding second and third row metals. Perturbation of the *d*-orbital splitting and the properties derived hereof, thus relates to the ligand, and whether this induces a low field-splitting (*weak field*), or a large field-splitting (*strong field*) environment. However, the majority of cluster catalysts comprises 4*d* and 5*d* metals coordinated by strong-field ligands.

Laine proposed a three-level scale to reflect the involvement of a given cluster in the catalytic cycle as schematized in **Figure 1** [20]. The highest level of sophistication necessitate that at least two of the cluster's metal centers are mechanistically required for the transformation. The combination of multiple metals (identical or different in chemical nature) typically leading to a distinct chemo-, regio- and stereoselectivity, as well as a significantly different activity from a mere additive effect, is considered as *synergism* or *cooperativity*. In this regard, specific combinations of various transition metals can afford clusters with unique stereoelectronic environments to satisfy a certain set of criteria for reactivity. On the other hand, a single metal center may mechanistically account for the transformation, while interacting with vicinal centers. The other metal thus acts as an *extended ligand*. The nature of this interaction may be explained from both a steric and an electronic perturbation of the center bound to the substrate, and thereby enhance the overall catalytic performance. Finally, the lowest level of sophistication suggests a cluster be required in at least one of the catalytic steps.

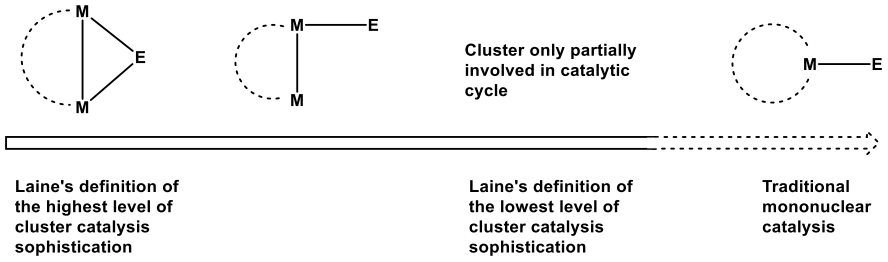

Figure 1. Three levels of sophistication a) multiple metal interactions with a substrate, b) a metal-substrate interaction is influence by a vicinal metal center either electronic, sterically or both, and c) single metal-substrate interaction, [20].

Laine's three-level scale of sophistication provides the basis for the following separate five criteria, also proposed by Laine, that suggest cluster mediated catalysis as:

1. An increasing amount of added catalysts results in a corresponding increase in turnover frequency (TOF).
2. Differences in product selectivity due to the use of a cluster catalyst (precursor), which mechanistically cannot be justified by a mononuclear compound.
3. A change in reaction conditions, or change in the catalyst, which favors metal-metal bond formation, induces an increased catalytic activity.
4. Mixed-metal cluster catalysis is suggested given a combination of at least two different metals enhance the rate of reaction or change product selectivity, which either fails to provide alone.
5. Chiral induction achieved employing asymmetric metal cluster (pre)catalysts. Chirality may reside on the basic skeletal- or metal-framework.

While these criteria provide an indirect indication of cluster catalysis, supplementary measurements are often required to ascertain the true nature of the catalyst. Such further measurement can include testing for agglomeration of colloids and nanoparticles, for example by a Hg(0) poisoning test. In addition, a catalyst (precursor) inhibition test, as well as recovery and recycling experiments, may provide even further insights into the nature of the true catalyst [21].

Moreover, it is important to emphasize that no methods alone should form the conclusion on the nature of the true catalyst, as immature conclusions may potentially be drawn [22].

1.2 Clusters: catalysts or precatalysts?

Polynuclear cluster catalysts are more often isolated as their corresponding precatalyst rather than as one of the catalytically active intermediates because of the high reactivity of the latter. Thus, the binary metal carbonyl dodecacarbonyl triruthenium, $Ru_3(CO)_{12}$, has been extensively used in small molecule activation, for example of H_2 [23–25] or CO [26–30], as well as more complex transformations, such as (cyclo)carbonylation [31–34] and C-H bond activation [35–38]. However, while highly active systems have been reported, mechanistic studies on these $Ru_3(CO)_{12}$ catalyzed reactions strongly suggest that the cluster acts a precatalyst and transforms into the active species prior to catalysis.

At high pressures of CO, $Ru_3(CO)_{12}$ is in equilibrium with its monomeric congener $Ru(CO)_5$, see **Scheme 2** [39]. This equilibrium has been shown to be highly accelerated by the presence of chloride [40]. Geoffroy and Dombek reported various nuclearity ruthenium structures resulting from different equilibria depending on temperature, CO pressure and the nature of a halide additive [41]. Thermal treatment afford tetranuclear butterfly structures in presence of chloride and bromide, whereas iodide promotes loss of CO resulting in a triruthenium-(μ_3-I) species.

Treating $Ru_3(CO)_{12}$ with dppe resulted in formation of the mononuclear species $Ru(CO)_3$(dppe) [42]. Interestingly, work by Dyson and Duckett demonstrates that, in polar solvents, the [Ru_3]-core stays intact despite the presence of phosphine, whereas apolar solvents induce cluster fragmentation, forming $Ru(H)_2(CO)_2(PPh_3)_2$ [43, 44]. Krische was able to isolate a mononuclear Ru-metallacycle from the fragmentation of $Ru_3(CO)_{12}$ in presence of PCy_3.[45] Chatani found that, under carbonylation of C-H bonds, fragmentation of the precatalyst $Ru_3(CO)_{12}$ into mononuclear Ru-complexes occurs [46–48]. Beller reported precatalytic amounts of $Ru_3(CO)_{12}$ mixed with phosphine ligands *in-situ* forms a mononuclear species [49–51]. Thus, there is significant evidence suggesting that $Ru_3(CO)_{12}$ behaves as a precatalyst for a variety of catalytically active mononuclear Ru-species.

In a similar fashion, treatment of $Fe_3(CO)_{12}$ with amine in THF was reported by Periasamy to fragment into two different compounds, a dinuclear $Fe_2(CO)_8$ and an amine-$Fe(CO)_4$ species [52–54]. Chini and Martinengo reported that the binary tetrarhodium carbonyl cluster, $Rh_4(CO)_{12}$ undergoes thermal decomposition (130 – 140 °C) under N_2, affording $Rh_6(CO)_{16}$ [55]. This decomposition was also observed to occur slowly in MeOH. The reaction of either tetra- or hexarhodium cluster with PPh_3 under a CO atmosphere afforded the dirhodium compound, $Rh_2(CO)_4(PPh_3)_4$. Chini later reported that $Rh_4(CO)_{12}$ forms an array of clusters varying in nuclearity at increasingly reducing conditions under a CO atmosphere [56]. Likewise, $Rh_6(CO)_{16}$ reacts with CO under reducing conditions to form anionic compounds of lower nuclearities, namely $[Rh_4(CO)_{11}]^{2-}$ and $[Rh(CO)_4]^-$ [57]. Fragmentation of $Rh_4(CO)_{12}$ was corroborated by Matsuda, who reported degradation under silylformylation of terminal alkynes using $Rh_4(CO)_{12}$ as precatalyst [58]. Longoni demonstrated that the transformation of tetracobalt dodecacarbonyl, $Co_4(CO)_{12}$, to a dicobalt compound, $Co_2(CO)_8$, is feasible at room temperature under approximately 1 bar of CO in ^{i}PrOH [59]. The equilibrium was further pushed towards the dicobalt in the presence of halide ions. These findings corroborate previously established decomposition patterns of the tetracobaltate clusters $[Co_4(CO)_{11}X]^-$, X = Br, I, or SCN, in Lewis-basic solvents.

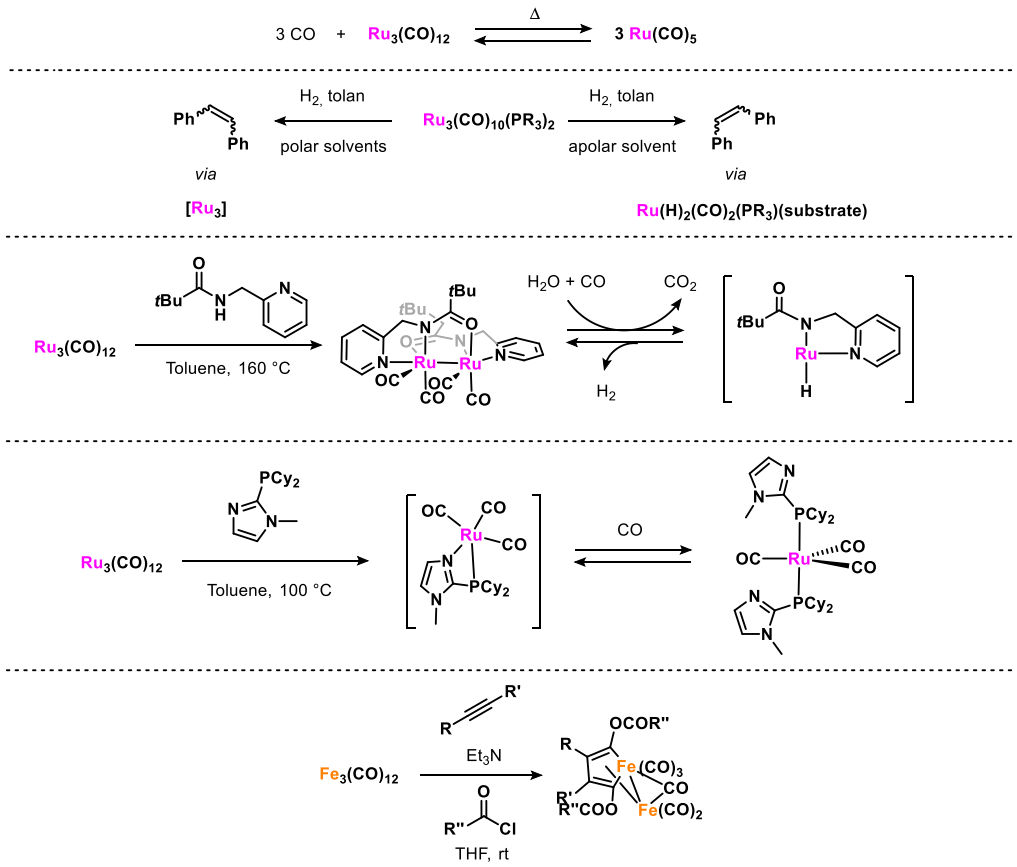

Scheme 2. Selected examples of fragmentations for catalyst precursors $Ru_3(CO)_{12}$ and $Fe_3(CO)_{12}$. Starting from the top, through the bottom, the reactions follow [39], [43, 44], [46–48], [49–51], and [52–54], respectively.

Watanabe studied various Ru-complexes as (pre)catalysts for the hydroacylation of olefins with an array of aldehydes [60]. The authors were able to recover $Ru_3(CO)_{12}$ from the reaction mixture where mononuclear complexes, such as Ru(COD)(COT) and $Ru(COD)_2$, had been employed as precatalysts. Among the screened potential catalysts, $Ru_3(CO)_{12}$ showed the best activity with 95% conversion and 50% yield. Moreover, changing the composition of the atmosphere significantly affected the amount of recovered $Ru_3(CO)_{12}$. Approximately 50 bar of Ar afforded a merely 5% recovery, whereas 20 bar of CO resulted in 60% recovery. The authors suggest that CO stabilize $Ru(CO)_5$ and $Ru_3(CO)_{12}$, either of which may be the active catalyst.

Similarly, Moore investigated the acylation of pyridine with CO and olefins **1** using $Ru_3(CO)_{12}$ as precatalyst, **Scheme 3** [61]. Under 10.3 bar of CO pressure and at 150 °C, 65% of a 13:1 mixture of ***n*-2** and ***iso*-2** was produced. During their studies, they observed that the ortho-metalated compound **3** decomposed to $Ru_3(CO)_{12}$ under the given reaction conditions albeit in the absence of an olefin. Thus, even though **3** was not observed in the catalytic reaction mixture, they inferred that the catalytic cycle is based on a triruthenium hydride species. They further corroborated their finding by performing kinetic studies that showed a first-order rate dependence on the $Ru_3(CO)_{12}$ concentration.

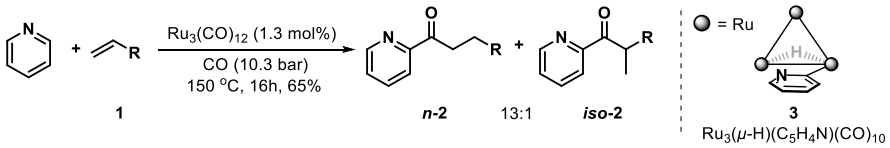

Scheme 3. Acylation of pyridine using $Ru_3(CO)_{12}$ as precatalyst, [61].

Related transformations exploiting chelate assisted C-H bond activation using $Ru_3(CO)_{12}$ as (pre)catalyst has since been reported by the groups of Murai and Chatani. This includes the reaction of 1,2-dimethylimidazole with *n*-hexene

(**1a**) under CO affording catalytic acylation of the imidazole with yields up to 77% of predominantly the linear product (up to >99:1) [62]. Interestingly, the authors propose the left triruthenium species **4** in **Figure 2** to be a key component in the catalytic cycle. However, it could not be ruled out that the monoruthenium complex **5** is catalytically active as well. Moreover, the two structures were suggested from a related triosmium cluster, $Os_3(C)_{10}(CH_3CN)_2$ [63], as well as the ortho-metalated species discussed by Moore in **Scheme 3**, to rationalize for the observed products.

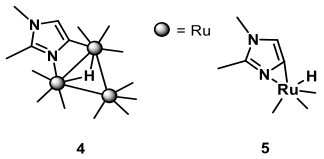

Figure 2. Two compounds with different nuclearity assumed to be central for the activation of C-H bond activation in 1,2-dimethylimidazole. Terminal CO molecules have been omitted for clarity, [62].

The general difficulty in ascertaining the true nature and nuclearity of the catalysts in various reactions is reflected in discussions in several subsequent reports using $Ru_3(CO)_{12}$ as precatalyst. One examples is the *N*-directed Ru-catalyzed carbonylation at a C-H bond in pyridylbenzenes, where analyses suggest the mononuclear species to be the catalytically active species [64]. Another example is the cyclocarbonylation of yne-aldehydes forming bicyclic *α*,*β*-unsaturated *γ*-butyrolactones, where the catalyst was merely defined as a Ru dihydride species [65]. In a third example, both $Ru_3(CO)_{12}$ and $Rh_4(CO)_{12}$ were found active in catalytic carbonylation at olefinic pyridylolefins *via* chelate assisted sp^2 C-H bond activation [66]. In this study, the reactivity patterns of the precatalysts were rationalized based on a previously reported triosmium structure **6** shown in **Figure 3** [67]. Likewise, Ru-catalyzed carbonylation of imidazoles via sp^2 C-H bond activation adjacent to the sp^2 *N* proceeds in high yields (up to 96%) and excellent linear selectivity (up to >99:1). The authors rationalize the observed products via an ortho-metalated trinuclear Ru-cluster as in **4** [68]. Finally, Ru-catalyzed carbonylation of aza-heterocycles provided C-H bond activation *β* to a directing nitrogen proceeding *via* **5** [69].

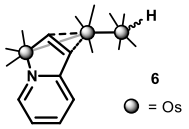

Figure 3. 5-membered metallacycle obtained from reaction of $Os_3(CO)_{10}(CH_3CN)_2$ with 2-vinylpyridine. Terminal CO molecules have been omitted for clarity, [67].

In this context, Chatani found that carbonylation of pyridin-2-ylmethylene *N*-substituted aromatic amides using $Ru_3(CO)_{12}$ as precatalyst produced a diruthenium complex with the substrate providing a chelating *N*,*N*-coordination environment to one of the Ru-centers [70]. While catalytically active, the compound was attributed as the resting state, as the presence of H_2O was necessary for a significant reactivity. As such, merely 16% product was observed after 3 days without the presence of H_2O, which should be compared to 55% after the same time span in the presence of two equivalents of H_2O. Moreover, the authors rationalized that the dinuclear species reacted under water-gas-shift conditions. A similar dinuclear species, also attributed as the resting state, was found in later studies on carbonylation of aromatic amides [46–48]. This compound, too, was fragmented in the presence of water, forming the mononuclear species.

Interestingly, work by Murai and Chatani on alkylation and vinylation of aromatic compounds revealed a catalyst nuclearity influence on the product regioselectivity [71]. Thus, as shown in **Scheme 4**, $Ru(H)_2(CO)(PPh_3)_3$ provides C-C bond formation *ortho* to the acetyl group of **7** leading to **9a**, whereas $Ru_3(CO)_{12}$ affords a selectivity *ortho* to the imine leading to **9b**. Hence, even though no further detailed mechanistic investigation were carried out, these observation suggest cluster catalysis based on, at least, the second criterion according to Laine.

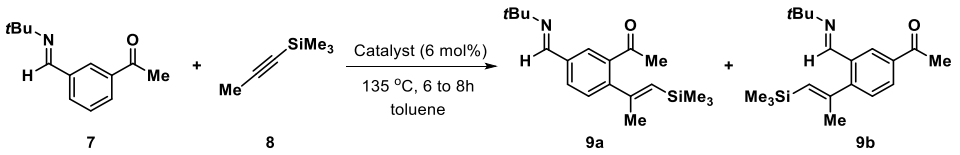

Catalyst	9a	9b
$Ru(H)_2(CO)(PPh_3)_3$	58%	0%
$Ru_3(CO)_{12}$	0%	49%

Scheme 4. Catalyst nuclearity affect the regioselectivity in vinylation of functionalized benzenes, [71].

These examples are meant to demonstrate the need for thorough mechanistic investigations to account for cluster catalysis and, if cluster catalysis is indicated, to elucidate the structure of the catalytically active cluster(s). Moreover, a trend is that polydentate ligands provide means of stabilizing a cluster framework during the catalytic cycle. They do so by enabling sufficient structural fluxionality for the various bond cleavages and formations throughout the catalytic transformation while retaining cluster integrity.

2 HOMONUCLEAR CLUSTERS IN CATALYSIS

2.1 Hydrogenation

Cabeza provided an example of a well-defined triruthenium cluster active in catalysis, where the preformed complex **10** catalyzes the hydrogenation of tolan (**11a**) to stilbene (**12a**), as shown in **Scheme 5** [72, 73]. The authors emphasize that the ampy-NH moiety affords a substrate coordination-wise regioselectivity towards the *cis* position to the *NH* coordinated ruthenium center, as CO substitution was consistently observed at this site. To elucidate the catalytic cycle, varying pressures of H_2 were used to establish rate-order dependence of substrate/catalyst ratio. At low H_2 pressures (low substrate to catalyst ratios), **10** undergoes β-hydride elimination to yield **10c**, followed by dissociation of tolan leading to **10d**. Subsequently, **10e** is formed by oxidative addition of H_2 to **10d**, followed by a fast hydrogenation of an incoming **11a**. Contrary, at high H_2 pressures (high substrate to catalyst ratios), **10** rearranges to **10a**, which then undergoes oxidative addition of H_2 forming **10b**. Hydride transfer and loss of **12a** with subsequent association of **11a** then leads to **10c**. Finally, a 1,2-migratory insertion completes the cycle. A later study of a structurally related cationic ruthenium cluster, $[Ru_3(\mu\text{-H})(\mu_3\text{-ampy})(\mu,\eta^1,\eta^2\text{-PhCH=CHPh})(CO)_8)]^+$, was reported by Cabeza as a catalyst precursor that promotes homogeneous catalytic hydrogenation of **11a** as well [74]. From kinetic studies indicating a first order rate-dependence with respect to the cluster, as well as spectroscopic analyses corroborating a trinuclear ruthenium complex as the only species in solution, the authors suggest a catalytic scheme analogous to the right hand side of **Scheme 5**.

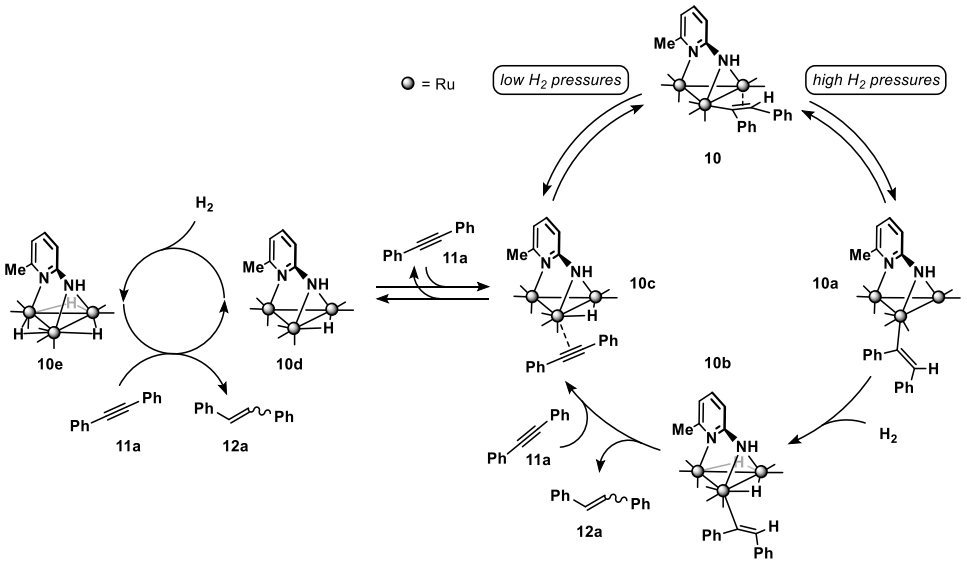

Scheme 5. Proposed mechanism by Cabeza of the hydrogenation of tolan (**11a**) to stilbene (**12a**) catalyzed by **10**. Terminal CO molecules have been omitted for clarity, [72, 73].

Sappa investigated a series of face-capping phosphinidene-bridged triiron clusters **13**, **Scheme 6**, as catalysts for the hydrogenation of **11a** as well as isomerization of ***cis*-12a** [75]. The catalytic activities of one of these clusters, $Fe_3(CO)_9(\mu_3\text{-P}t\text{Bu})_2$ (**13c**), was compared with that of a shape-wise similar tetraruthenium cluster, $Ru_4(CO)_{13}(\mu_3\text{-PPh})$ (**14**), which showed that for hydrogenation of **11a**, **14** is greater than one order of magnitude more active albeit with loss of ***trans*-12a** selectivity. Thus, whereas the iron-based **13c** had a TOF(1h) of 5 h^{-1} with **a *trans*-/*cis*-12a** ratio of 1.5:1, the ruthenium-based **14** showed a TOF(1h) of approximately 130 h^{-1} with a ratio of close to 1:1. It is difficult to assess the precise role and effect of the metal core due to the difference in nuclearities. However, the use of phosphinidene-bridging ligands demonstrates the cluster stabilizing power of μ_3-bridging X_2L-type ligands.

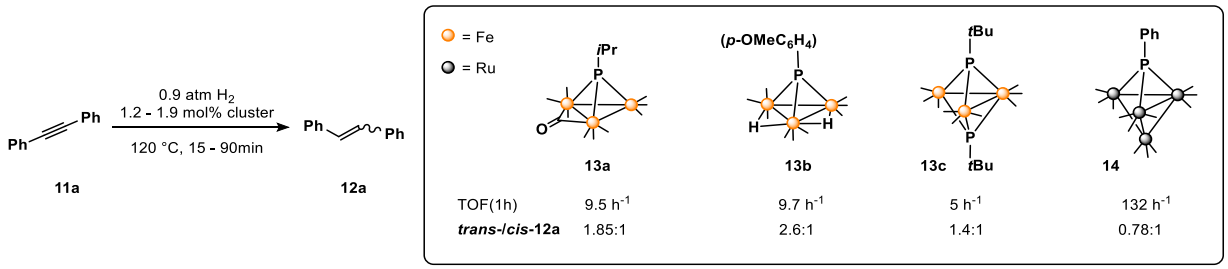

Scheme 6. Three structurally related face-capped triiron cluster compared to a face-capped tetraruthenium cluster for the hydrogenation of **11a** to ***trans*-12a** and ***cis*-12a**. Terminal CO molecules have been omitted for clarity, [75].

More recently, Algarra, Llsuar, and Basallote reported the incomplete cubane-type Mo_3S_4 cluster **15**, **Scheme 7**, as catalyst for the partial hydrogenation of alkynes (**11**) [76]. The authors rationalize a mechanism based on experimental and computational studies, which invoke transformation *via* the edge-bridging sulfur groups rather than at the metal centers. A dithiolene adduct (**15a**) is formed between two of the bridging sulfurs and the alkyne, analogous to adsorption to MoS_2 surfaces. The remaining edge-bridging sulfur cleaves the σ-bond in H_2, resulting in intermediate **15b** with one (μ-S)-H and a C-H bond. Two competing pathways account for formation of either of the (*E*) or (*Z*) alkene. The former undergoes an isomerization step and subsequently reductive elimination, whereas the latter forms without prior isomerization. Using 12 mol% of the catalyst for 65 hours under 100 bars pressure of H_2 at 150 °C in CH_3CN resulted in 62% conversion of **11a**, of which 85% was ***cis*-12a**.

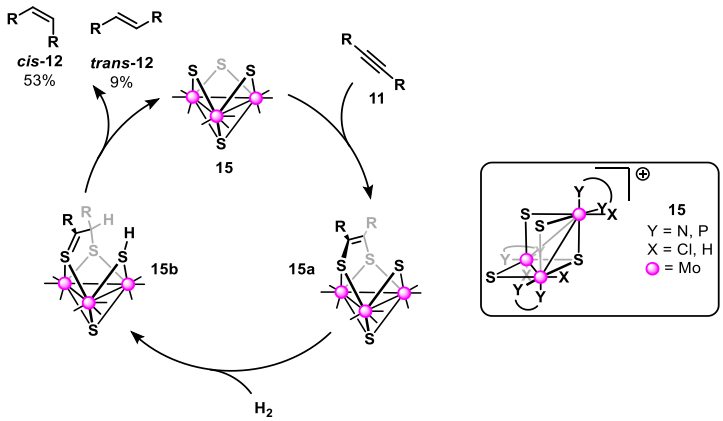

Scheme 7. Partial hydrogenation of **11** *via* bridging sulfur atoms, rather than the metals of **15**. Terminal CO molecules have been omitted for clarity, [76].

Bonnet studied chalcogenide face-capped triruthenium hydrido clusters, $(\mu\text{-H})_2Ru_3(\mu_3\text{-Y})(CO)_5(dppm)_2$ Y = O (**16*O***), S (**16*S***), as precatalysts for the hydrogenation of **1** to alkanes **17** as seen in **Scheme 8** [77]. The authors discuss possible mechanisms for the observed products, and suggests a transient species, **16*O*a1** and **16*O*a2**, wherein a Ru-Ru bond is broken to accommodate alkene coordination. While substitution of μ_3-O with μ_3-S did not increase catalytic activity, they did not provide sufficient framework stability as some fragmentation product was observed. However, no fragmentation was observed for the clusters where the one or two of the edges was bridged by a dppm-ligand. As such,

the authors conclude a synergism between the face-capping atom and the phosphine ligand, resulting in both increased stability of the cluster, and an increased catalytic activity. Furthermore, the authors propose a catalytic scheme invoking the breaking of a Ru-Ru bond, which is rationalized from kinetic studies showing a first order rate-dependence with respect to alkene, in addition to an isotopic labelling study, showing that a single hydride is transferred to the olefin.

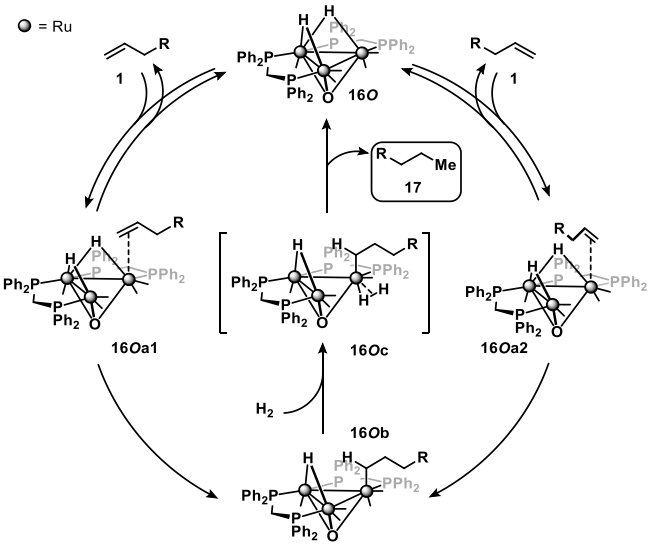

Scheme 8. Face-capping oxygen and dppm ligands of **16*O*** provide positive interactions that ensures the cluster integrity throughout the catalytic hydrogenation of olefins as proposed by Bonnet. Terminal CO molecules have been omitted for clarity, [77].

Haupt reported that the treatment of dirhenium complexes, $Re_2(\mu\text{-}P(p\text{-}XC_6H_4)_2)(CO)_8$, X = H, F, with H_2 afforded tri- and tetranuclear rhenium clusters (**18** and **19**, respectively) [78]. These were found to be active catalysts in both hydrogenation and isomerization of **1a**, of which a distinct selectivity for hydrogenation was observed for the fluorine-substituted arenes (**18b** and **19b**), **Table 1**. Ligand substitution for $p\text{-}FC_6H_4$ resulted in an increase in TON along with suppression of isomerization reaction. Cluster **18b** and **19b** are evidently stronger Lewis acids, thus resulting in a more facile coordination to **1a**. The authors suggest cluster catalysis based on the recovered amount of intact clusters. A catalytic cycle was rationalized based on their observations, and comparing the reactivity to that of the known triosmium cluster, $Os_3(\mu\text{-}H)_2(CO)_{10}$ [4]. As such, the proposed cycle proceeds analogously to traditional mononuclear catalysis; (*i*) formation of cluster-alkene π-complex, (*ii*) alkene insertion into the (μ-H)-Re bond, (*iii*) oxidative addition of H_2, and finally (*iv*) reductive elimination of **17a**.

Table 1. Treatment of **1a** with H_2 is affected by electronic properties of the organic ligand in **18** and **19**. Terminal CO molecules have been omitted for clarity, [78].

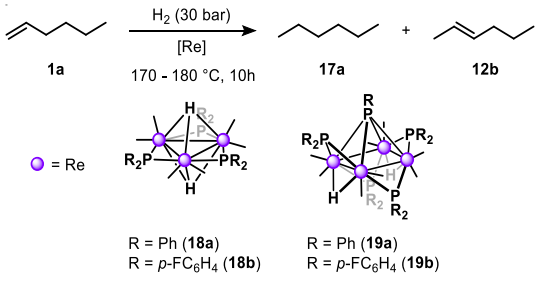

Catalyst	Loading [mol%]	Conversion [%] (TOF [h^{-1}])	
		17a	**12b**
18a	1.6×10^{-2}	28.6 (184)	40.4 (260)

19a	8.3×10^{-3}	23.8 (288)	39.6 (480)
18b	9.0×10^{-3}	56.4 (630)	8.3 (92)
19b	8.5×10^{-3}	63.5 (750)	21.1 (250)

Araujo investigated the selectivity in the catalytic partial hydrogenation of 1,5-cyclooctadiene (**20**) employing a range of tetrairidium clusters [25]. While bulk iridium as well as mononuclear $IrCl(CO)(PPh_3)_2$ afforded full hydrogenation to cyclooctane (**23**), $Ir_4(CO)_{11}PPh_2H$ (**24**) and $Ir_4(CO)_{12}$ afforded partial hydrogenation to **21** and **22** with up to 58% selectivity albeit at a lower conversion, **Table 2**. Kinetic measurements established a first-order rate-dependency with respect to **20**, whereas the various iridium clusters had a similar value (~0.0015 min^{-1}) suggesting a transformation of the catalyst precursors. The lack of nanoparticles, a lack of change in reactivity in presence of Hg, and an observed product selectivity difference, work in support of cluster catalysis.

Table 2. Hydrogenation of **20** using various Ir catalyst precursors. Terminal CO molecules have been omitted for clarity, [25].

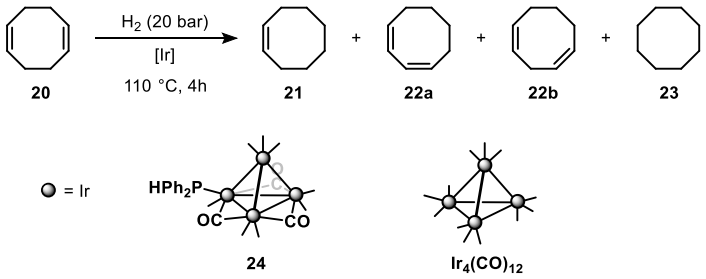

Catalyst	Conversion [%]	Selectivity [%]			
		21	**22a**	**22b**	**23**
Ir on activated carbon	100	-	-	-	100
$IrCl(CO)(PPh_3)_2$	100	-	-	1	99
24	44	47	18	33	2
$Ir_4(CO)_{12}$	40	58	14	14	14

From Wangelin's studies on $Fe(hmds)_2$, hmds = $N(SiMe_3)_2$, for the catalytic hydrogenation of alkenes, discrete metal clusters ranging from four to seven in nuclearity were obtained, each containing metal-metal bonds, **Scheme 9** [79]. Preliminary reactions demonstrated that **25** afforded catalytic hydrogenation of *α*-methylstyrene **1b** to the alkane **17b** of merely 5%. However, under reducing conditions (5 mol% DIBAL-H) 25% yield was achieved, which in presence of additional reductant resulted in >99% yield.

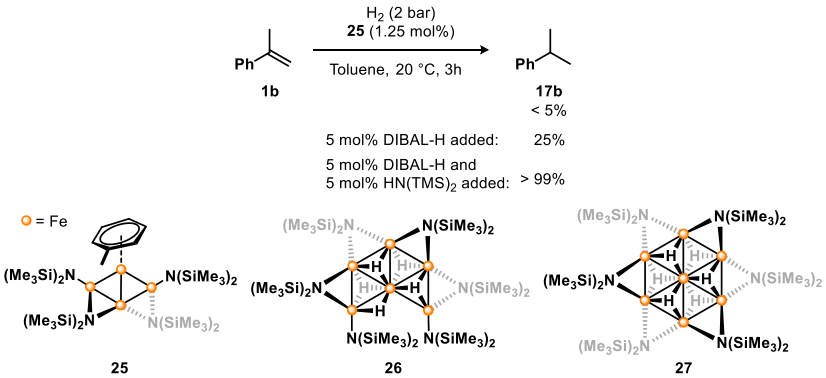

Scheme 9. Low-valent heteroleptic iron clusters varying in nuclearity, resulting from treatment of $Fe(hmds)_2$ with DIBAL-H, [79].

Wangelin synthesized a low-valent 2D heteroleptic planar Mn_6 cluster **28**, and provided an account on its catalytic properties for the hydrogenation of alkenes, alkynes and imines under reducing conditions [80]. Preparation of the cluster, or *in-situ* formation, afforded the same yields of **17b** (97%) from **1b** using equimolar amount of the reductant DIBAL-H:Mn in *n*-hexane at 20 °C. On the contrary, hydrogenation of sterically encumbered alkenes (or alkynes), such as **21a** to **23a**, was achieved using reductant/Mn in 2:1, **Table 3**. Moreover, it was unclear whether the cluster or a mononuclear Mn species was responsible for the catalysis.

Table 3. 2D heteroleptic planar Mn_6 cluster **28** as catalyst for the hydrogenation of **1b** and **21a**, [80].

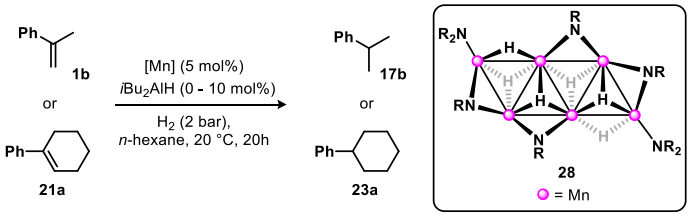

Catalyst	$^{i}Bu_2AlH$ [mol%]	**17b** [%]	**23a** [%]
28	-	0	
28	5	97	
$Mn(hmds)_2$	10	97	
$Mn(hmds)_2$	5		-
$Mn(hmds)_2$	10		>99

Matteoli investigated the influence of two different chiral phosphine-ligated tetraruthenium clusters in asymmetric hydrogenation of olefins, as well as *α*,*β*-unsaturated acids **29**, such as tiglic acid (**29a**) and **29b**, and their corresponding esters, such as **31a** [81]. The difference in electronic properties of the substrates was sought to provide mechanistic insight, such as competing isomerization reactions, enhanced substrate-catalyst interactions, and steric congestion. The structures of the precursors were determined by both single-crystal X-ray diffraction, as well as ^{1}H and ^{31}P NMR, which demonstrated a *P*,*P*-coordination environment at a single Ru center, **32**, **Table 4**. Based on these experimental findings, the authors emphasize that the presence of a carboxylic moiety in the substrate enhances the substrate-catalyst interaction. Moreover, they conclude the BINAP ligated cluster (**32a**) in general affords the better properties, and the presence of an additional ligand may increase catalytic activity. No elaborate studies on nuclearity and retention hereof were reported, nor was any tentative mechanism proposed.

Table 4. Asymmetric hydrogenation of **29a**, **29b**, and **31a** using tetraruthenium clusters **32** or **33** having chiral ligands as catalysts. Terminal CO molecules have been omitted for clarity, [81–84].

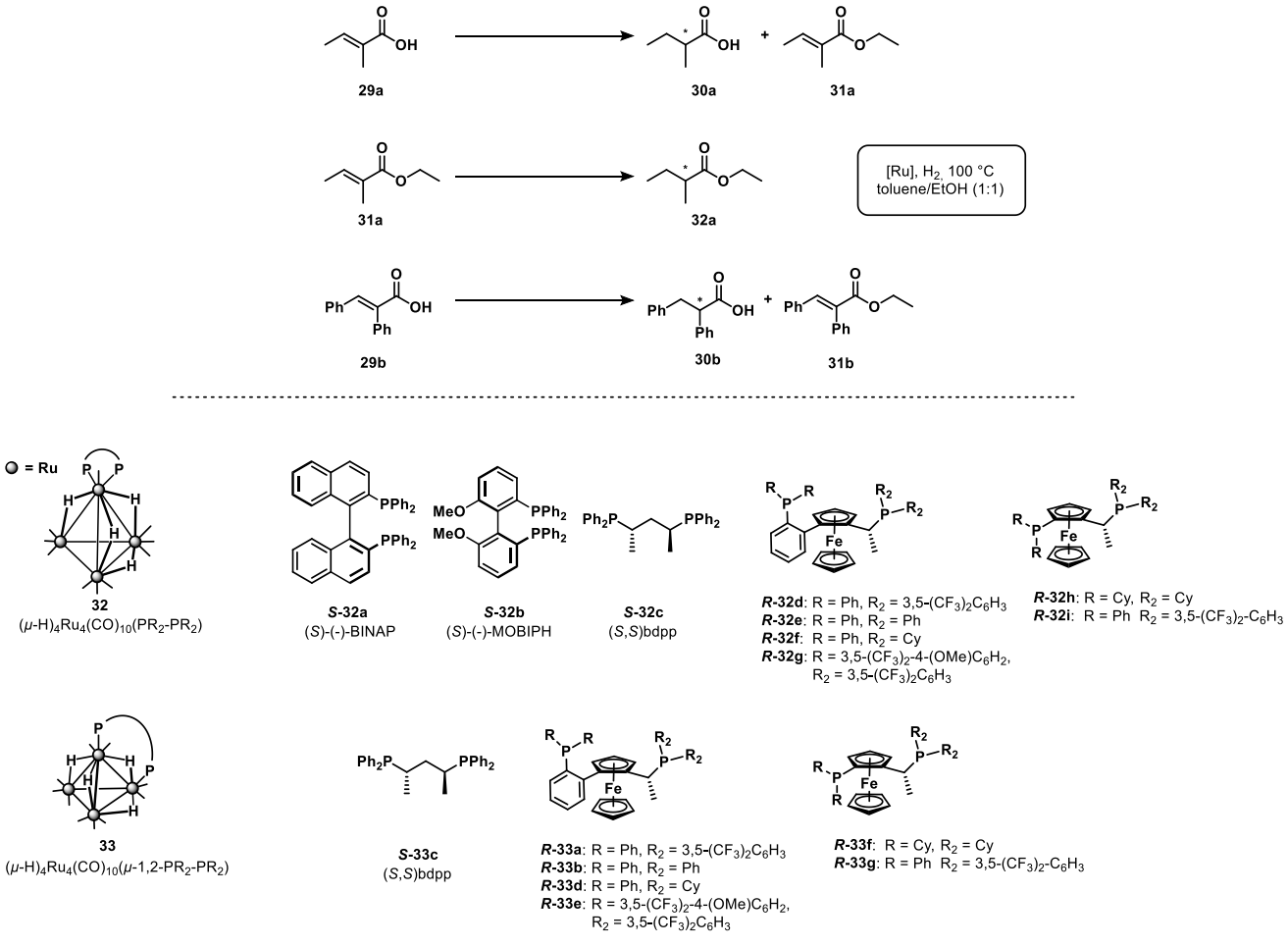

Substrate	Catalyst (loading [mol%])	H_2 pressure [bar]	Reaction time [h]	Conversion [%]	Product	Selectivity [%]	Yield [%]	*ee* [%]	Configuration
29a	***S*-32a** (0.05)	130	93	91	**30a**	-	85	29	(*R*)
29a	***S*-32b** (0.05)	130	72	100	**30a**	-	94	17	(*S*)
31a	***S*-32a** (0.05)	130	234	87	**32a**	-	87	3	(*R*)
31a	***S*-32b** (0.05)	130	253	100	**32a**	-	100	2	(*S*)
29a	***R*-32c** (0.1)	50	48	85	**30a**	94	-	45	(*R*)
29a	***S*-32c** (0.1)	50	48	75	**30a**	92	-	43	(*S*)
29a	***R*-33c** (0.4)	50	48	100	**30a**	95	-	42	(*R*)
29a	***S*-33c** (0.4)	50	48	100	**30a**	92	-	44	(*S*)
29a	***R*-32d** (0.4)	50	24	100	**30a**	100	-	93	(*S*)
29a	***R*-33a** (0.4)	50	24	99	**30a**	99	-	82	(*S*)
29a	***R*-33a** (0.4) + Hg(0)	50	24	100	**30a**	100	-	87	(*S*)
29a	***R*-33b** (0.4)	50	24	100	**30a**	100	-	58	(*S*)
29a	***R*-33b** (0.4) + Hg(0)	50	24	100	**30a**	100	-	62	(*S*)
29b	***R*-33a** (0.4)	50	24	100	**30b**	90	-	66	(*R*)
29b	***R*-33b** (0.4)	50	24	100	**30b**	83	-	63	(*R*)
29a	***R*-33d** (0.4)	50	24	99	**30a**	100	-	54	(*R*)
29a	***R*-33e** (0.4)	50	24	87	**30a**	100	-	77	(*S*)
29a	***R*-33f** (0.4)	50	24	100	**30a**	90	-	-	-
29a	***R*-33g** (0.4)	50	24	100	**30a**	96	-	-	-

Nordlander investigated two sets of stereoenriched tetraruthenium clusters, (μ-H)$_4$Ru$_4$(CO)$_{10}${μ-1,1-(*R*/*S*, *R*/*S*)-bdpp}(***R*-32c** or ***S*-32c**, respectively) and (μ-H)$_4$Ru$_4$(CO)$_{10}${1,2-(*R*/*S*, *R*/*S*)-bdpp} (***R*-33c** or ***S*-33c**, respectively), as catalysts for the asymmetric hydrogenation of **29a** under milder conditions [82]. Lowering the pressure of H_2 from 130 to 50 bar resulted in three distinct observations: high conversion (75 – 100%), interconversion from the bridging **33c** to the chelating **32c**, and a product distribution strongly affected by the ligand enantiomer; (*R*, *R*) forms (*R*), likewise (*S*, *S*) resulting in (*S*). As the activities of ***S*/*R*-33c** were nearly identical to ***S*/*R*-32c**, and the recovered cluster was of the latter structure, cluster catalysis by structure ***S*/*R*-32c** was argued. While the possibility of lower-nuclearity species forming from degradation is not excluded, the activity of these being responsible for the conversion is unlikely. The authors argue that in such a scenario, the activity of [$H_4Ru_4(CO)_{12}$]-systems would be independent of the ligands, whereas they find the opposite to be true. Despite not having determined the exact sequence of elementary steps, a tentative account on the experimental findings is presented in **Scheme 10**. Starting from **32cg**, the oxidative addition of H_2 is discussed to be stereoselective due to the orientation of *P*-phenyl substituents. Accordingly, introduction of **29a** to the coordination-sphere of **32c** follows either of two pathways: (*i*) ligand substitution forming **32ce**, or (*ii*) homo or heterolytic cleavage of a Ru-Ru bond forming **32ca**, permitting coordination of **29a**, resulting in **32cb**. Stepwise hydride insertion is followed by reductive elimination, regenerating **32c**. The latter route is argued to be more probable because of a low CO pressure makes reassociation unlikely.

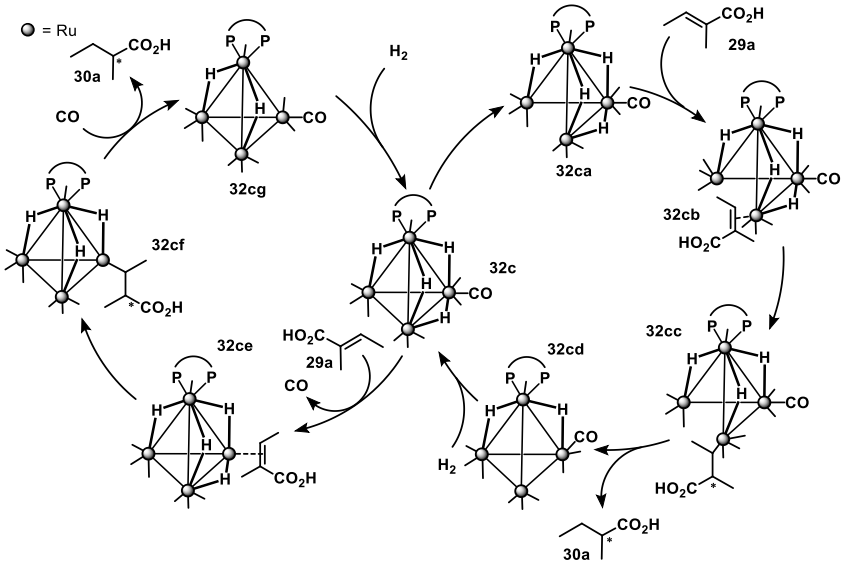

Scheme 10. Catalytic cycles involved in hydrogenation of **29a** leading to **30a** by cluster **32c** as proposed by Nordlander. The low CO pressure is suggested to disfavor the left hand pathway, as CO reassociation is unlikely. Remaining terminal CO molecules have been omitted for clarity, [82].

Continued work by Nordlander investigated the changes in cluster stability and activity in the asymmetric hydrogenation of **29a** induced by various chiral phosphine ligands [85]. While improvement was observed over the parent hydrido cluster, (μ-H)$_4$Ru$_4$(CO)$_{12}$, the authors noted varying conversion (70 - 95%), with poor increase in enantioselectivity (up to 23% *ee*), along with thermal decomposition. Cluster catalysis is invoked, as the decomposition products were insufficient in providing similar catalytic activity, as well as provided different products than those observed. The authors relate these findings to their prior study, and suggest that a better enantioselectivity can be achieved by employing ligands with a significant steric bulk proximal to the substrate. To this end, Nordlander prepared Walphos substituted tetraruthenium clusters (**33a,b**) and reported up to excellent enantioselectivity (30 – 93% *ee*) in the hydrogenation of various α,β-unsaturated carboxylic acids [83]. From spectroscopical and single-crystal X-ray diffraction analysis, an unusual bonding of the phosphine ligand was found; one coordinates equatorially whilst the other axially, resulting in chiral cluster frameworks and thus potential diastereomeric mixtures. Nevertheless, NMR analysis corroborates the presence of only a single diastereomer. A Hg(0) poisoning test and recovery experiment suggest (small amounts of) cluster fragmentation albeit the authors dismiss the significance of the colloidal

material, due to the significantly difference observed in catalyst activity with respect to yield and selectivities. Moreover, the authors emphasize an interconversion of isomers of chelating and bridging diphosphines during catalysis, and they suggest suppressing this interconversion may result in even higher stereoselectivity.

A series of tetraruthenium hydrido clusters was substituted with Josiphos- (**32h, i** and **33f, g**) and Walphos phosphines (**32d, e, f, g** and **33d, e**) to assess the steric and electronic influence of the ligand on the hydrogenation of **29a** [84]. Whereas the Josiphos substituted clusters demonstrated poor catalytic properties as well as degradation, the Walphos clusters demonstrated both excellent conversion (99 – 100%), product selectivity (99 - 100%), and enantioselectivity (92% *ee*), **Table 4**. Interestingly, an interconversion opposite to that previously established was observed, transforming the 1,1-chelating into 1,2-bridging diphosphines (**32** to **33**). This observation is argued by the authors to origin in strain relief transitioning from a nine membered "dimetallacycle" ring to the eight membered ring. Suppression of this isomerization is suggested to result in an increased enantioselectivity. While spectroscopic analyses and catalyst poisoning tests demonstrated that the combination of cluster, hydrogen pressure and temperature afforded the majority of the transformation, the free ligand was found to promote the reaction with 68% *ee* albeit at a mere conversion of 23% after 72h.

Nordlander explored the analogous phosphine-rhenium clusters of the Josiphos and Walphos-families and observed that, as for the ruthenium clusters, the Walphos-family ligand afforded better catalyst precursors in the asymmetric hydrogenation of **29a** [86]. While the trirhenium clusters demonstrated poor conversion (15%) and enantioselectivity (13% *ee*), the corresponding dinuclear complexes afforded superior conversion (88%) and selectivity (57%). Moreover, the ligand discrepancy is suggested to relate to a potential wider bite angle of the Walphos.

Furthermore, Singh and Nordlander investigated the effect of a face-capping chalcogenide to provide stability of the cluster framework in a triruthenium cluster under hydrogenation of **29a** [87]. Thus, employing the Walphos-ligand affords two diastereomers of the Ru_3-cluster **34**, **Scheme 11a**. Cluster mediated catalysis is strongly suggested based on spectroscopic analyses demonstrating an intact organometallic species in solution and neither diastereomers had interconverted after the reaction. The authors provide mechanistic insights by combining their experimental observations with DFT calculations, and rationalize a catalytic cycle invoking an initial dissociation of a CO *trans*-positioned to the phosphine leading to **34a**, **Scheme 11b**. Thereby an unsaturated cluster is formed, permitting the formation of a π-complex (**34b**), which undergoes alkene insertion (**34c**). Subsequent oxidative addition of H_2 at the same Ru-center (**34d**) results in reductive elimination regenerating the cluster concurrently with formation of the hydrogenation product (**30a**). Moreover, the authors conclude that the face-capping chalcogenide ensures cluster integrity throughout the transformation.

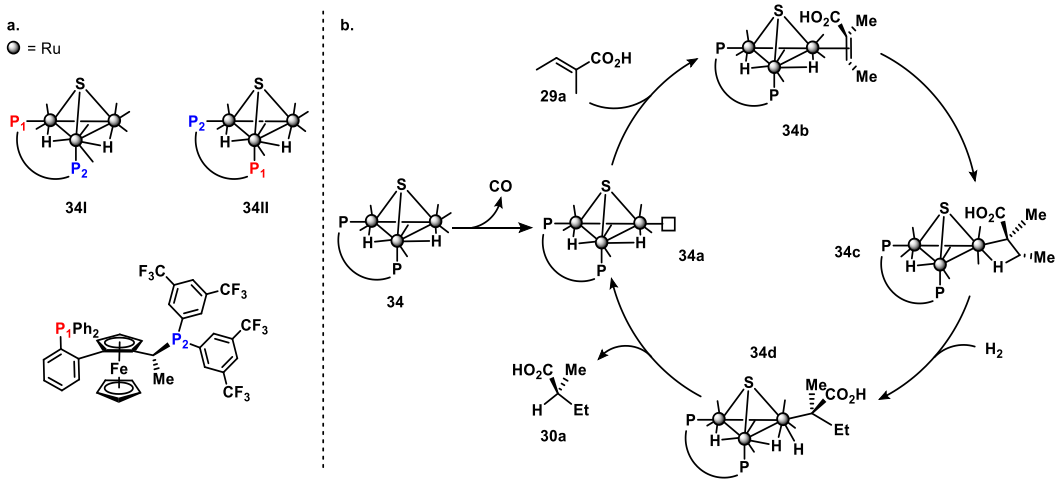

Scheme 11 a. The two Ru_3-cluster diastereomers **34I** and **34II**. **b.** Catalytic scheme for the asymmetric hydrogenation of **29a** to **30a** as proposed by Nordlander. Terminal CO molecules have been omitted for clarity, [87].

A more recent study by Nordlander investigated the use of chiral binaphthyl mono-substituted phosphiranes as ligands in use with the tetraruthenium hydrido cluster for asymmetric hydrogenation of **29a** [88]. While the clusters demonstrated catalytic activity, no enantioselectivity was observed. As no products associated with cluster fragmentation was found, cluster catalysis is suggested by the authors. Moreover, based on their comprehensive studies, Nordlander suggests that asymmetric induction in cluster catalyzed alkene hydrogenation reactions is, in large, determined by the properties of the ligand and that bidentate phosphine provides more beneficial properties relative to the monodentate congeners.

Ikariya investigated the asymmetric Meerwein-Ponndorf-Verley reduction of ketones **35** to alcohols **36** by mixing $Ru_3(CO)_{12}$ with chiral diiminodiphosphine ligands in the presence of isopropanol, **Table 5** [89]. Evidence in support of *in-situ* formation of a triruthenium cluster is presented by combining spectroscopical measurements, reactivity differences compared to a mononuclear ruthenium complex (the latter is inactive), as well as preparation and test of catalytic competence of a related anionic species. Additionally, kinetic studies suggest first-order rate-dependency with respect to the cluster concentration. Moreover, while the addition of base affected the conversion of the sterically encumbered ketone **35c**, the enantioselectivity remained generally similar. Thus, treating **35c** with $Ru_3(CO)_{12}$ in presence of **L2** and base afforded 90% *ee*, whereas in the absence of base 94% *ee* was obtained.

Table 5. Asymmetric transfer hydrogenation of **35** to **36** by *in-situ* formed triruthenium clusters, [89].

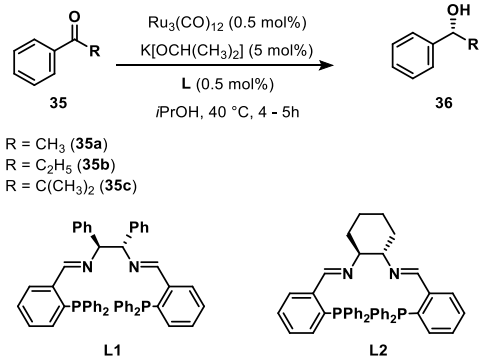

R	Ligand	Base present	Time [h]	Yield [%]	*ee* [%]
$CH(CH_3)_2$	**L1**	No	5	48	>99
		Yes	4	79	>99
	L2	No	5	30	94
		Yes	4	66	90
C_2H_5	**L2**	No	5	72	92
		Yes	4	93	92
CH_3	**L1**	No	5	91	81
		Yes	4	96	82

Rio and Gossage investigated the asymmetric hydrogenation of acetophenone **35a**, as well as the asymmetric Diels-Alder reaction of cyclopentadiene **37** and acrolein **38a**, employing catalytic amounts of each of the compounds **39**-**40** (0.5 mol%) acquired from treating $Ru_3(CO)_{12}$ with three different chiral aminooxazolines, **Figure 4** [90]. Single-crystal X-ray diffraction revealed that two of the three clusters possess a triangular face-capped Ru_3-core (**39a** and **39b**), where the amido unit binds two Ru-centers and the oxazoline nitrogen atom coordinates to the remaining Ru-center. In the third complex (**40**), the amido and hydrido spans the same Ru-Ru edge. The authors tested the mentioned reactions using $Ru_3(CO)_{12}$ as precatalyst mixed with the respective ligands. They observed conversions lower than 5% in the hydrogenation reaction, whereas the Diels-Alder reaction showed up to 20% conversion. Contrary, when using either of the preformed precatalysts **39**-**40**, excellent conversion is seen (99%) with TOF(10h) values of 144 - 200 h^{-1}

albeit with poor enantioselectivities ranging between 18 – 20% ee in the hydrogenation. The authors suggest that the prepared clusters form catalytically active hydrido compounds *in-situ*. They rationalize their conclusion based on the observation that addition of KOH increases the TOF(10h) from 65 to 200 h^{-1} and elevates the conversion from 51 to 99%. In the absence of catalyst precursors, the [4+2]-cycloaddition achieved approximately 20% conversion within 2 hours, whereas the use of the precursors afforded 80% conversion in the same timespan, with a TOF(10 min) of 25 h^{-1}.

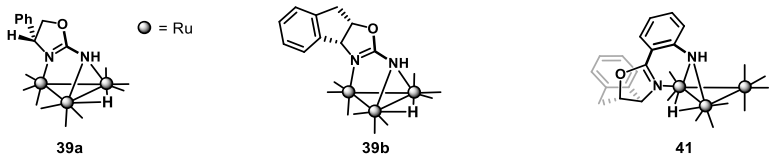

Figure 4. Three triruthenium clusters **39**-**40** derived from chiral aminooxazolines. Terminal CO molecules have been omitted for clarity, [90].

Llusar and Beller employed the incomplete cubane-type Mo_3S_4-cluster, $[Mo_3S_4X_3(Y_2)_3]^+$ (**15**), **Scheme 7**, in several settings with variation of the terminal ligands, X and Y. The hydrido dmpe ligated $[Mo_3S_4]$ cluster, $[Mo_3S_4H_3(dmpe)_3]BPh_4$ (**15c**), was found to catalytically reduce functionalized nitroarenes **41** to aminoarenes **42**, and the extent of conversion was affected by the source of reductant [91]. While H_2 provided merely 5% yield, a mixture of HCO_2H/Et_3N = 5:2, afforded up to >99% conversion with yields up to >99% of the corresponding **42** for an array of compounds as shown in **Scheme 12**. In a later study, they reported chemoselective reduction of **41** and azoarenes **43** in the presence of other reduction-susceptible functional groups, such as ketones and esters, using the trihydridocluster $[Mo_3S_4Cl_3(dmen)_3][BF_4]$ **15d,** dmen = *N*,*N*′-dimethylethylenediamine [92]. Later, the scope was expanded to include additional functional groups, **Table 6** [93]. Of the screened catalyst precursors, the cluster having a *N*,*N*-bidentate ligand, $[Mo_3S_4Cl_3(dnbpy)_3][PF_6]$ **15e**, was found to provide the optimal conditions. When using a 5 mol% catalyst loading, quantitative yields were obtained under 20 bar of H_2 and 70 °C in MeOH. To account for cluster integrity during the transformation, the reaction mixture was analyzed after four hours by ESI-MS, and no other ions corresponding to species of lower-nuclearity were observed. Further, the catalyst was recovered and reused, which afforded a modest yield of 52%.

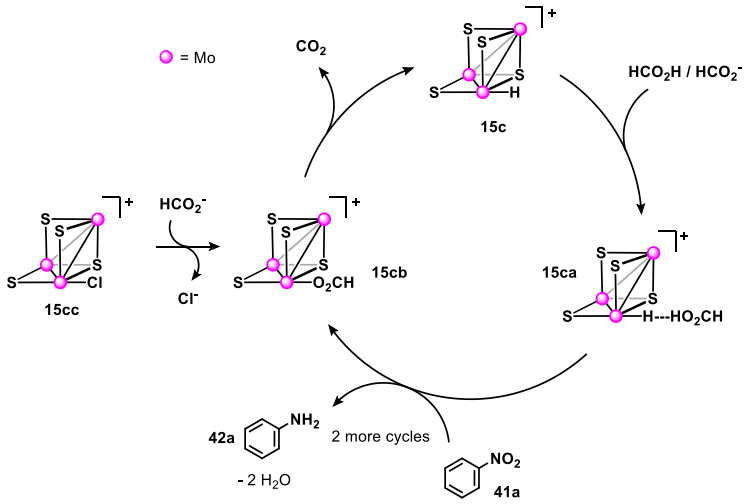

Scheme 12. Catalytic scheme proposed by Llusar and Beller for the cubane-type cluster **15** catalyzing the reduction of **41a** to **42a**. Terminal, chelating phosphines, and hydrides/chlorides have been omitted for clarity, [91].

Table 6. Chemoselective reduction of functionalized **41** to **42** catalyzed by **15e,** [93].

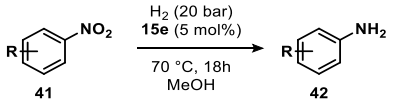

41	Conversion [%]	Yield [%]
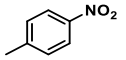 **41b**	>99	>99
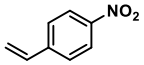 **41c**	98	85
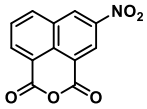 **41d**	>99	99
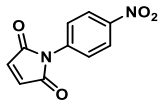 **41e**	>99	70
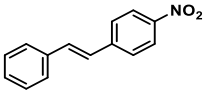 **41f**	>99	95

The incomplete cubane-type cluster **15d** was also found by Llusar and Beller to afford catalytic reductive amination of **41a** with benzaldehyde **44** using 6 mol% catalyst loading under approximately 20 bar of H_2 at 70 °C in THF on a 4 mmol scale to form *N*-benzylaniline **42g, Scheme 13** [94]. The authors account for cluster integrity throughout the transformation based on ESI-MS showing no ions of lower-nuclearity as well as ^{1}H NMR of the reaction mixture revealing intact cluster. Moreover, the cluster was recovered and used in a recycling experiment, which afforded full conversion with 90% yield of **42g**.

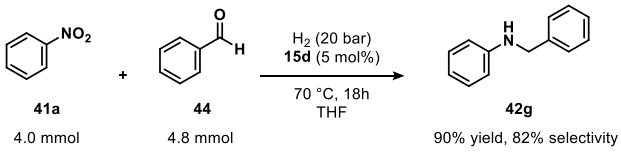

Scheme 13. Reductive amination using incomplete cubane **15d** as catalyst precursor, [94].

Suzuki and Takao studied the neutral polyhydrido triruthenium cluster, $\{(Cp^*Ru(\mu\text{-}H)\}_3(\mu_3\text{-}H)_2$, **45** in **Scheme 14**, for the hydrogenation of diazenes **43** and hydrazines **46**, **Table 7** [95]. As such, **45** activated the *N*-*N* bond of **46** to afford asymmetric capped bis- and mono-(μ_3-imido) clusters, **45a** and **45b**, respectively (left hand side of **Scheme 14**). Only the latter reacted with H_2 to provide **42a** and regenerate **45**. Under catalytic amounts of **45** (0.12 mol%), H_2 (approximately 100 bar), at 100 °C in EtOH, **46** was converted to **42a** in 31%. Despite the high pressure of H_2 suppressing the formation of the inactive complex **45a**, most of **45** was converted into this inactive species over time.

Table 7. Hydrogenation of **43** and **46** using **45** as catalyst, [95].

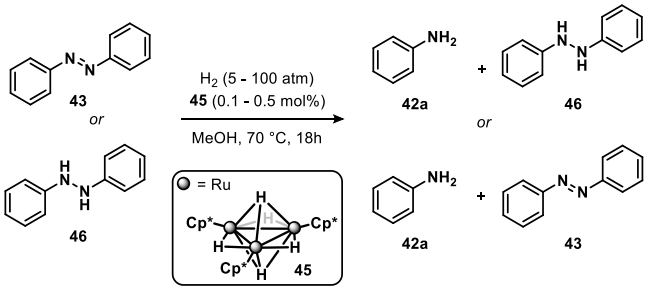

Loading of **45** [mol%]	Pressure H_2 [atm]	Substrate	Conversion [%]	Selectivity (**42a**/**46**) or (**42a**/**43**)
0.50	5	**43**	13	3.5:1
0.40	100		68	9.1:1
0.10	5	**46**	72	1.7:1
0.10	100		31	14.9:1

Cluster **45** was also reported by Takao as an active catalyst for the hydrogenation of benzonitrile **47a**, as shown on the right hand side of **Scheme 14** [96]. At approximately 10 bar of H_2 and 110 °C in MeOH, 93% conversion of **47a** was achieved with 82% selectivity towards benzylamine **48a**. Further increase in temperature to 130 °C achieved 98% conversion albeit at a lower product selectivity of 48%. Introducing a bridging carbonyl to **45**, thus affording cluster **49**, resulted in a higher catalytic performance, allowing the transformation to occur at lower temperatures as well as providing a higher selectivity. The authors speculate that the CO withdraws sufficient electron density from the Ru_3-core to prevent a simultaneous coordination of two **47a** substrates. Thus, at approximately 10 bar of H_2 and 120 °C in THF, 98% conversion was observed with a 93% selectivity towards **48a**. Based on extensive analyses, including crystal-structures, (decomposition) products obtained from stoichiometric reactions, the authors rationalize a catalytic cycle shown on the right hand side in **Scheme 14**.

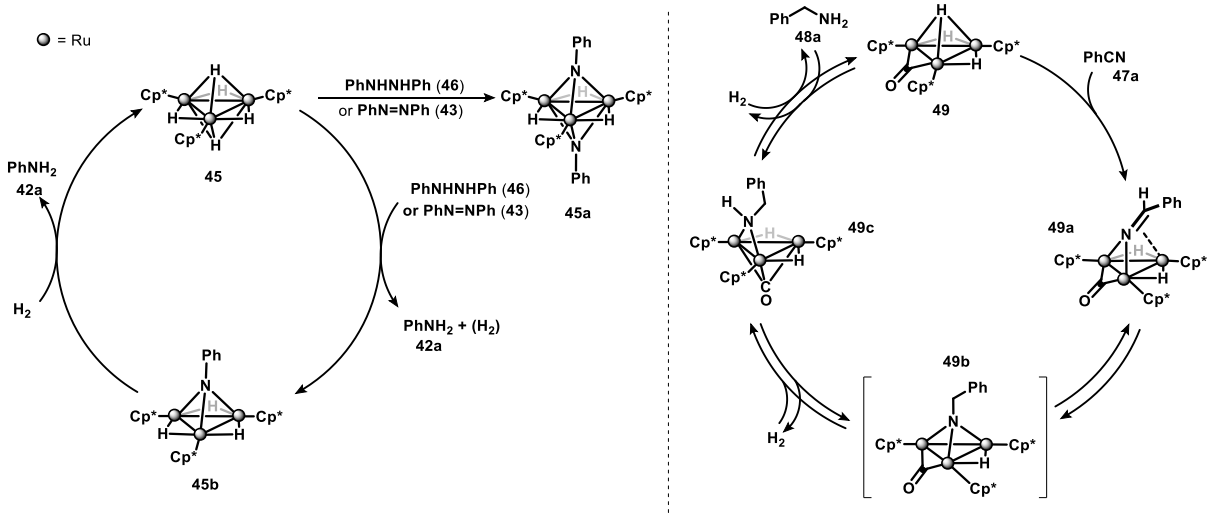

Scheme 14. Catalytic schemes for the hydrogenation of hydrazine as proposed by Suzuki [95], and of benzonitrile as proposed by Takao, [96]. Structural modification *via* a bridging carbonyl resulted in a compound with better catalytic behavior.

Research into efficient CO_2 hydrogenation catalysis is an active area of research, and while typical examples comprise mononuclear complexes based on, for example, iron [97], cobalt [98], ruthenium [99], and iridium [100], Inagaki recently reported a trinuclear iridum cluster **50** working as a photocatalytic CO_2 hydrogenation catalyst [101]. Whereas

conventional catalysis invoke high pressure and temperature for this reaction, **50** provided approximately 60% yield under 10 bars of pressure (H_2/CO_2 = 1:1) at room temperature. The authors suggest a catalytic cycle as shown **Scheme 15**, invoking initial coordination of CO_2 leading to **50a**, which is followed by insertion into the Ir-H bond leading to **50b**. Reductive elimination leads to **50c** while concomitantly forming an acid-basic adduct. Finally, subsequent oxidative addition of H_2 regenerates **50**. While both irradiation and base are necessary for the reaction to proceed, the effect of irradiation remains unclear. The authors suggests that its involvement is to facilitate hydride dissociation forming a vacant coordination-site for CO_2. However, evidence is presented that suggests further involvement by enhancing the reaction with CO_2.

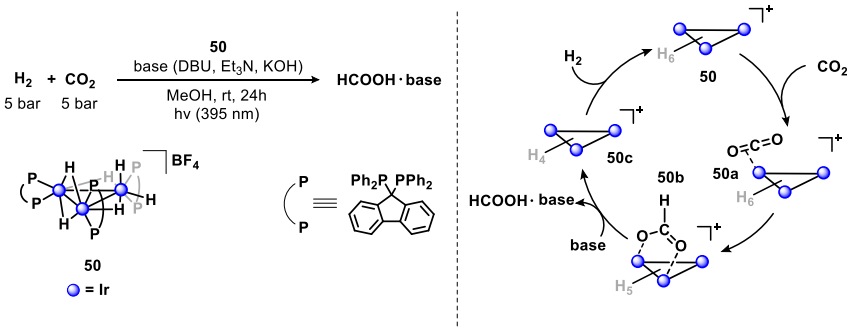

Scheme 15. Catalytic hydrogenation of CO_2 using trinuclear complex **50** as proposed by Inagaki. The diphosphine ligands are omitted for clarity, [101].

2.2 Carbonylation

Whitmire studied the homologous series of chalcogenide capped triironclusters, $[Et_4N]_2[Fe_3(CO)_9E]$, E = S (**51*S***), Se (**51*S***), and Te (**51*Te***), for the carbonylation of methanol to methyl formate **52**, while concurrently providing insight into the effect of main-group chalcogenides on cluster stability, as well as on the reactivity pattern [102]. Kinetic studies established a first-order rate dependence with respect to cluster concentration, that in conjunction with a lack of activity of the related mononuclear iron complexes, $Fe(CO)_5$ and $[HFe(CO)_4]^-$, worked to support cluster catalyzed transformation. Despite the almost identical rates in formation of **52** between the various chalcogenide clusters, the authors find substantial differences in activation energy (43, 76 and 72 kJ for **51*S***, **51*Se*** and **51*Te***, respectively). This discrepancy between formation rates and activation energies are explained by the deduced preexponential factors, where E = S contains a less favorable value (3.5×10^3 for **51*S***, *vs.* approximately 2.0×10^7 for **51*Se*** and **51*Te***, respectively). From these values, and in addition to a readily isolation of the open Te complex $[Te\{Fe(CO)_4\}_3]^{2-}$ [103] not observed for **51*S***, the authors conclude a variation in the rate-determining step, despite a similar rate-law. The proposed catalytic scheme shown in **Scheme 16**, invoke a catalytically active species that undergoes Fe-Fe bond breakage, which **51*S*** strongly disfavor. While a tentative mechanism involving rupture of a Fe-Fe bond, the authors limit the discussion to on M-M bond opening of a dianionic species in presence of CO.

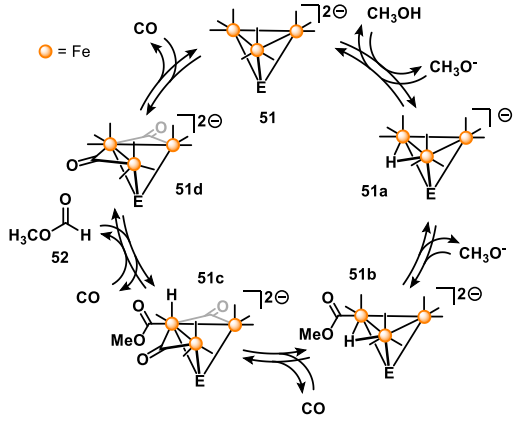

Scheme 16. The catalytic cycle in carbonylation of MeOH using the triiron chalcogenide cluster **51** homologue series (E = S, Se or Te) as proposed by Whitmire. Terminal CO molecules have been omitted for clarity, [102].

By using $Ru_3(CO)_{12}$ as catalyst precursor in junction with *N*-methylpiperidine, Mitsudo was able to afford cross carbonylation affording hydroquinones **54** from alkynes **11** and 2-norbonenes **53** [104]. While catalyst (precursor) screening demonstrated a distinct catalyst activity between triruthenium (up to 85% yield) and the mononuclear complex (trace), thus satisfying Laine's second criterion, diruthenium complexes afforded only a slightly lower yield (up to 76%) compared to the polynuclear precursor, **Table 8**. Moreover, no studies into the concrete structure of the active catalyst were provided.

Table 8. Cross carbonylation of **53** with **11b,** [104].

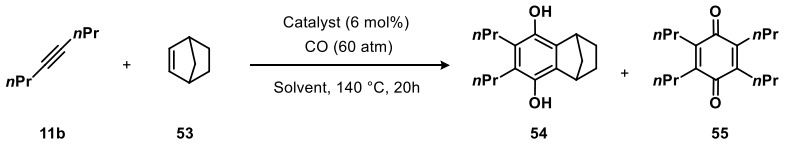

Catalyst	Solvent	Yield [%]	
		54	**55**
	Toluene	61	35
$Ru_3(CO)_{12}$	THF	51	32
	N-Methylpiperidine	85	trace
$[RuCl_2(CO)_3]_2$	*N*-Methylpiperidine	76	4
$RuCl_2(PPh_3)_3$	*N*-Methylpiperidine	trace	trace

Hydroformylation

Süss-Fink found indirect evidence that the anionic cluster $[Ru_3(\mu\text{-H})(CO)_{11}]^-$ **56** remained intact while catalyzing hydroformylation of ethylene to yield aldehyde **57a**, as shown in **Scheme 17** [105]. The authors were able to ascertain the sequence of elementary steps in the catalytic cycle using an isotopic labeling method. Thus, by mixing **56** with CF_3CO_2D and ethylene in THF, they were successful in trapping the deuterated intermediate, $[Ru_3(\mu\text{-D})(\mu\text{-}\eta^2\text{-}OCCH_2CH_3)(CO)_{10}]$, which enabled them to locate the position of the bridging hydride by ^1H and ^2H NMR. In addition, they were able to establish that the hydride transfer to ethylene precedes hydrogen incorporation.

Further studies, using propylene (**1c**) as substrate probed the selectivity as a function of temperature, pressure and solvent [106]. Generally, the cluster was found to provide chemoselective formation of aldehydes rather than alcohols independent of the conditions. On the contrary, control of regioselectivity (*n* over *iso*) was feasible, and under 10 bar of total pressure (CO/H_2 = 2:1) at 75 °C in diglyme, *n*-butanal (**57b**) was produced in practically quantitative yield (*n*/*iso* = 73). Importantly, the authors provided spectroscopically evidence that no fragmentation occurs during the reaction.

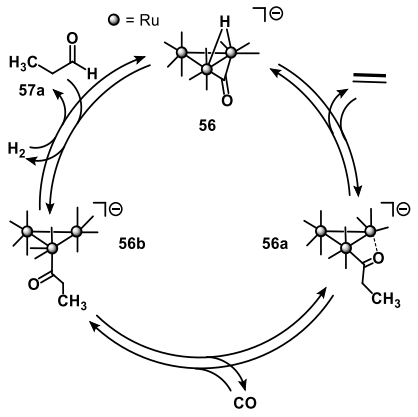

Scheme 17. Mechanism of the hydroformylation of ethylene to **57a** catalyzed by **56** as proposed by Süss-Fink. Terminal CO molecules have been omitted for clarity, [105].

Süss-Fink further investigated the hydroformylation of olefins (**1**), and changes resulting from substituting CO in $Ru_3(CO)_{12}$ with sterically demanding diphosphines [107]. Single-crystal X-ray diffraction unambiguously established four structures, one of which was found having an unusual μ_1-η^2 coordination (chelating) **58**, opposed to μ_2-η^2 (bridging) **59**-**61**, **Figure 5**. In DMF at 80 °C, both cluster-types demonstrated catalytic activity towards hydroformylation. Moreover, the clusters were largely recovered unaltered. The maximum TON value in the hydroformylation of ethylene was observed for $Ru_3(CO)_{10}$(F-dppe), F-dppe = bis(perfluoro-diphenylphosphino)ethane **60**, obtaining 429 cycles, compared to merely 157 cycles for $Ru_3(CO)_{12}$.

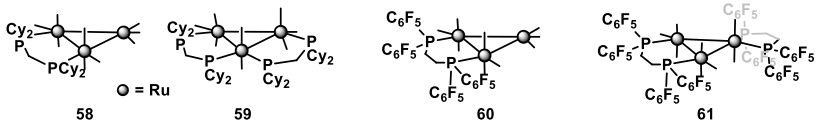

Figure 5. Various ligated triruthenium clusters as catalysts for the hydroformylation of **1**. Terminal CO molecules have been omitted for clarity, [107].

Pittman reported the use of two different cobalt clusters, **62**, and **63**, catalysts for achieving hydroformylation of 1- and 2-pentene with a predominantly linear selectivity, **Table 9** [108, 109]. A high yield of the intact cluster, as well as a different reactivity compared to $Co_2(CO)_8$, work to support cluster mediated catalysis. The authors suggest that the μ_3-C ligand of cluster **62**, and the bridging PC_6H_5 ligands of cluster **63**, discourages fragmentation into lower nuclearity species. A small selectivity difference (*n*/*iso*) was observed between **62** and **63**, 5.4 vs. 2.6 in favour of the *n*-isomer ***n*-57b**, respectively. Further, the authors note that whereas an elevated temperature reduced selectivity, a pressure increase enhanced the selectivity. For cluster **62**, at 90°C a selectivity of 5.4 was achieved, which was more than halved to 2.2 at 130°C, despite reaching almost full conversion at roughly a fifth of the time. The authors further investigated cluster **63**, and the catalytic properties of a phosphine-substituted homologue **64** for hydroformylation of 1- and 2-pentene [110]. The high yield of recovered cluster **63** (95%), the lack of other organometallic species, as well as a reactivity difference compared to $Co_2(CO)_8$, works to support cluster-mediated catalysis. Moreover, single-crystal X-ray diffraction was used to establish the structural configuration of cluster **64**. Interestingly, only cluster **63** was recovered from the reaction mixture were **64** was used originally.

Table 9. Hydroformylation of 1-pentene by tri- and tetracobalt clusters, **62** and **63**, [108–110].

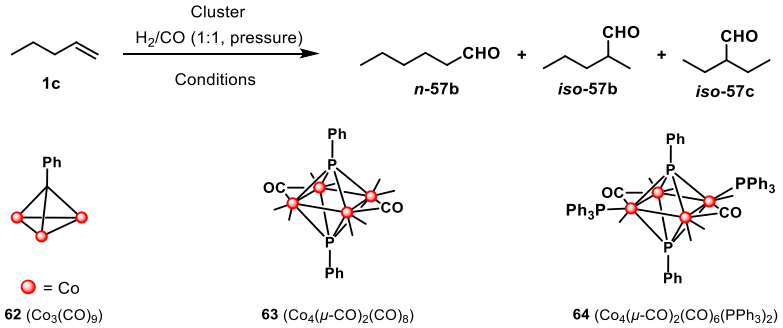

Cluster	Loading [mol%]	Substrate	Temp [°C]	Pressure [bar]	Solvent	Time [h]	Yield aldehyde [%]	Selectivity **n-57b / (iso-57c+iso-57c)**
62	0.36	**1c**	90	61 - 56	C_6H_6	104	57.5	5.4
			130	63 - 54		22	99.7	2.2
63	0.36	**1c**	130	48 - 44	C_6H_6	88	62.5	2.6
			150	50 - 44		23.5	84.2	1.9

Lavigne observed **65** in **Scheme 18c**, as a catalyst for the hydroformylation of tolan (**11a**), forming α-phenylcinnamaldehyde **38b** [111, 112]. Ligand substitution demonstrated two distinct reactivities, of which one was important in the catalytic cycle. Whereas PPh_3 resulted in migratory insertion of CO to **11a** leading to **65a**, coordination of CO afforded the vinyl group to undergo migratory insertion leading to **65b**. This step is described to occur by an σ-π motion. As such, under sufficient CO pressure the migration of the vinylic group is argued to constitute an important intermediate in the catalytic cycle. Oxidative addition of H_2 then enables reductive elimination, forming **38b** and hydride compound **65c** that can react with **11a** and conclude the cycle. Moreover, the cluster was active for up to six catalytic cycles.

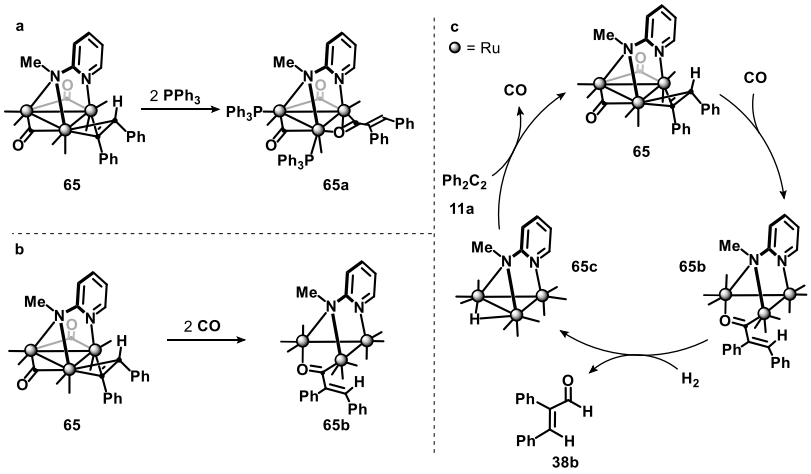

Scheme 18. Hydroformylation of **11a** using face-capped triruthenium cluster **65** as catalyst as proposed by Lavigne. Terminal CO molecules have been omitted for clarity, [111, 112].

Hydrocarbonylation

Jun reported a chelation-assisted hydroesterification of **66** using sodium formate **67** as the C_1-source and 2-phenylethanol **68** as alcohol to provide ester **32b**, **Table 10** [113]. ^{13}C-labeling experiments established the carbonylic carbon in **69** originated from **67**. Thermal decomposition of **67** was further substantiated by pH measurements showing

an increase from 6.9 to 9.1 after an hour of heating at 170 °C, as well as trapping of CO in a Rh(I) complex. The role of 2-pyridinemethanol is explained in terms of a five-membered metallacycle, concluding the mechanism to consists of a chelation-assisted hydroesterification, and transesterification. While the nuclearity of the catalyst(s) was not addressed directly, considering the various precatalysts employed, the difference in product distributions satisfy Laine's second criterion, thus suggesting cluster catalysis.

Table 10. Hydroesterification of **66** catalyzed by an *in situ* mixture of $Ru_3(CO)_{12}$ and 2-pyridinemethanol, [113].

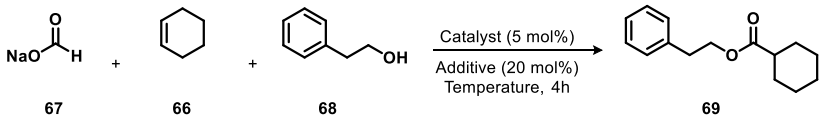

67 66 68 69

Catalyst	Additive	Temperature [°C]	Yield [%]
$Ru_3(CO)_{12}$	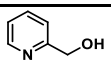	170	97
$Ru_3(CO)_{12}$	None	170	0
$[Ru(p\text{-cymene})Cl_2]_2$	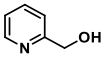	150	0
$Rh_4(CO)_{12}$		170	0

Chang demonstrated the hydroesterification of various alkenes (**1**) employing catalytic amounts of $Ru_3(CO)_{12}$ to afford products ***n*-32c** or ***iso*-32c** with predominantly linear selectivity (up to > 99:1), **Table 11** [114]. Comparing of a number of catalyst precursors resulted in a significant product variation between the triruthenium species relative to di- and monoruthenium compounds, with the two latter severely lacking activity. No further studies to ascertain the nature of the catalyst were provided.

Table 11. Hydroesterification of **1a** using $Ru_3(CO)_{12}$ as catalyst precursor, [114].

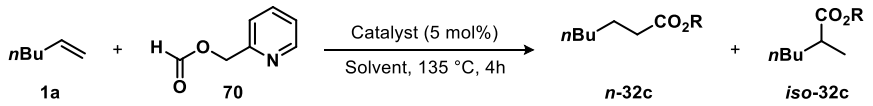

1a 70 *n*-32c *iso*-32c

Catalyst	Solvent	Conversion [%] (*n*:*iso*)	Decarbonylation [%]
$Ru(COD)Cl_2$	Toluene	8	5
$[RuCl_2(p\text{-cymene})]_2$	Toluene	4	-
$Ru_3(CO)_{12}$	Toluene	99 (57:43)	53
	DMF	>99 (74:26)	<1

A later study by Chang found that using $Ru_3(CO)_{12}$ in DMSO worked to provide conditions for regioselective catalytic hydroesterification of alkynes, whereas DMF provided beneficial conditions for dienes [115]. No experiments were done to address the structure of the catalyst, nor was ruthenium-sources of varying nuclearities investigated. However, a triruthenium species **71**, shown in **Scheme 19**, was isolated from another study on cooperative coupling using Ru and Pd, thus suggesting a polynuclear nature of the catalyst [116]. A later study found that, whereas DMF suppressed decarbonylation for hydroesterification, the opposite was true in hydroamidation [117]. Utilizing CH_3CN as solvent provided conditions affording varying yields (53 – 76%) of predominantly linear selectivity.

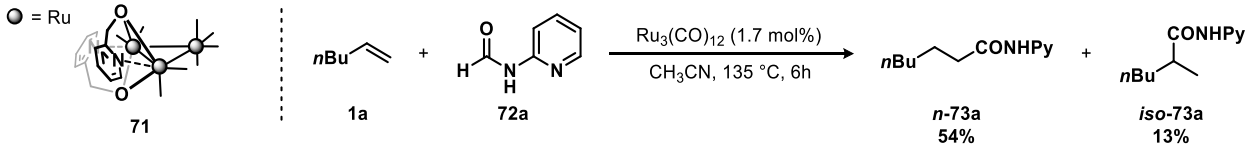

Scheme 19. Stoichimetric reaction of pyridylmethylalcohol with $Ru_3(CO)_{12}$ resulting in a *N*,*O*-chelated cluster. Hydroamidation **1a** with **72a** leading to mixtures of ***n*-73a** and ***iso*-73a**, respectively, using $Ru_3(CO)_{12}$ as precatalyst. Terminal CO molecules have been omitted for clarity, [117].

Following these results, Chang demonstrated that co-catalytic amounts of halide salts worked to enhance the ruthenium-catalyzed hydroesterification of olefins **1** and alkynes such as ^{n}Pr-CC-^{n}Pr **11b** [118]. While the presence of halide has been reported to promote cluster fragmentation (*vide supra*), the authors invoke that this equilibrium is relevant only at high pressures of CO, as opposed to their conditions (absence of CO, and a maximum of 110 °C in DMSO). Rather, based on spectroscopic data, the role of halide was argued to promote dissociation of CO ligand. As such, using Bu_4NI as additive afforded excellent yields (up to 99%) with predominantly linear selectivity (up to >98:2) in the hydroesterification of **1**.

Formyl addition of **72b** to **53** leading to **74** was successfully achieved by Kondo and Mitsudo using a catalyst precursor system comprising the anionic triruthenium hydrido cluster **75**, $[PPN][Ru_3H(CO)_{11}]$, PPN = bis(triphenylphosphine)iminium, and PCy_3, **Table 12** [119]. From screening a range of catalyst precursors, the mononuclear compound Ru(COD)(COT) demonstrated good conversion and similar regioselectivity (*exo*:*endo*) to that of **75**, albeit at a significantly reduced yield of 16% compared to 97%. The more simple $Ru_3(CO)_{12}$ also showed a *exo*:*endo* regioselectivity in the same range (84/16), but with significantly lower conversion of merely 26%. While these differences in conversions and product distributions satisfies Laine's second criterion, further studies could potentially shed more light on the nature of the catalytically active species.

Table 12. Alkene insertion into formyl bond using anionic triruthenium cluster, [119].

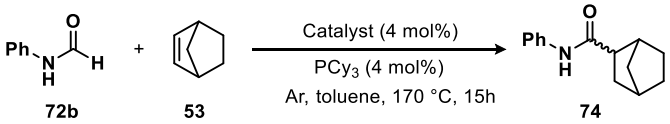

Catalyst	Conversion [%]	Yield [%]	*exo:endo*
$Ru_3(CO)_{12}$	26	18	84/16
75	100	97	71/29
$[Ru(\eta^6\text{-}C_6H_6)Cl_2]_2$	91	-	-
Ru(COD)(COT)	74	16	82/18

Cyclocarbonylation

Takahashi demonstrated that $Ru_3(CO)_{12}$ is an efficient catalyst (precursor) for cyclocarbonylation to selectively afford γ- and δ-lactones, such as **77a**, from allenylic alcohols, such as **76a** (91 – 99% yield), **Scheme 20** [120]. When substituting to mononuclear ruthenium complexes, such as $RuCl_3 \cdot x\ H_2O$ and $RuCl_2(PPh_3)_3$, catalytic activity was observed albeit with lower yields of 82% and 41%, respectively. Additionally, related metalcarbonyls demonstrated no activity. Investigation of the reaction conditions found that absence of additive Et_3N reduced the yield to approximately 60 %. Moreover, while the nuclearity of the actual catalyst was not addressed, the catalyst precursor nuclearity was shown to affect the yield of product formation.

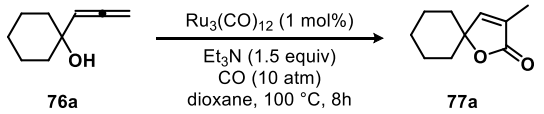

Scheme 20. Triruthenium $Ru_3(CO)_{12}$ of **76** affording γ- and δ-lactones, [120].

A subsequent study on the same reaction demonstrated a linear correlation of TOF with respect to the $Ru_3(CO)_{12}$, in accordance with Laine's first criterion [121]. Labelling studies revealed the formation of two furanone-based products, of which tautomerisation to **77** occurs at elevated temperature in presence of Et_3N and ruthenium. To conclude their findings to a catalytic cycle, **Scheme 21,** the authors argue for an initial formation of a π-allyl complex. This suggestion is based on two observations, (*i*) excess addition of MeOH did not increase the rate of carbonylation, and (*ii*) the isolation of π-allyl adducts of both $Fe_2(CO)_9$ and $Os_3(CO)_{12}$.

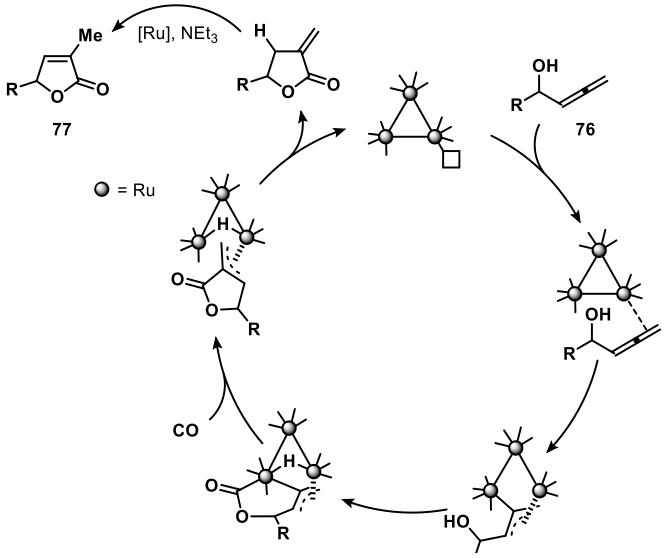

Scheme 21. The catalytic cycle for cyclocarbonylation of **76** to yield **77** using $Ru_3(CO)_{12}$ as catalyst, as proposed by Takahashi. Terminal CO molecules have been omitted for clarity, [121].

With reference to the work by Takahashi, Tsubuki and Honda reported that the use of $Ru_3(CO)_{12}$ in catalytic amounts under atmospheric pressure of CO selectively affords cyclocarbonylation of homoallenylic alcohols **78** to either five- or six-membered lactones, such as **76**, **Scheme 22** [122]. The nature of the solvent was found to affect the formation of *endo* vs. *exo* product. Whereas acyclic tertiary amines resulted in complex mixtures, using cyclic tertiary amines resulted in a predominantly *endo* selectivity in varying yields 58 – 76%. Of the various solvents, 2,4,6-collidine resulted in a *endo-exo* distribution of 3.0:1. Additionally, the solvent affected the necessary pressure for cyclocarbonylation. Using Et_3N, pressures below five atmospheres resulted in approximately 10% yield, while 2,4,6-collidine afforded up to 79% yield under atmospheric pressure of CO. The catalyst nuclearity was not addressed, nor was any other ruthenium sources investigated as potential catalysts.

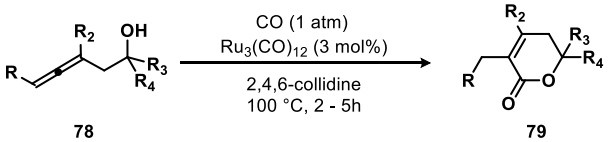

$R_1 = R_3 = R_4 = H$, $R_2 = C_5H_{11}$, 5h, 73%

$R_2 = R_3 = R_4 = H$, $R_1 = C_5H_{11}$, 3h, 76%

Scheme 22. Cyclocarbonylation of **78** to **79** under atmospheric pressure of CO using $Ru_3(CO)_{12}$ as (pre)catalyst, [122].

2.3 Miscellaneous

Hydrosilylation

Nagashima reported that the acenaphthylene face-capped triruthenium cluster, **80** [6], undergoes a distinct hydrogenation of the arene-moiety, affording hydrogenation of the C-C double bond within the six membered ring of the ligand to provide **81**, shown in **Scheme 23** [7]. A later study revealed the resultant oxidative addition adduct of silanes to **75** provided clusters with retained integrity, **82** [123].

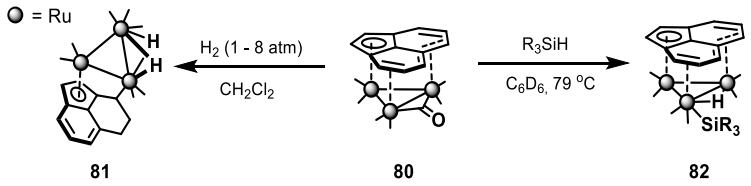

Scheme 23. Treatment of triruthenium-acenaphthylene cluster **80** with molecular hydrogen affording a distinct hydrogenation of the ligand **81**, or provides an oxidative addition adduct with silanes **82**. Terminal CO molecules have been omitted for clarity. [6, 7, 123]

The same study disclosed **80** as an efficient catalyst precursor for the hydride addition to *α*,*β*-unsaturated carbonyls **83** to afford either **84** or **85**, as well as for ring-opening polymerization of THF to polymeric ether **86**, **Table 13**. Up to full selectivity of the hydride addition was achieved by pairing **83** with the appropriate silane. As such, employing diphenylsilane resulted in 1,2-addition to yield **84**, whereas dihydrosilanes resulted in 1,4-addition providing **85**. Interestingly, ring-opening polymerization of THF provided a selective M_n in the range of 10^3 – 10^5, a process commonly initiated in strongly acidic media. The authors suggest a transient species, structurally resembling **82**, based on an induction period, as well as ^{1}H NMR studies of the reaction mixture showing similar resonances. Moreover, **82** was preparatively synthesized albeit under thermally different conditions than those in the catalytic cycle (79 °C *vs.* 40°C). These observations thus suggests cluster catalysis.

Table 13. Initial discovery using **80** as precatalyst. Terminal CO molecules have been omitted for clarity, [123].

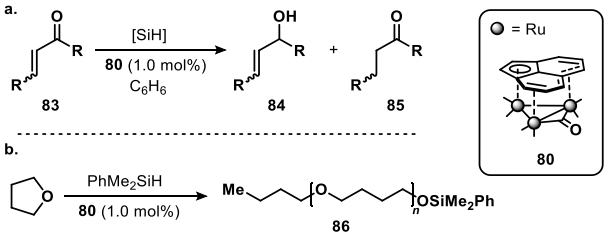

a. Substrate	[SiH] (1 equiv.)	Time [h]	Yield [%]	**84:85**	b. THF/SiH	Temperature [°C]	Time [h]	Yield [%]	M_n	$\frac{M_w}{M_n}$
	$(HSiMe_2)_2(CH_2)_2$	1	80	12:88	20	40	20	40	5500	1.4
	Ph_2SiH_2	4	93	91:9						
	$(HSiMe_2)_2(CH_2)_2$	1	94	94:6	100	40	20	44	16000	1.5
	Ph_2SiH_2	2.5	74	100:0						

Nagashima provided further reports on selective reduction of functional groups using **80** as catalyst precursor. For example, addition of tertiary amines, such as Et_3N, as additive afforded selective reduction of the amide unit in ketoamide compounds [124]. In another example, the presence of Me_2S in mixtures of aldehydes and ketones selectively suppressed reduction of the ketones [125]. Furthermore, under neutral conditions **80** catalyzes the cleavage

of the C-O bond in a range of functionalities containing the C-O^{t}Bu unit, including *N*- and *O*-Boc as well as ^{t}Bu-esters and ^{t}Bu-ethers [126]. Further substrate selectivity was demonstrated by varying the source of silane. To this end, reduction of carboxylic acids using monofunctional silanes afforded the corresponding silylether, whereas bifunctional silanes provided the aldehyde [127]. Finally, bifunctional silanes were further employed in dehydration of amides [128].

Variation of the substituents changes the reactivity from vinyl ether polymerization to a [1,3] O to C rearrangement. A stereo-electronic-activity relationship of the substituents in the substrate **87** concluded that, H as α-substituent (R') generally results in polymerization, shown in **Scheme 24** [129][130] On the other hand, when R' is different from H, in addition to a vinyl substituent that form a stabile cation, such as furfuryl vinyl ether or *p*-methoxybenzyl vinyl ether, rearrangement was observed, **Table 14**. Moreover, the addition of excess hydrosilane resulted in a step-wise formation of the corresponding silylether going through an initial [1,3] O to C rearrangement to the corresponding carbonylic moiety, followed by reduction, finally forming the silylether. While using 10 mol% PhMe2SiH selectively provide **88**, a complete reversal in selectivity was achieved using 130% of the silane and using 1 mol% **80** providing **89**.

Table 14. Alkoxysubstituent promoting rearrangement over polymerization, [130].

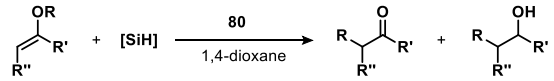

87 88 89

Substrate	[SiH] [mol%]		Catalyst [mol%]	T [°C]	t [h]	Conv. [%]	Yield [%]	**88**:**89**
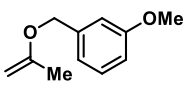	$PhMe_2SiH$	(10)	0.1	50	1	>99	88	100:0
		(130)	1	50	1	>99	91	0:100
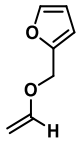	$PhMe_2SiH$	(20)	0.1	50	3	12	12	100:0

The polymerization is described by a cationic mechanism initiated by a heterolytic cleavage of the H-SiR_3 bond, resulting in an ion pair consisting of R_3Si^+-[H-Ru_3]$^-$ (**90d**). The siliconium ion then adds to the terminal carbon of **83** leading to **90a**, which is followed by propagation of the monomer (**90b** and **90c**) and terminated by hydride transfer providing the polymerization product **91**, as shown in **Scheme 24**. The Lewis acidity of the siliconium species is proposed to be insufficient for activating compounds bearing electron withdrawing substituents. End group analysis using deuterium corroborates the authors' suggested mechanism and observations regarding insertion of alkene between the Si and H bond in R_3Si-H.

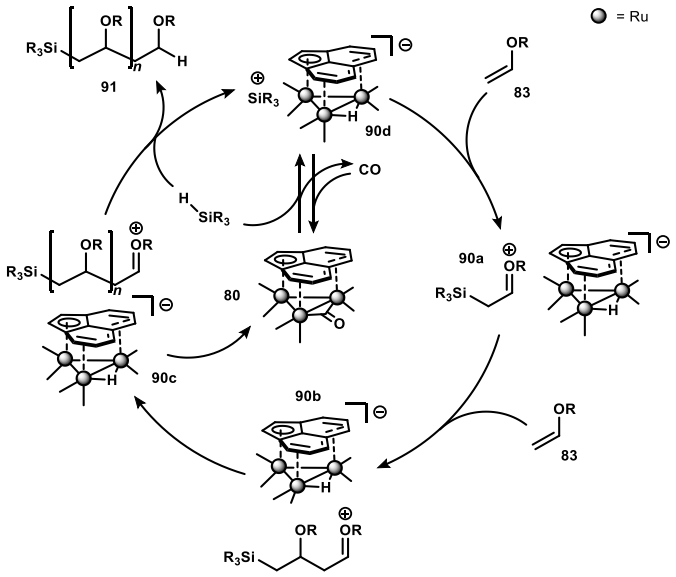

Scheme 24. Catalytic scheme for the polymerization of ethers to **91**, exemplified by polymerization of vinyl ether **83**, as proposed by Nagashima [129]. Terminal CO molecules have been omitted for clarity.

Hydrodefluorination

Catalytic hydrodefluorination of perfluoropyridine **91** to tetrafluoropyridine **92** was achieved using the incomplete cubane-type cluster, $[M_3S_4H_3(dmpe)_3]^+$ M = Mo (**15c**), W (**93a**), of which **93a** was reported by Llusar to afford a superior TON value of 90 [131]. Using 1 mol% catalyst loading and Me_2PhSiH as silane source afforded 90% yield under microwave conditions. Under the applied conditions, no cluster degradation was observed, and any reaction was only observed in the presence of the cluster. Mechanistic accounts were rationalized from DFT studies suggesting an initial phosphine dissociation from the cluster permitting M-H/C-F σ-bond metathesis. This compound, in turn, undergoes M-F/Si-H σ-bond metathesis that is concluded by re-coordination of the phosphine ligand as shown in **Scheme 25**. To assess the influence of the phosphine ligands on catalytic activity, Llusar reported in a later study the activity of the dppe congeners, $[M_3S_4H_3(dppe)_3]^+$, M = Mo (**15f**), W (**93b**) [132]. Approximately 90% yield was achieved at a significantly lower temperature (115 *vs*. 180 °C) and catalyst loading (0.7 *vs*. 1.0 mol%, respectively). Thus, substitution for less basic chelating phosphine was found to afford higher catalytic activity.

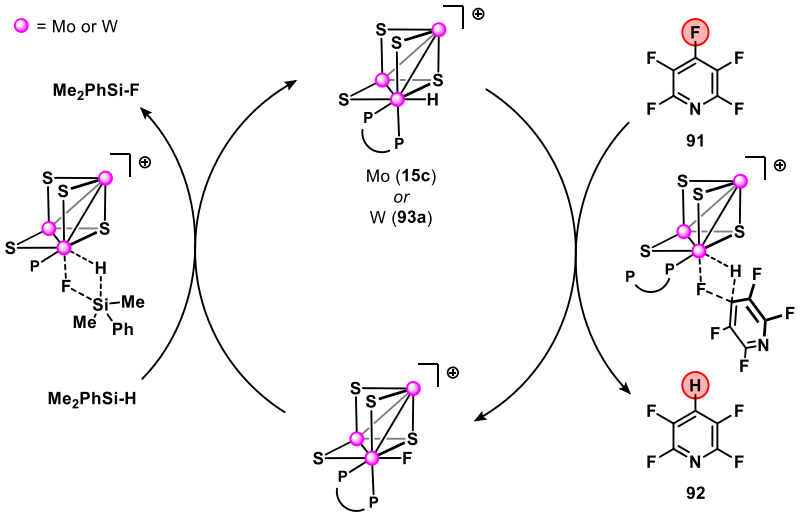

Scheme 25. Catalytic regioselective hydrodefluorination of **91** to **92** using the high valent clusters **15c** or **93a**, as proposed by Llusar. For clarity, ligands have been omitted on residual metal centers, [131].

Dehydrogenation reactions

Yi demonstrated that the tetraruthenium complex, {[(PCy_3)(CO)RuH]$_4$(μ_4-O)(μ_3-OH)(μ_2-OH)}, **94**, is a highly effective catalyst for the Oppenauer oxidation of primary (62 – 85%) and secondary alcohols (79 – 98%), **Table 15** [133]. The authors were able to recover **94** after the reaction, which by ^{1}H NMR spectra showed no changes. Further, the activity was found to remain the same throughout five cycles. In addition, the activity of **94** was greater than either of the parent compounds, RuHCl(CO)(PCy_3)$_2$ and [(PCy_3)$_2$(CO)RuH](μ-H)(μ-OH)[RuH(CO)PCy_3], which afforded merely 30% and trace conversions, respectively. Additional two mononuclear ruthenium complexes were tested, of which neither afforded any oxidation. This drastic difference suggests cluster catalysis according to Laine's second criterion. Moreover, the transformation was concluded to proceed by cooperative interaction, as Hammett studies demonstrate an outer-sphere mechanism, as well as a sigmoidal curve-shape for the initial reaction rates. As such, the substrate seemingly binds to multiple ruthenium centers. Finally, a Hg(0) poisoning test indicates homogeneous-phase catalysis.

Table 15. Dehydrogenation of **68** to **88** using a tetraruthenium cluster **94** as catalyst. Terminal CO molecules have been omitted for clarity [133].

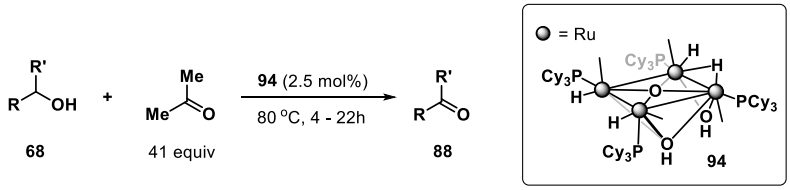

Substrate	Time [h]	Conversion [%]	Yield [%]
	18	100	62
	18	100	94
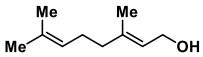	3.5	95	85
	16	83	79
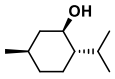	6	100	98

Using the same ruthenium cluster, **94**, Yi demonstrated its ability as an efficient catalyst for the dehydrogenation of unreactive C-H bonds in amines and carbonyls, resulting in TON values up to 20,000 within 2h at 200 °C [134]. Additional mechanistic insights were obtained by phosphine inhibition and labeling studies, demonstrating that the cluster undergoes dissociative activation, as a significant reduction in TON was observed following increasing equivalents of phosphine. Further, the transformation was established to occur *via* a reversible C-H activation at the vinylic position of *tert*-butylethylene (TBE). From these findings, Yi later reported a tandem one-pot setup for dehydrogenation-alkylation of hydrocarbons to provide a variety of aromatic compound, using a combination of tetraruthenium cluster **94** and the cationic monoruthenium species [(η^6-C_6H_6)RuH(CO)(PCy_3)]BF_4 [135]. This method worked to afford a highly regio- and stereoselective protocol for the one-pot dehydrogenation-alkylation and insertion of **1** to ketones, such as **88a**, **Table 16**.

Table 16. Tandem one-pot dehydrogenation-alkene insertion using two ruthenium catalysts, [135].

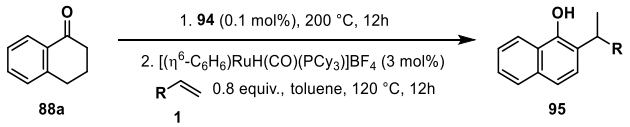

1	95	TON
	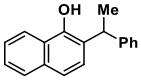	364
	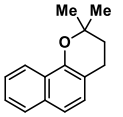	310
	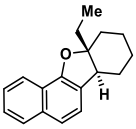	284

Suzuki reported that cluster **45** is active for the catalytic dehydrogenative coupling of electron-donating 4-substitued pyridine compounds **96** to yield 4,4'-dimethyl-bipyridine **97**, **Scheme 27** [136]. Cluster **45** treated with excess pyridine reacted *via* a C-H bond cleavage at the α-position resulting initially in the formation of an edge-bridge pyridyl species **45d**, which for electron-withdrawing functional groups transformed into the thermodynamically favored face-capped μ_3-pyridyl complex, **45e, Scheme 26**.

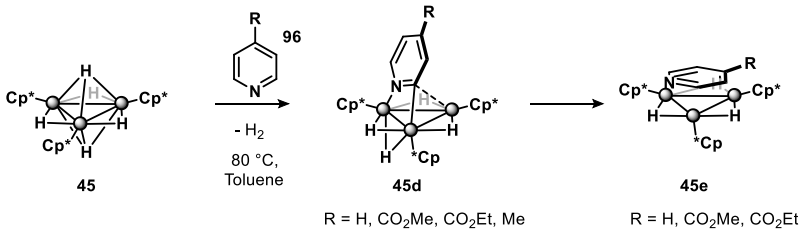

Scheme 26. Transformation of the pentahydrido triruthenium cluster **45** with pyridines, [136].

Using 0.2 mol% of **45** at 180 °C, dehydrogenative coupling forming **97** was achieved in turn-over number of 80 after 120 hours. The reaction in general provided moderate yields of the coupling products. However, it constitutes a rare example of reactions that utilize C-H bond activation for C-C bond formation, **Table 17**. The authors noted strongly coordinating solvent suppressed the reaction, as demonstrated by the difference in yields by one order magnitude between DME (2%) and mesitylene (20%). Moreover, the lack of products observed for electron-withdrawing substituents is suggested to relate to formation of **45e**.

Table 17. Dehydrogenative coupling of **96** leading to **97** using **45** as catalyst precursor, [136].

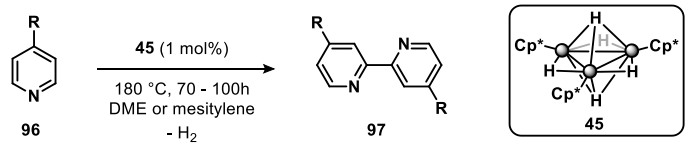

R	Time [h]	Solvent	Yield [h]
Me	72	DME	2
Me	72	Mesitylene	20
Me	100	Mesitylene	43
4-pyridyl			27
NMe_2			23
CO_2Et			trace
OMe			8

While a full mechanistic account remained unclear, the authors provide a tentative mechanism based on an initial oxidative addition of a C-H bond at the α-position to give **45f**, **Scheme 27**. This is followed by the coordination of a second pyridine compound giving **45g**, which promotes loss of hydrido ligands as H_2. The second pyridine compound undergo C-H bond scission to provide **45h**, which *via* a rupture of a Ru-Ru bond permits for reductive elimination (**45i**). Finally, regenerating the Ru-Ru bond, releasing **97**, and allowing oxidative addition of a new pyridine compound closes the catalytic cycle by reforming **45g**.

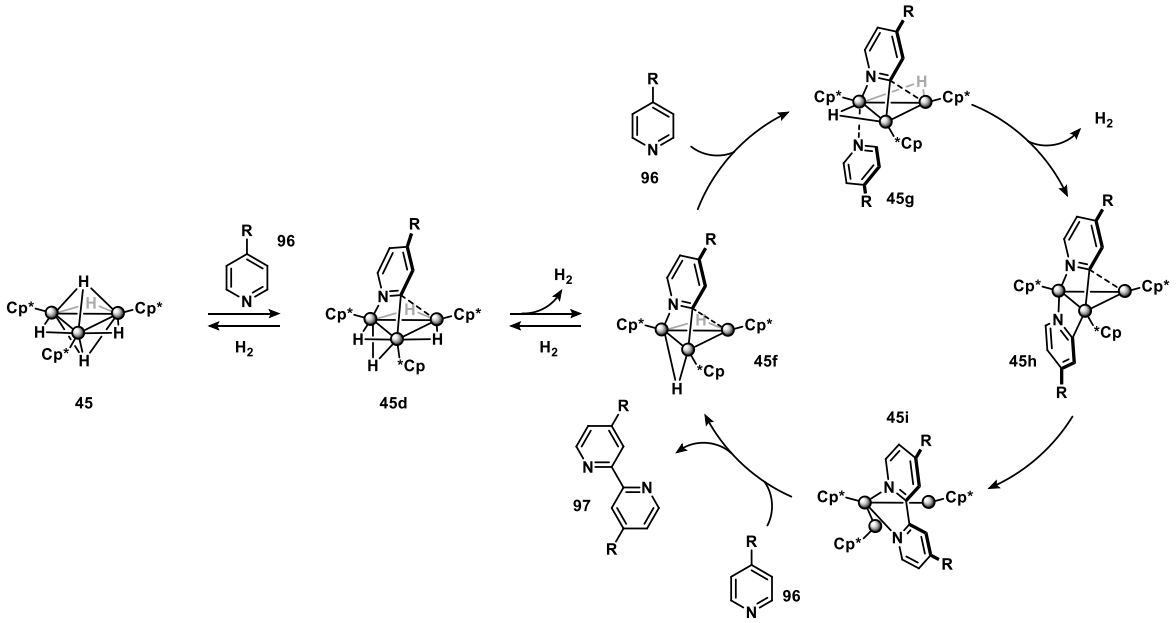

Scheme 27. Tentative mechanism involved in dehydrogenative coupling of **96** leading to **97** using **45** as catalyst precursor, as proposed by Suzuki, [136].

Hydration

Subsequent studies disclosed insights into the nature of the cooperative catalytic interactions by employing cluster **94** in the hydration of nitriles **47** to amides (either **47c** or **47d**), **Scheme 28** [8]. By comparing the binding differences between benzonitrile **47a** and methacrylonitrile **47b** to **94**, and based on a Hill coefficient of approximately three, it was found that likely only **47a** demonstrated multiple binding interactions. Thus, three sites are able to bind **47a**, whereas **47b** was found to have a lower binding affinity. Consequently, **94** does only demonstrate cooperativity when reacting with **47a**. Single-crystal X-ray structure of a tetraruthenium-MeCN adduct **94a** revealed insight into the nature of the cluster, which upon MeCN coordination undergoes transformation of three structural features: (*i*) μ_3-OH to μ-OH, (*ii*) rearrangement of hydrides from terminal to bridging, and (*iii*) increased bond length between the ruthenium centers opposite to the nitrile. Moreover, the same adduct was found to provide four times the catalytic activity compared to **94**. From kinetic studies, it was demonstrated that only electron-poor arenes undergo cooperative transformation to a significant extent. This observation is suggested by the authors to relate to Ru-Ru bond rupture leading to cluster fragmentation from electron-rich arenes. Furthermore, DOSY NMR studies demonstrated that the active species is mononuclear under transformations of electron-rich arenes, corroborating the postulate. Finally, a Hg(0) poisoning test concluded homogenous phase catalysis.

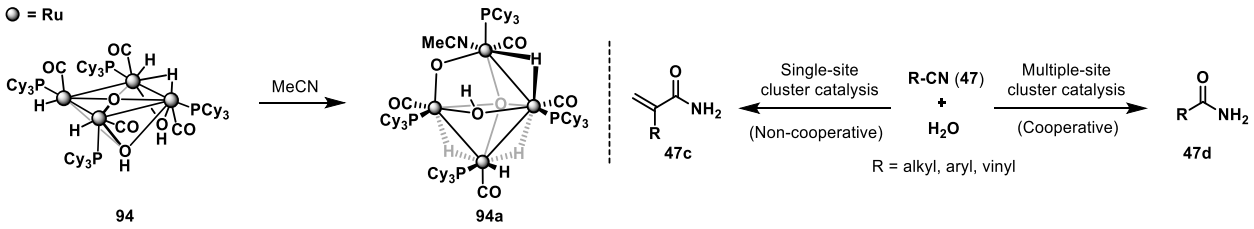

Scheme 28. MeCN adduct of tetraruthenium cluster (**94**) demonstrating retention of nuclearity. Electronic properties of the nitrile affects the interaction with the cluster, electron-poor resulting in multiple-site catalysis, [8].

Cycloaddition

Kleij investigated the octanuclear zinc clusters **100**, resulting from a conglomeration of four symmetrical Zn_2-Schiff-bases, as potential catalyst precursors for the cycloaddition of CO_2 to oxiranes **98** leading to carbonates **99**, **Scheme 29** [137]. Single-crystal X-ray diffraction demonstrated two distinct zinc sites, of which the coordination environment and geometry of the "inner" site, was argued to be a consequence of the nature of the "outer" site. Moreover, the former has a single water molecule associated, whereas the latter is exclusively coordinated by the phenoxo ligands. Spectroscopic and chromatographic analyses established an intact spherical cluster-entity. In methylethylketone, after 68h of reaction time, 0.63 mol% of **100** afforded 87% yield of **99**, **Scheme 29**.

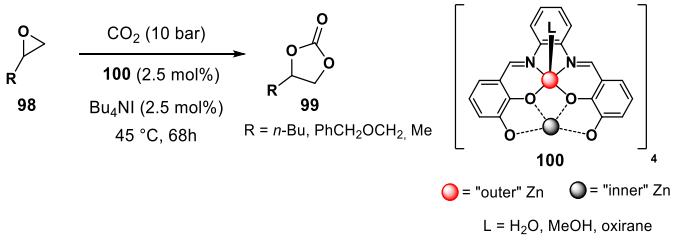

Scheme 29. Using an octazinc cluster **100** for the cycloaddition of CO_2 to oxiranes **99**, [137].

A later study by Kleij assessed the catalytic activity of **100** by introducing functional groups varying in electronic properties, as well as using asymmetric Schiff bases as building blocks, **Table 18** [138]. Higher TON values were observed when employing electron-donating groups, which was accounted for in terms of a lower Lewis acidity of the zinc metals. On the contrary, employing electron-poor ligand backbone substituents resulted in a facile ligand dissociation and thus lower substrate turnover. Comparing the turnover number reveal a difference by a factor of approximately 1.5 between the methoxy and nitro-substituted cluster, at 417 vs 271, respectively. Notably, mononuclear Zn-salen complexes showed similar activities as **100** did.

Table 18. Cycloaddition of **98a** with CO_2 leading to **99a** using **100** as catalyst, [138].

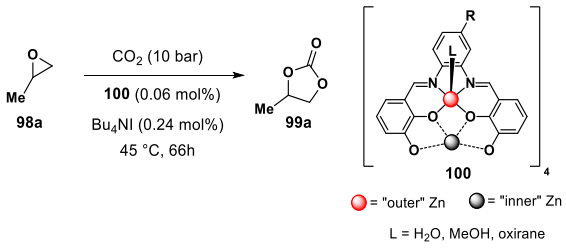

R	Yield [%]	Selectivity [%]	TON
H	61	>99	254
OMe	100	>99	417
NO_2	65	>99	271

Using iodide as additive, Chang reported reaction conditions that selectively afford either 5-*exo*-, or 6-*endo*-cyclization of formamides **101** using catalytic amounts of $Ru_3(CO)_{12}$, **Scheme 30** [139]. Based on their prior results combined with those of Geoffroy and Dombek [41], the authors suggest the halide bridged triruthenium species **102**, $[Ru_3(CO)_{10}(\mu\text{-I})]^-$, as the catalytically active species for producing the 5-*exo*-cyclization **101b**. The lack of either product using other catalyst precursors, such as $Os_3(CO)_{12}$, and $Ru(PPh_3)_4H_2$, combined with their prior findings, supports cluster mediated catalysis.

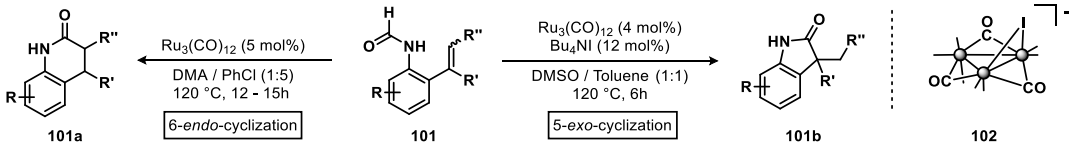

Scheme 30. Regioselective cyclocarbonylation of **101** to yield either **101a** or **101b**. Terminally bound CO ligands have been omitted for clarity, [139].

Exploring the chemistry of alkyne ligands for polynuclear architectures, Wangelin prepared the first examples of a heteroleptic alkynyl-Mn cubane structure **103**, shown in **Scheme 31** [140]. Based on their previous studies on $Fe(N(SiMe_3)_2)$ complexes in cyclotrimerization of phenylacetylene **104a** to provide either **105a** or **105b**, cluster **103** was employed as catalyst. Both the cluster and the parent compound, $Mn(hmds)_2$ was found to be moderately active in the same reaction. While $Mn(hmds)_2$ achieved 37% yield with a distribution of **105a**/**105b** of 1.5:1, cluster **103** afforded 41% yield with the same product distribution.

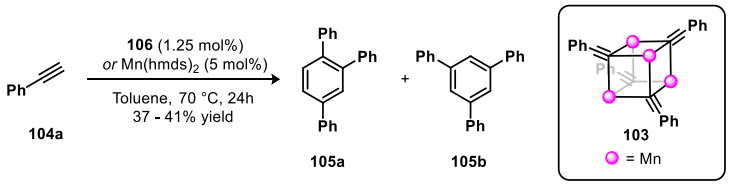

Scheme 31. Cyclotrimerization of **104a** to either **105a** or **105b** using cubane Mn_4-Alkynyl cluster **103** as catalyst. Hmds ligands have been omitted for clarity, [140].

Further catalytic studies on **103** found that the cluster is active in the hydrogenation of alkenes, such as α-methylstyrene **1b**. Using 1.3 mol% cluster in toluene at 70 °C under 5 bars pressure of H_2 for 20 hours resulted in full hydrogenation. Interestingly, a significant difference between **103** and $Mn(hmds)_2$ in the hydrogenation of **11a** was observed. Whereas $Mn(hmds)_2$ afforded full conversion, **103** afforded merely 30%.

3 HETERONUCLEAR CLUSTERS IN CATALYSIS

3.1 Hydrogenation

For the selective hydrogenation of COD (**20**), low valent heterometallic clusters were studied by Pittman and Braunstein, **Table 19** [141]. All of the clusters **106** were moderately active as hydrogenation catalysts, however considerable amount of isomerization products were observed as well. To assess whether the ligand (PEt_3 *vs*. PPh_3) or the combination of metals was more influential on the activity, the clusters' activities were compared at 100 °C. Of the group six metals, the Mo-PEt_3 clusters favored monohydrogenation over the PPh_3 congeners. While the choice of group ten metal had a much less pronounce effect, the Pd-PEt_3 clusters were in general more active. As such, the nature of phosphine ligand significantly affected the activity. At 100 °C and under approximately 14 bar of H_2 in THF with a 0.12 mol% catalyst loading, approximately 70% selectivity of the mono hydrogenated product was achieved using the $(\eta^5\text{-Cp})_2Pd_2(\mu_3\text{-CO})_2(\mu\text{-CO})_4Mo_2(PEt_3)_2$ cluster.

Table 19. Planar triangulated low valent heterometallic cluster used as selective hydrogenation catalyst of **20** using **106** as catalyst (precursor), [141].

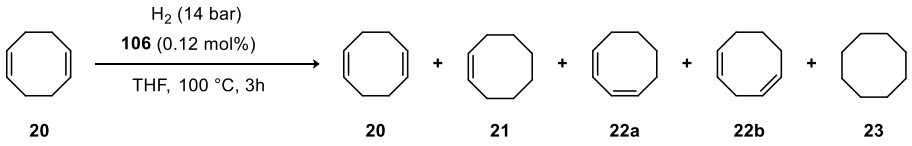

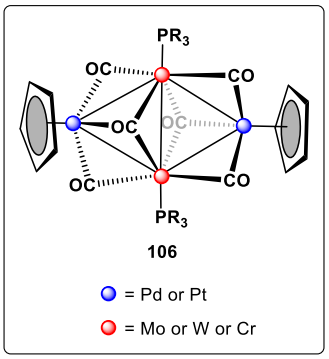

M	M'	R	Selectivity [%]				
			21	**22**	**23a**	**23b**	**24**
Pd	W	Et	7.0	24.5	61.3	7.2	trace
		Ph	7.7	4.4	79.0	7.9	1.0
Pd	Mo	Et	2.6	70.4	23.7	3.0	0.4
		Ph	12.9	22.2	51.1	13.0	0.7
Pt	W	Et	-	18.7	77.7	trace	3.6
		Ph	-	0.6	95.6	trace	3.8
Pt	Mo	Et	trace	61.1	32.1	-	6.8
		Ph	0.3	19.3	79.5	trace	0.9
Pd	Cr	Et	-	15.7	83.8	trace	0.5

Cluster mediated hydrogenation and isomerization of diolefins **107** were established by Sappa and Tiripicchio, using tetrahedral heterometallic clusters **108** comprising a triangular array of the group eight metals capped by a Ni-Cp unit, **Table 20** [142, 143]. From the well-defined tetrahedral bimetallic osmium cluster, $CpNiOs_3(\mu\text{-H})_3(CO)_9$ **108*Osa***, the authors hypothesise a similar structure of the ruthenium congener, $CpNiRu_3(\mu\text{-H})_3(CO)_9$ **108*Rua***. While both **108*Osa*** and **108*Rua*** were found catalytically active, spectroscopic analysis established a poor stability of **108*Rua***, as decomposition was observed within 40 minutes. Fragmentation is further supported by comparing the amount of **1c** found using **108*Osa*** and **108*Rua***. While **108*Osa*** provide up to 22% after 240 minutes, only 2% is found for the **108*Rua*** within the first 30 minutes. The authors suggests the role of the capping group to provide a "trans-effect" that promotes the dissociation of CO, as isomerization predominantly was observed as it was lost. Comparing the reactivity of $HRu_3(CO)_7(\mu\text{-}PPh_3)_3$ to $(Cp)NiRu_3(\mu\text{-H})_3(CO)_7(PPh_3)_2$ **108*Rud*** a similar selectivity for isomerization is seen.

Further insights were disclosed on changes in catalytic activity induced by various phosphine ligands, by substituting the tetrahedral bimetallic **108*Ru*** and **108*Os*** clusters [144]. The ruthenium clusters were again observed to decompose within the first 40 minutes. While monosubstituted PPh_3 clusters, $(Cp)NiRu_3(\mu\text{-}H)_3(CO)_8(PPh_3)$ **108*Rub***, were less active than **108*Rua***, the doubly substituted clusters, such as **108*Rud***, clusters generally demonstrate a higher turnover than the respective parent clusters. This observation led the authors to conclude that isomerization precedes hydrogenation. The lack of recovered degradation $Ru_3(CO)_{12-n}L_n$ products from the reaction mixture supports catalysis by an intact $[Ru_3]$-cluster framework. Moreover, the phosphine is suggested to lower hydride acidity rather than promoting the dissociation of CO ligands.

Table 20. Hydrogenation of pent-1,4-diene using Ni-Cp faced-capped clusters. Terminal CO molecules have been omitted for clarity, [142–144].

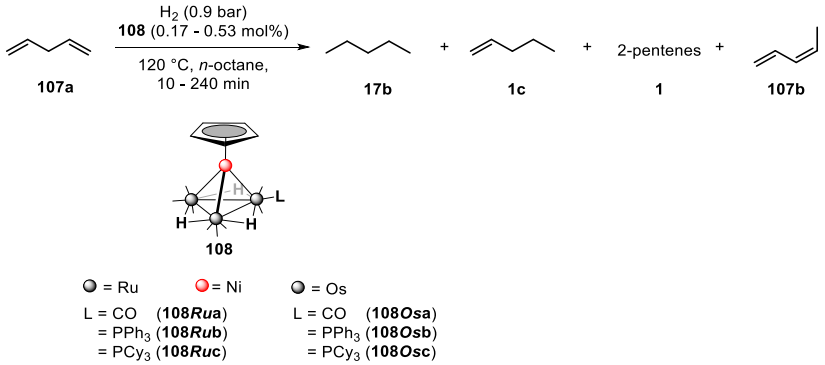

Cluster	Catalyst loading [mol%]	Time [min]	Composition [%] Unreacted	**17b**	**1c**	**1**	**107b**	TON
$HRu_3(CO)_7(\mu\text{-}PPh_3)_3$	0.20	10	93	-	3	-	4	39
		20	82	trace	4	-	15	95
		40	53	1	14	-	32	240
108*Rua*	0.37	10	98	-	0	-	2	12
		20	95	1	1	-	3	27
		30	91	1	2	-	5	42
108*Rub*	0.22	10	100	-	trace	-	-	1
		20	98	-	trace	-	2	9
		30	91	-	2	-	6	39
		40	90	-	4	-	8	54
108*Rud*	0.18	10	91	trace	1	-	8	52
		20	62	0	4	-	35	215
		30	40	0	6	-	54	337
		40	36	0	8	-	55	356
108*Ruc*	0.28	10	64	0	3	-	32	130
		20	54	0	9	-	37	167
		40	49	0	11	-	40	184
108*Osa*	0.53	60	79	0	6	15	-	79
		120	68	5	21	7	-	68
		240	71	3	22	3	-	71
108*Osb*	0.17	60	94	trace	1	-	6	36
		120	92	trace	1	-	7	45
		240	87	1	5	-	7	74
108*Osb*	0.17	60	94	0	1	-	5	33
		120	86	1	2	-	11	79
		240	68	2	4	-	26	186

Concluding their studies on hydrogenation and isomerization of (cyclic) dienes, the combined findings are summarized by the authors who suggest a catalytic cycle shown in **Scheme 32**. Either [$NiRu_3$] or [$NiOs_3$] act in the cycle that initially work by ligand substitution of a terminally bound ligand **L** from **108** with **107c** leading to **108d**. Substitution is followed by either of two pathways. Loss of the CpNi unit results in cluster degradation forming **108e** and cluster-mediated isomerization products, whereas hydride insertion results in a vacant site (**108f**), which permit for oxidation addition of H_2, followed by reductive elimination. This step generates product **1** and cluster **108g**, which undergoes ligand association by either **L** or **107c**, thus closing the cycle.

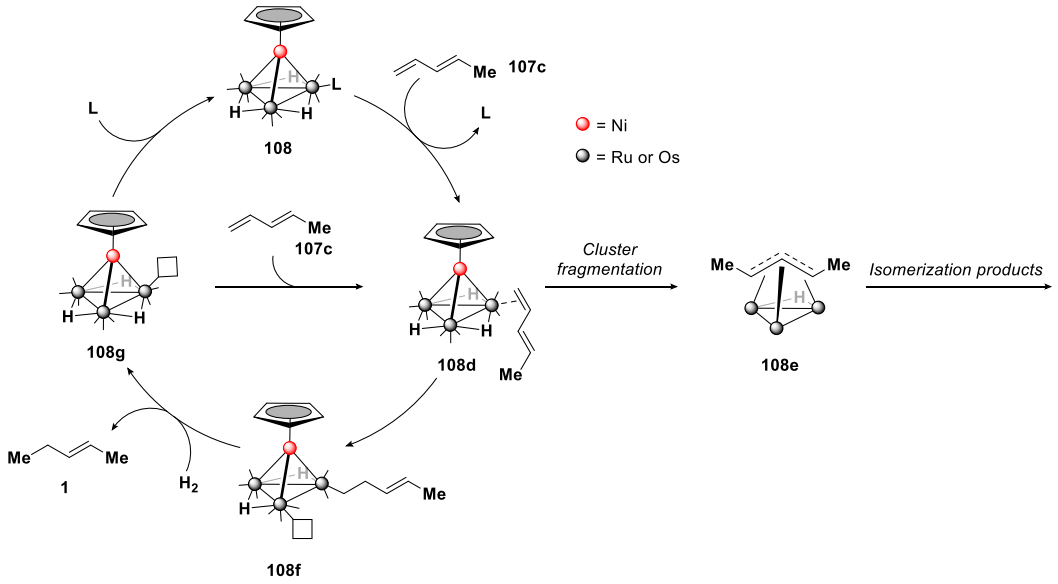

Scheme 32. Catalytic scheme for the selective hydrogenation of **107** in presence of **108** as proposed by Sappa and Tiripicchio. Fragmentation of the cluster results in isomerization products. Terminal CO molecules have been omitted for clarity, [142–144].

Hydrogenation of **103a** was demonstrated by Pittman and Braunstein by employing the same triangulated planar clusters **106** as in **Table 19** to selectively afford partial hydrogenation of **103a** to styrene **1d** [141]. Of the various combinations, the use of $(\eta^5\text{-Cp})_2Pt_2(\mu_3\text{-CO})_2(\mu\text{-CO})_4Mo_2(PEt_3)_2$ achieved 99% selectivity at 60 °C under approximately 14 bar of H_2. Hydrogenation of *n*-hexyne **103b** demonstrated that terminal alkyl alkynes readily hydrogenated to the corresponding alkene as well.

A mixed-metal Ru-Pt cluster **109**, $Pt_3Ru_6(CO)_{20}(\mu_3\text{-}PhC_2Ph)(\mu_3\text{-H})(\mu\text{-H})$, was prepared by Adams as a catalyst precursor for the selective partial hydrogenation of **11a** [145]. To assess ligand exchange, and to provide evidence in support of cluster catalysis, **109** as well as the ditolylacetylene homologue **110**, $Pt_3Ru_6(CO)_{20}(\mu_3\text{-}TolC_2Tol)(\mu_3\text{-H})(\mu\text{-H})$, were used in labelling studies, that demonstrated incorporation of reagents [146]. Additionally, kinetic studies revealed first order rate-dependence with respect to cluster concentration, whereas CO had an inverse first order dependence. Further kinetic studies of appropriate (fragmentation) species afforded TOF values of insufficient magnitude (up to 3 h^{-1} *vs* up to 82.4 h^{-1} for **109**). Thus, the empirically derived activation parameters suggest cluster catalysis. Similar results with respect to rate order dependency, as well as labelling studies, were observed when using **109** as catalyst precursor for the hydrosilylation of **11a** [147].

To ascertain the active site for the transformation, and to account for the interplay between Ru-Pt, a homologue of **109** containing the labile ligand Me_2S was used for the partial hydrogenation of **11a** [148]. The initial reaction rate (20 min) was three times as large using this homologue, which the authors argue is a result of more facile ligand dissociation. In spite of the high catalytic activity, the cluster interconverts back to **109** under the reaction conditions, which precluded a detailed kinetic account. The authors conclude that the transformation of both H_2 and **11a** necessarily must take place at the Ru_3-triangle, with a tentative explanation that the Ru-Pt interaction originates in an electron donation from the latter transition metal. Thus, a catalytic transformation of **11a** is proposed to follow the

mechanism shown in **Scheme 33**. The initial step proceeds *via* ligand (CO) dissociation resulting in an electronically unsaturated species with a vacant coordination site (**109a**), which then undergoes oxidative addition of H_2 to provide **109b**. A μ_3-bridging H is argued based on structures of related fragments, and the subsequent interaction to **11a** at the free ruthenium triangle promotes the formation of a C-H bond from the hydride and the originally coordinated alkyne. The resulting vinyl ligand, with *cis*-positioned phenyl groups, then becomes triply coordinated to the cluster (**109c**), that further promote a hydride transfer to form the ***cis*-12a**. Moreover, steric encumbering was found to favor product dissociation. The authors note that at a high substrate loading and after several catalytic cycles, fragmentation and alkene adducts play a significant role in the loss of catalytic activity.

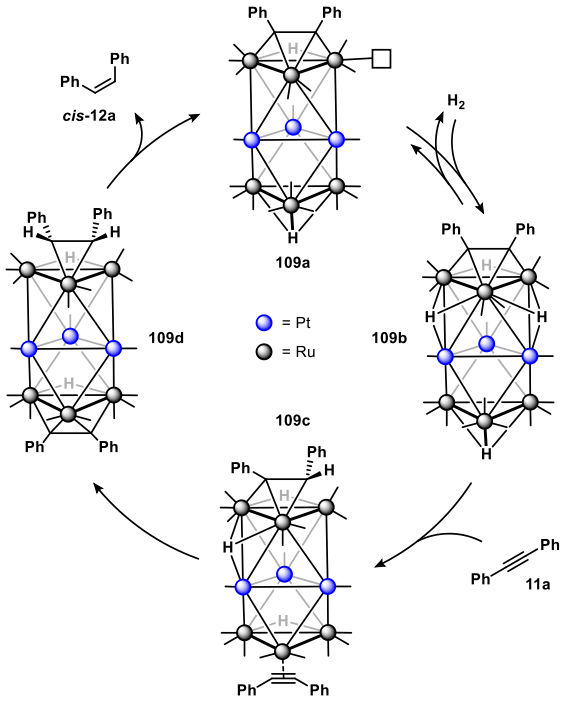

Scheme 33. Catalytic scheme for hydrogenation of **11a** by a formation of a vacant coordination site, followed by formation of two triply bridging hydrides as proposed by Adams. Coordination of **11a** to the unencumbered ruthenium triangle promotes insertion of one hydride to the originally coordinated alkyne. Terminal CO molecules have been omitted for clarity, [148].

Further insight on the Ru-Pt interaction was provided using the mixed-metal hexanuclear cluster **111**, $Ru_5(CO)_{14}(\mu\text{-H})_2(\mu_6\text{-C})[Pt(P^tBu_3)]$, demonstrating that the Pt was involved in activation of hydrogen and **103a** [14]. The hexanuclear $[Ru_5Pt]$ was found in an equilibrium with the open structure **111a**, **Scheme 34**. Treatment of **111** with **103a** at 40 °C resulted in a platinum-capped square-pyramidal pentaruthenium cluster, with the alkyne bridging a $PtRu_2$ triangle **111b**. Subsequent treatment with H_2 at elevated temperature (80 °C) regenerated **111** along with the production of **1d**. Overall, the TOF was 20 h^{-1}.

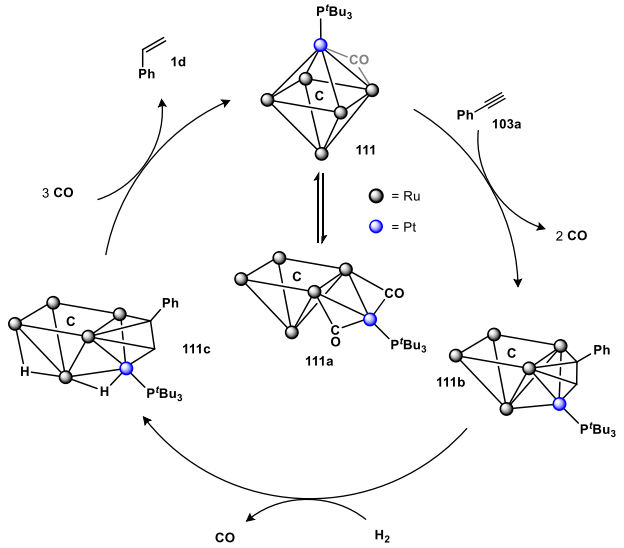

Scheme 34. Probing the role Pt plays in transformation of alkynes in the related layer segregated Ru-Pt cluster, Adams prepared a hexanuclear Ru-Pt compound, in which Pt is connected to substrate activation rather than an extended ligand. Terminal CO molecules have been omitted for clarity, [14].

3.2 Carbonylation

Echavarren studied a series of polynuclear gold clusters, of which the pentabimetallic $Au_4^IAg^I$ cluster **112** was found to catalyze carbonylation of various primary amines **42** to ureas **113** with up to 99% yield [149]. In support of cluster catalysis, **112** was recovered and reused, which afforded a yield of 73%. In addition, the lack of an induction period suggests that catalysis is taking place in the homogeneous phase. Conducting a Hg(0) poisoning test was precluded as the mercury reacted with **112**. From the optimized reaction conditions, a broad scope of **42**, including sterically demanding examples, were carbonylated to the corresponding urea compounds **113**, **Table 21**.

Table 21. Catalytic carbonylation of primary amines using $Au_4^IAg^I$ cluster, [149].

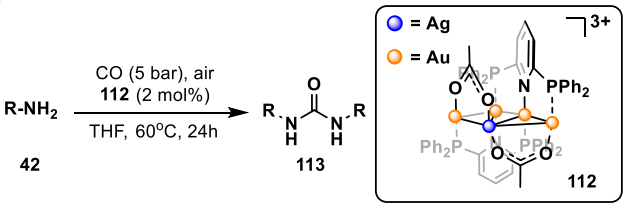

42	113	Yield [%]
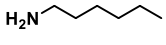 **42h**	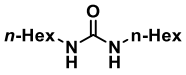	93
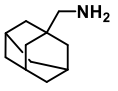 **42i**	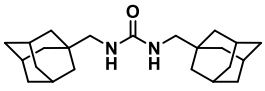	88
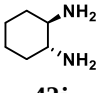 **42j**	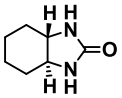	92
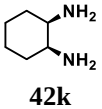 **42k**	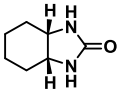	89

Hydroformylation

Pittmann and Braunstein found that two different clusters containing Co and Pt, a triangular (**114**) and a butterfly cluster (**115**), respectively, **Table 22**, was active in hydroformylation of *n*-pentene (**1c**) to mixture of ***n*-57b** and ***iso*-57b** [141]. The chemical nature of the coordinating atoms in the chelating ligand was found to significantly influence the activity of **114**. Comparing the reactivities between complexes of dppe, $Ph_2P(CH_2)_2PPh_2$ (**114*P***), and dpae, $Ph_2As(CH_2)_2AsPh_2$ (**114*As***), ligated clusters respectively, showed that whereas **114*As*** was inactive, **114*P*** afforded a yield of approximately 39% at 80 °C (*n*/*iso* = 3.7:1). The authors suggest the reactivity difference to origin from retention of cluster integrity, of which only dppe aids towards this, based on the amount of recovered compound. Using 0.11 mol% catalyst loading of **115** provided 85% conversion with a predominantly linear selectivity (*n*/*iso* = 4:1) at 100 °C.

Table 22. Triangular (**114**) and butterfly (**115**) PtCo mixed-metal complexes as catalysts for the hydroformylation of **1c** to mixtures of ***n*-57b** and ***iso*-57b**. Terminal CO molecules have been omitted for clarity, [141].

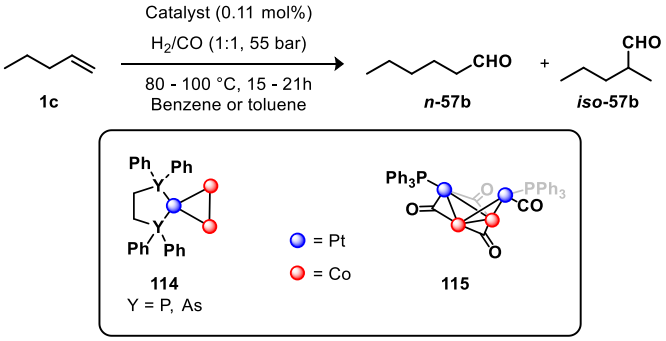

Catalyst	Temperature [°C]	Time [h]	Conversion [%]	Yield [%] ***n*-57b**	***iso*-57b**
114P	80	21	39	3.7	8.2
114As	80	22	0	-	
115	62	17	trace	trace	trace
	75	18	16.5	14	2.5
	100	17	85.4	63.5 (+7.3% 1-hexanol)	14.6

To investigate the postulate that polydentate μ_3-ligands suppress cluster fragmentation, whilst accommodating M-M bond rupture to facilitate (catalytic) transformations, a series of face-capped triangular mixed-metal clusters **116**-**121**, **Table 23**, were prepared by Pittman for the catalytic hydroformylation of **1c** to mixtures of ***n*-57b** and ***iso*-57b** [150]. Under the conditions for transformation of **1c**, isomerization competition was observed. Most notably for the clusters **116**, **119**, and **121**. While cluster **116** initially (7h) catalyze the hydroformylation of **1c**, extending the reaction time (24h) significantly lowers the selectivity, due to hydroformylation of the 2-pentenes (**1**). Fragmentation was suspected for **121** and, as such, its activity was compared to that of $Co_2(CO)_{10}$. Interestingly, they showed nearly identical activities, thereby indeed indicating a fragmentation of **121** to a lower nuclearity complex. Moreover, the authors conclude cluster mediated catalysis for clusters **116** through **120** based on a lack of evidence supporting the presence of lower nuclearity species, as well as the amount of recovered cluster (> 90% yield). Finally, the transformation is suggested to proceed *via* a metal-metal bond cleavage, and the μ_3-ligand likely works to retain cluster integrity throughout the catalytic cycle.

Table 23. Tetrahedral clusters with μ_3-briding ligands **116**-**121**, investigated by Pittman as catalyst (precursors) for the hydroformylation of **1c** to mixtures of ***n*-57b** and ***iso*-57b**. Terminal CO molecules have been omitted for clarity, [150].

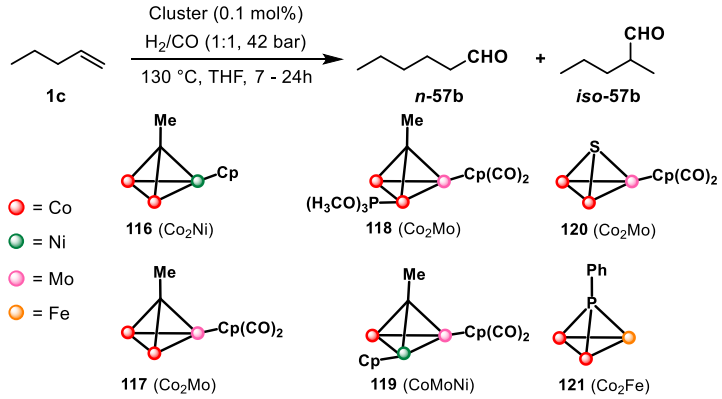

Catalyst	Time [h]	Alcohols [%]	**57b** [%]	Selectivity (*n*/*iso*)
116	7		21	2.6
	24	11	88	0.6
117	24		14	2.4
118	24		26	2.9
119	24		8	3.2
120	24		2	only ***n*-57b**
121	24	1.2	90	1.4
$Co_2(CO)_8$	24	1.0	92	1.5

Gervais and Kalck observed that the heterometallic d^0-d^8 [$ZrRh_2$] cluster **122** $(\eta^5\text{-Cp})_2Zr(CH_2PPh_2)_2Rh_2(\mu\text{-}S^tBu)_2(CO)_2$ afforded catalytic hydroformylation of **1a**, under mild reaction conditions [151, 152]. Approximately 90% conversion to mixtures of of ***n*-57c** and ***iso*-57d** was achieved at 80 °C at a pressure of approximately 5 bars of H_2/CO (1:1), with predominantly linear selectivity (*n*/*iso* = 2:1), **Table 24**. The authors speculate that the role of Zr is to act as an electron reservoir. Choukroun provided further insight on the role of Zr by introducing sterically encumbered zirconocene substituents at the cyclopentadienyl group [153, 154]. Single-crystal X-ray diffraction of the ^{t}Bu homologue of **122** revealed a disruption of the Zr-S interactions, consequently changing the coordination environment of Zr from a pentacoordinate to that of pseudo-tetrahedron. However, the role of Zr is in large suggested to ensure that the Rh-centres remain vicinal thereby warranting a cooperativity between the two Rh-centers.

Table 24. Hydroformylation of **1a** to mixtures of ***n*-57c** and ***iso*-57d** using the trinuclear bimetallic cluster **122** as catalyst (precursor), [153, 154].

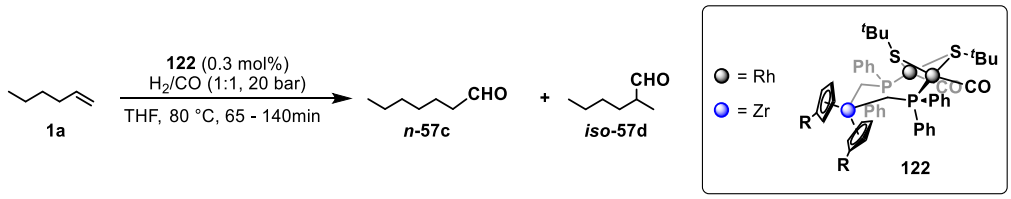

R	Time [min]	Conversion [%]	Selectivity (*n*/*iso*)
H	65	56	2.1
	115	96	2.0
^{t}Bu	70	38	2.2
	140	97	1.8

Similarly, Ciriano, Oro and Claver provided insight on cluster compounds **123** comprising the early transition metal titanium and late transition metal rhodium, [$TiRh_3$], in the hydroformylation of **1a** and **1d** [155]. Probing **123** with monodentate phosphine and phosphites, the authors were able to ascertain the active catalyst to exist in an equilibrium between a bis- (**123a**) and a tris ligated (**123b** and **123c**) compound type, as shown in **Scheme 35**. A previous study by Ciriano and Oro on the iridium homologue further corroborated this equilibrium [156]. Thus, using 0.5 mol% of precatalyst **123** at 80 °C under approximately 5 bar of H_2/CO (1:1) in toluene with PPh_3 in a P/Rh ratio of four, **1a** was converted in 96% to **57c** with a predominantly linear selectivity of 78%. On the contrary, 88% conversion of **1d** to **57d** was achieved, at a slightly higher pressure of approximately 30 bar in THF, with an interestingly *iso*-selectivity of 89%.

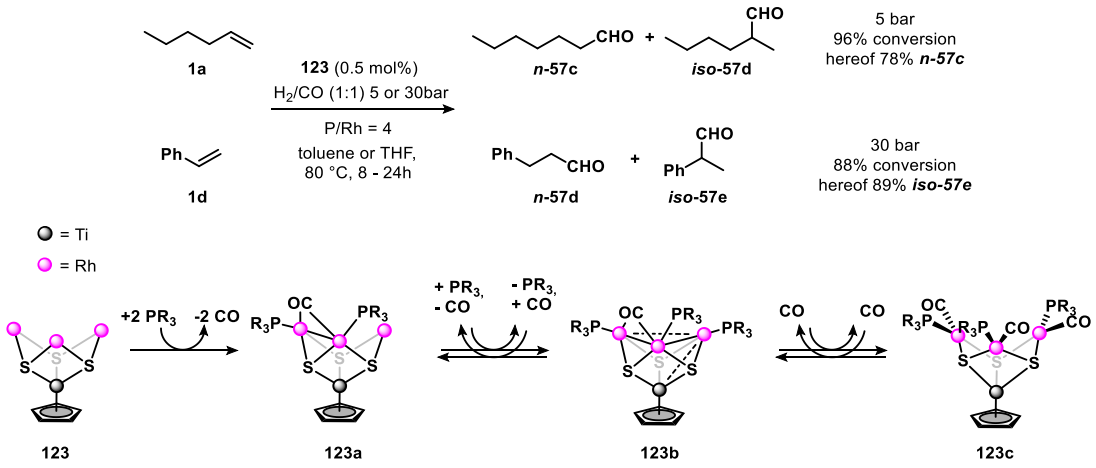

Scheme 35. Hydroformylation of **1a** to mixtures of ***n*-57c** and ***iso*-57d** as well as of **1d** to mixtures of ***n*-57d** and ***iso*-57e** using **123** as catalyst precursor. Terminal CO molecules have been omitted for clarity, [156].

Haupt investigated the synergism between Rh and Mn as well as between Rh and Re, [$M_2Rh(\mu\text{-}PCy_2)\text{-}(\mu\text{-}CO)_2(CO)_8$, M = Re (**124*Re***), Mn (**124*Mn***)], **Table 25**, for the hydroformylation of **1a** [157]. The Rh-Mn cluster **124*Mn*** was found to catalyze isomerization to **1e** and **1f** with predominantly *trans*-selectivity with TOF values of up to 473 h^{-1}.

On the contrary, the Rh-Re complex **124*Re*** achieved hydroformylation to **57c** with TOF values of up to 246 h^{-1} with predominantly linear selectivity (*n*/*iso* = 3.4).

Table 25. Triangular mixed-metal RhM_2, M = Mn (**124*Mn***) and Re (**124*Re***) as catalysts for the hydroformylation of **1a** to mixtures of ***n*-57c**, ***iso*-57d**, **1e**, and **1f**. Terminal CO molecules have been omitted for clarity, [157].

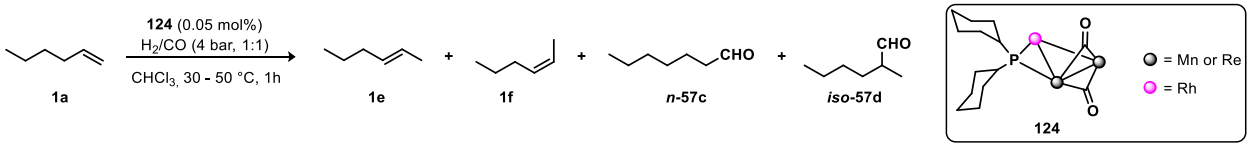

124	Temperature [^{0}C]	**1f** TOF [h^{-1}]	**1e** TOF [h^{-1}]	***n*-57c** TOF [h^{-1}]	***iso*-57d** TOF [h^{-1}]
124*Re*	30	5	20	58	26
	50	79	162	190	56
124*Mn*	30	104	152	12	4
	50	187	286	43	12

3.3 Miscellaneous

Hydrosilylation

As previously discussed by Pittman, the use of non-fluxional ligands in metal-carbonyl clusters, such as the face capping μ_3-ligands used in **Table 23**, serve to inhibit cluster fragmentation under thermal catalysis. Pittman and Vahrenkamp present evidence to support this proposal by using such μ_3-ligated clusters as catalyst precursors in the photoinitiated reaction between Et_3SiH and acetophenone (**35a**) leading to either hydrosilylation (**125**) or Mukaiyama silyl enol ether formation (**126**) [158]. In the absence of both **121** and irradiation (λ = 254 or 355 nm) no reaction was observed, and the amount of recovered **121** after photolysis was up to 98%. A higher quantum yield was observed using irradiation at 254 nm, which is discussed in relation to a possible mechanism invoking loss of a CO ligand. Whereas high-energy irradiation results in a metal-ligand charge transfer that consequently destabilizes the M-CO bonds, low energy light merely results in M-M bond cleavage that readily reform, **Scheme 36**.

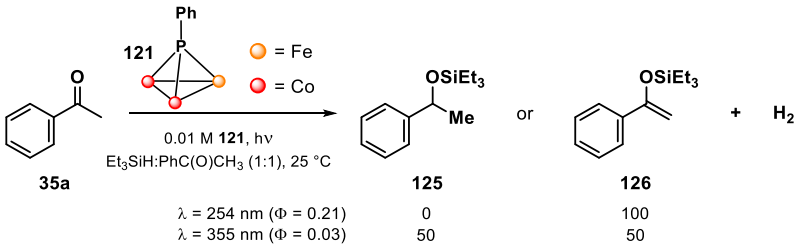

Scheme 36. Photoinitiated catalytic (dehydrogenative) silylation of **35a** leading to **125** or **126** using **121** as catalyst. Terminal CO molecules have been omitted for clarity, [158].

Dehydrogenation reactions

Shapley investigated the activity of a trinuclear bimetallic cluster **127** complex comprising Ru and the group ten metals, (dppe)M(μ_3-S)$_2${Ru(N)Me_2}$_2$, M = Ni (**127*Ni***), Pd (**127*Pd***), and Pt (**127*Pt***), for the dehydrogenation of **65f** to **44**, **Table 26** [19]. A bond length variance of approximately 0.2 Å between Ni and Ru centers was observed in **127*Ni***, of which the shorter distance (2.9 Å) was suggested by the authors to stem from a two-electron interaction from Ru to Ni. This is rationalized based on the relative small HOMO-LUMO gap between Ni and Ru. On the contrary, the Pt-Ru bonds were both found to be equidistant (3.16 Å) in **127*Pt*** [159]. Comparing the activity of **127*Pt*** cluster at 18.8 and 44 bars pressures of O_2, respectively, the authors established that an increase in O_2 pressure does not increase the oxidation rate. This observation is suggested to be due to that O_2 and **65f** likely compete between the same binding sites at the cluster. Additionally, an increase in the concentration of O_2 lowers the CO_2 and thus the cluster solubility.

While **127*Ni*** demonstrates a direct metal-metal interaction, its effect on catalytic activity is not addressed. The conversion difference of approximately 20% (in toluene) is also not addressed in detail, [19].

Table 26. Catalytic dehydrogenation of **65f** leading to **44** employing hetero-trinuclear cluster **127** as catalyst. $scCO_2$ denote supercritical CO_2 [19].

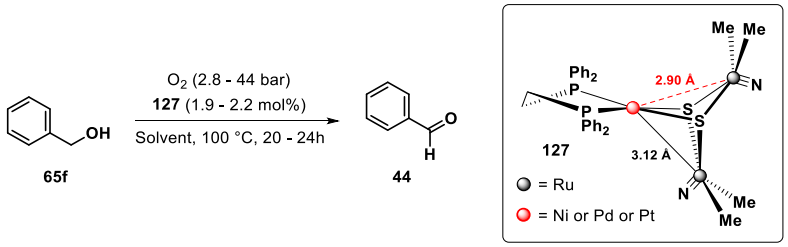

127	Solvent	Pressure O_2 (total pressure) [bar]	Time [h]	Conversion [%]	TON	TOF [h^{-1}]
127*Ni*	Toluene	2.8 (2.8)	24	53	18.5	0.8
127*Pd*				32	3.63	0.2
127*Pt*				35	7.06	0.3
127*Ni*	$scCO_2$	10 (120)	20	19	9.57	0.5
127*Pt*				11	5.97	0.3
127*Pt*		18.8 (120)	20	32	15.99	0.8
127*Pt*		44 (129)	20	22	10.70	0.5

Takao studied the homologue series of triangular trimetallic clusters comprising the group nine metals and Ru, $Ru_2M(\mu\text{-}H)_3(\mu_3\text{-}H)(\eta^5\text{-}Cp)_3$, M = Co (**128*Co***), Rh (**128*Rh***) and Ir (**128*Ir***), for the dehydrogenative coupling of 4-substituted pyridines **96** to bipyridines **97**, **Table 27** [160]. Compared to the all ruthenium cluster **45**, a significant increase in TOF (3h) (from 0.1 h^{-1} to 0.3 h^{-1}) was achieved by substituting one Ru-atom for Co. Interestingly, poor to no reactivity was observed for **128*Rh*** and **128*Ir***, respectively.

Analysis of the intermediate **128*Co*a** was indicative of an electron transfer from the Co center to the ligand forming monoanioic $dmbpy^{\bullet-}$ species, which was supported by spin-density DFT calculation demonstrating a negative value residing at the ligand, and positive values at the Co-center. As such, the Co is suggested to be in oxidation state 2+, adopting a d^7 electron configuration. Evan's method was used to determine a μ_{eff} (297.7K) of 2.5μ_B, consistent with a triplet state of **128*Co*a**. For unsubstituted bipyridines, the lower LUMO energy level hampers the electron-transfer. Treatment of **128*Co*a** with pyridine demonstrated a facile ligand dissociation of dmbpy, **Scheme 37**. Prior to dissociation of dmbpy, electron transfer from the $dmbpy^{\bullet-}$ species to the Co^{2+} is required.

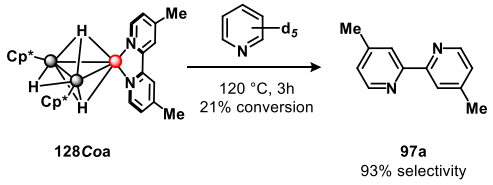

Scheme 37. Release of dmbpy ligand from **128*Co*a** by substitution with pyridine, [160].

Using a 5 mol% catalyst loading in heptane at 140 – 180 °C for 3 days afforded up to 87% yield. To support cluster catalysis, the authors monitored the reaction by ^1H NMR to analyze the reaction products. In addition, a key intermediate was structurally characterized using single-crystal X-ray diffraction, showing cobalt coordinated in a chelating-fashion by the bipyridine adduct. Moreover, **128*Co*** was completely converted at the end of the reaction, and

loss of catalytic activity stem from fragmentation to mononuclear species, which the authors found to be catalytically inert.

Table 27. Catalytic dehydrogenation of **96** to **97** using **128*Co*** as catalyst, [160].

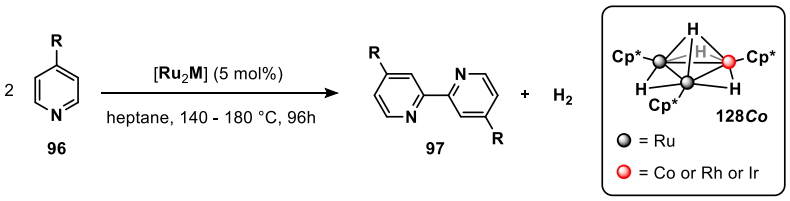

Ru_2M	R	Temperature [°C]	Yield [%]
Ir	Me	180	Trace
Rh	Me	180	16
Co	Me	180	87
	^{t}Bu	180	76
	NMe_2	140	58
	OMe	140	trace
	CO_2Et	140	0
	CF_3	180	0

Wong reported the pentanuclear bimetallic cluster $Os_4Au(\mu\text{-}H)_3(CO)_{12}(PPh_3)$, **129**, as catalyst towards oxidative carbonylation of aniline (**42a**) in methanol [161]. Catalytic formation of methyl phenylcarbamate **130** was effected using **129** with 93% conversion and an 82% selectivity, compared to approximately 40% selectivity demonstrated by the two tetraosmium clusters, $Os_4(\mu\text{-}H)_4(CO)_{12}$ and $[N(PPh_3)_2]Os_4(\mu\text{-}H)_3(CO)_{12}$, **Table 28**. Moreover, the two latter clusters formed the byproducts *N*-methylaniline **42h** and formaniline **67b** not observed for **129**. Lowering the concentrations of substrate and cluster in MeOH resulted in an increase of conversion at the expense of the selectivity towards **130**. The lack of byproducts formed by **129** lead the authors to suggest two different mechanisms for **129** relative to the tetraosmium clusters.

Table 28. Carbonylation of **42a** using pentanuclear bimetallic [Os_4Au] cluster **129** as catalyst. Terminal CO molecules have been omitted for clarity, [161].

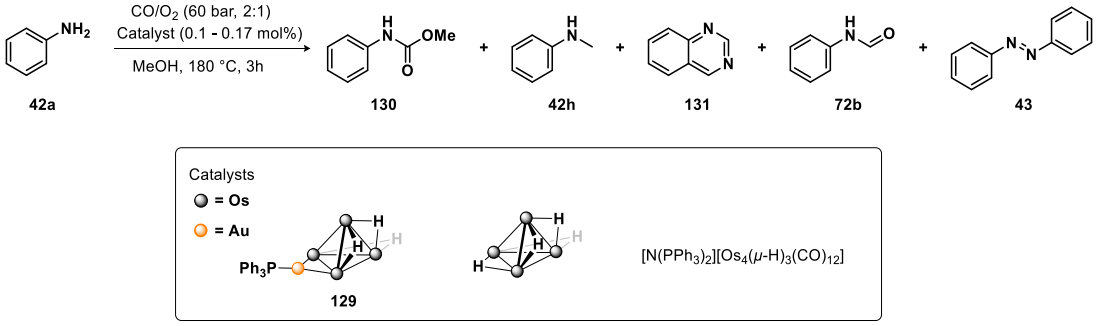

Cluster	Loading [mol%]	TOF [h^{-1}]	MeOH [mL]	Conversion [%]	Selectivity [%] **130**	**42h**	**131**	**72b**	**43**
129	0.13	248	3	93	82	-	10	-	-
	0.13	267	20	100	-	-	37	-	39
$Os_4(\mu\text{-}H)_4(CO)_{12}$	0.17	42	3	21	41	30	4	8	5
	0.17	126	20	63	-	12	-	-	28
	0.10	33	3	10	43	37	8	7	5

$[N(PPh_3)_2]Os_4(\mu\text{-}H)_3(CO)_{12}$	0.10	333	20	35	-	22	-	-	78

Addition reactions

Hidai has provided several accounts on the mixed-metal sulfide cubane-type cluster $[MMo_3S_4]$ as catalyst precursors for various transformation of alkynes (**104**, **132, 142, 144**), olefins (**1d, 157**), and hydrazines (**46**). For example, $[PdMo_3S_4(H_2O)_9Cl]Cl_3$ (**133**) and $[PdMo_3S_4(tacn)_3Cl]Cl_3$ (**134**), tacn = 1,4,7-triazacyclononane, cubane-type clusters were found to be highly regioselective towards *trans*-addition of alcohols to alkynoic acid esters **132** leading to **135**, **Table 29** [162]. Cluster catalysis is suggested based on the combined observations that spectroscopic analyses indicate a single organometallic species in the reaction mixture, and that neither of the parent compounds $[Mo_3S_4(H_2O)_9]Cl_4$ nor Pd-black provide sufficient catalytic activity.

Table 29. Proposed catalytic cycle for conversion of **132** to **135** using **134** as catalyst precursor, [162].

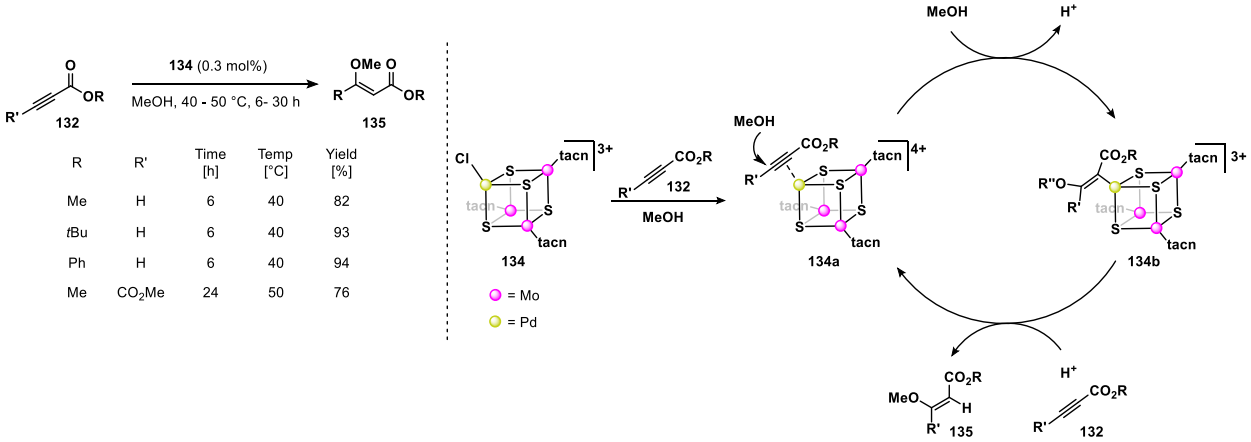

Cluster **134** was reported to catalyze the stereoselective addition of alkyl and aryl substituted hydrogen carbonates **137** to electron-deficient alkynes, such as **136a**, **Table 30** [163]. To support the suggestion of cluster catalysis, the reactivity of **134** was compared to that of **133**, as well as to those of other appropriate mononuclear Pd, Ru, and Rh complexes. Whereas **133** provided transformation at a much lower rate than **134** did, neither of the mononuclear complexes resulted in any detectable transformation, which satisfies Laine's second criterion on cluster-mediated catalysis. Additionally, spectroscopic analyses substantiate a single organometallic species in the reaction mixture. Moreover, **134** demonstrated a TON(18h) of 2500. The role of the cubane-type cluster is twofold and is suggested to (*i*) activate the acetylenic species, and (*ii*) suppress side reactions. The mechanism suggested by the authors follow analogously to that in **Table 29**.

Table 30. Stereoselective catalytic addition of carboxylic acids to electron deficient alkynes, [163].

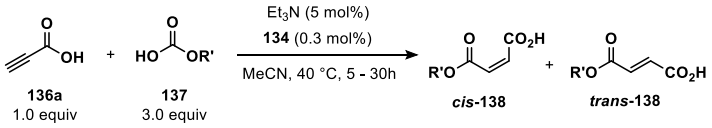

R'	Time [h]	Conversion [%]	Yield [%]	*cis*:*trans*
Me	8	90	62	98/2
Ph	5	92	76	98/2
m-ClC_6H_4	10	96	72	97/3

Regioselective addition of alcohols across triple bonds was catalyzed by the triangular mixed-metal sulfide cluster comprising Ir_2M, M = Pd (**139*Pd***), Pt (**139*Pt***), **Table 31** [164], where substituting Pd for Pt afforded a less selective

cluster. Cluster catalysis is suggested based on the combination of recovered cluster, and lack of selectivity when employing lower nuclearity catalysts. A later study by Hidai provided further insights to the transformation, where it was shown that the electronic properties of the arene in **104** affected the selectivity, as electron donating groups in the *p*-position was found to decrease the regioselectivity [165]. The combined findings are concluded in the presented cycle below. The authors suggest a catalytic cycle that is initiated by ligand substitution at the palladium center of chloride for the alkyne **104**, resulting in **139a**. Addition of the first equivalent of alcohol and protonolysis results in a alkoxyvinyl cluster **139b**, which further undergoes addition of alcohol to form **140**.

Table 31. Regioselective alcohol addition to **104** leading to **140** or **141** using **139** as catalyst precursor, [164, 165].

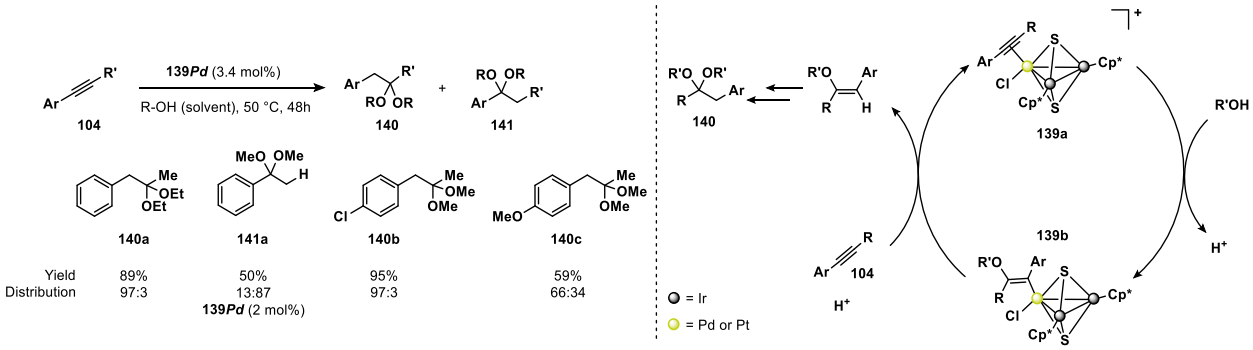

Cycloaddition

In a later study, Hidai employed cluster **134** to demonstrate its applicability in the cyclization of various alkynoic acids **142a** to furanone type product **143a**, **Scheme 38** [166]. Cluster catalysis is strongly implied based on kinetic studies revealing a first order rate-dependence with respect to the cluster, an approximately 20 fold rate enhancement relative to mononuclear Pd complex, $PdCl_2(PhCN)_2$, as well as spectroscopic measurement showing intact catalyst throughout the reaction. A TON(19h) value of 100000 was reported in the cyclization of the simplest compound, using a 0.001 mol% catalyst loading in MeCN at 40 °C (97% yield).

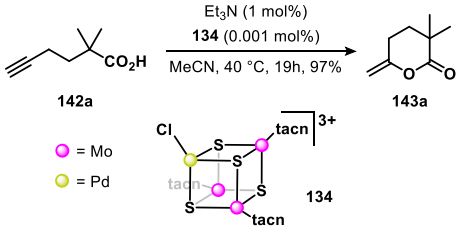

Scheme 38. Cyclization of **142a** to **143a** using **134** as catalyst precursor, [166].

Continued efforts to provide insight into the catalytic activity of cubane-type clusters **134** were provided by Hidai in the cyclization of aminoalkynes **144** to **146**, **Scheme 39** [167]. Changing the Pd-precursor to either $Pd(dba)_2$, dba = bis(dibenzylideneacetone), or Pd(ma)(nbd), ma = maleic anhydride, and nbd = nobornadiene, resulted in corresponding cubane-type clusters $[(Cp^*Mo)_3PdS_4(dba)][PF_6]$, **145a** and $[(Cp^*Mo)_3PdS_4(ma)][PF_6]$**145b**, respectively. Both **145a** and **145b** showed a high catalytic activity in the intramolecular cyclization of **144**, affording up to 98% yield. These findings are in stark contrast with when employing PPh_3, which afforded merely 6% yield. This observation was accounted for as to due to a difficult ligand-substrate substitution in the former systems. Insights on the mixtures was provided by UV-vis measurements substantiating an intact cluster entity. Using a 1 mol% catalyst loading of $[(Cp^*Mo)_3PdS_4(dba)][PF_6]$ **145a** in THF at 60 °C led to near quantitative yields.

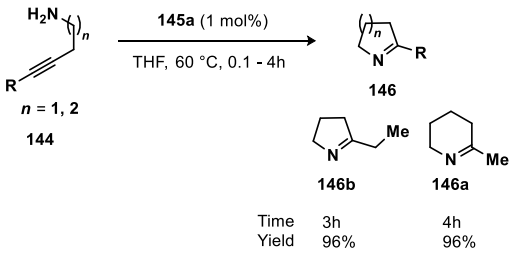

Scheme 39. Catalytic intramolecylar aminoalkyne cycloaddition of **144** leading to **146** using **145a** as catalyst precursor, [167].

Substituting Ni for Pd and tacn for Cp* in **134** provided the COD-dimer of the cluster [{(Cp*Mo)$_3$(μ_3-S)$_4$Ni}$_2$(μ,η^2:η^2-cod)][PF$_6$]$_2$, **147** [168]. A monomeric cluster was generated by treating **147** with dimethyl acetylenedicarboxylate, resulting in the singly alkyne-Ni coordinated cluster **148, Scheme 40**. The alkyne coordination to the Ni-center is suggested to result from the π-accepting properties of the Mo$_3$S$_4$-framework, thus lowering the electron-density at the Ni center. While both **147** and **148** demonstrated catalytic activity, neither of the parent compounds, [(Cp*Mo)$_3$(μ_2-S)$_3$(μ_3-S)][PF$_6$] and Ni(COD)$_2$, provided any activity in the cyclization. Based on the lack of catalytic activity of the parent compounds as well as prior observations, the authors propose the catalytic cycle by a single cluster shown in the **Scheme 41**.

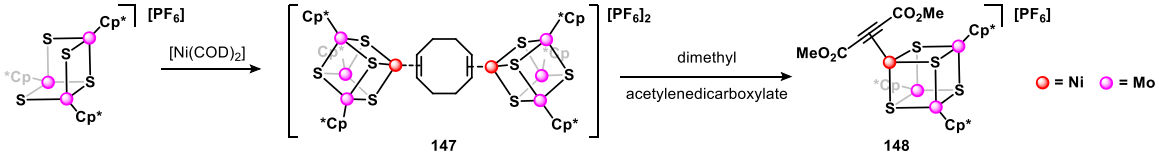

Scheme 40. Preparation of [NiMo$_3$S$_4$]-cubane type clusters **147** and **148,** [168].

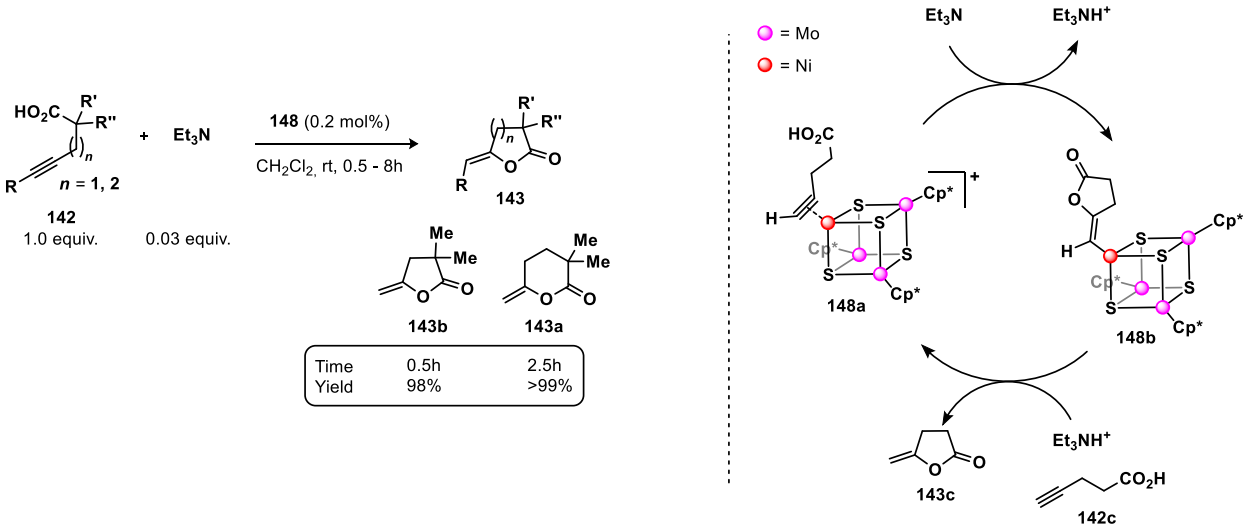

Scheme 41. Left: Intramolecular cyclization of **142** leading to **143** using **148** as catalyst precursor. Right: Catalytic cycle for the cyclization of **142** to **143** using **148** as catalyst, as proposed by Hidai, [168].

Llusar and Pérex-Prieto reported asymmetric induction in the catalytic intra- and intermolecular cyclopropanation of olefins, such as **149** and **1d**, with α-diazoketo units leading to **150** and **152**, respectively, by using catalytic amounts of stereoenriched mixed-metal cubane-type CuMo$_3$S$_4$-clusters, **153-156**, **Table 32** [169]. Optically pure trinuclear frameworks were prepared stereoselectively *via* cluster excision of the polymeric unit, {Mo$_3$S$_7$Cl$_4$}$_n$, using the chiral chelating phosphine ligand, (*R/S*, *R/S*)-Me-BPE. The resulting cluster chirality was preserved as Cu was introduced to the framework. Single-crystal X-ray diffraction in combination with circular dichroism was used to establish two

enantiopure compounds. Preliminary studies of the intramolecular cylopropanation reaction showed that the parent Mo_3S_4-framework **15** was catalytically inactive. Furthermore, spectroscopic analysis confirmed the racemic cubane-cluster, **156**, stayed intact throughout the reaction. Based on the preliminary results of the racemic cluster, the chiral cluster 153 was employed under the same reaction conditions, affording a low enantiomeric excess of merely 25% *ee*.

Additionally, clusters **153-156** were employed in an intermolecular cyclopropanation, resulting in E/Z ratio of up to 2.6 and with low enantioselectivity. The low selectivity is suggested to relate to the addition of alkenes to the Cu-carbene species, which is insufficiently sterically encumbered. As such, the authors suggest that an increase of steric bulk at the coordination-sphere of the Cu-center likely will be beneficial for the stereoselectivity. Pérez-Prieto proposed the involvement of the cluster **153** to occur by either of two mechanisms, namely (*i*) halide dissociation [at the Cu-center], or by (*ii*) Cu-S/Se bond cleavage [170]. To this end, analogues were prepared; substituting Cl with Br, and S for Se. Whereas the enantiomeric ratios were effectively identical for the chloride- and bromide cluster, the rate was decreased by substitution of S for Se, **Table 32**, indicating that the latter mechanism is more likely.

Table 32. Chiral induction using enantiopure $CuMo_3S_4$-clusters **153** and **156** as catalyst precursors for the cyclopropanation of **149** [169], as well as the intermolecular cyclopropanation of **1d** [170].

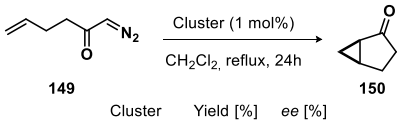

Cluster	Yield [%]	*ee* [%]
156	95	-
153	84	25
[Mo_3S_4]	-	-

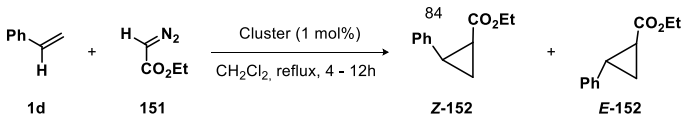

Cluster	Time [h]	Yield [%]	*E*/*Z*	***Z*-152** *ee* [%]	***E*-152** *ee* [%]
156	80	80	2.4	-	-
		88	2.6	21	20
153	5	77	2.3		
154	5	41	2.6		
155	12	70	2.6		

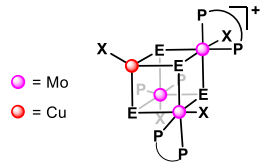

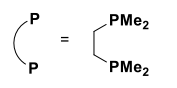

E = S, X = Cl (**156**)

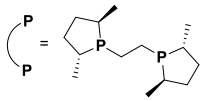

E = S, X = Cl (**153**)
E = S, X = Br (**154**)
E = Se, X = Cl (**155**)

Allylation

Cluster **145** was further used to afford regioselective allyllation of amines, such as **42h**, leading to **158**, **Scheme 42** [171]. Using 50 mol% H_3BO_3 as additive, near quantitative yields were reported within 4 hours with 5 mol% catalyst loading. As in the aforementioned study, the ligation was found to affect the catalytic activity, and only dba afforded a catalytically active cluster. Of the mononuclear compounds, only $Pd(PPh_3)_4$ was able to provide any transformation albeit at lower yield (70 *vs* 96%). The authors concluded that the Mo_3S_4-framework act as a sterically encumbered ligand, thus suppressing formation of branched product. A tentative mechanism was provided by the authors, initiated by ligand substitution going from **145** to **145b**. The allylic hydroxyl group in turn coordinates to the boric acid. Subsequent nucleophilic attack to the π-allyl intermediate **145c** regenerates **145a** concurrently with product formation. The authors suggest the $[(Cp^*Mo)_3S_4]$ unit may be regarded in terms of an extended ligand.

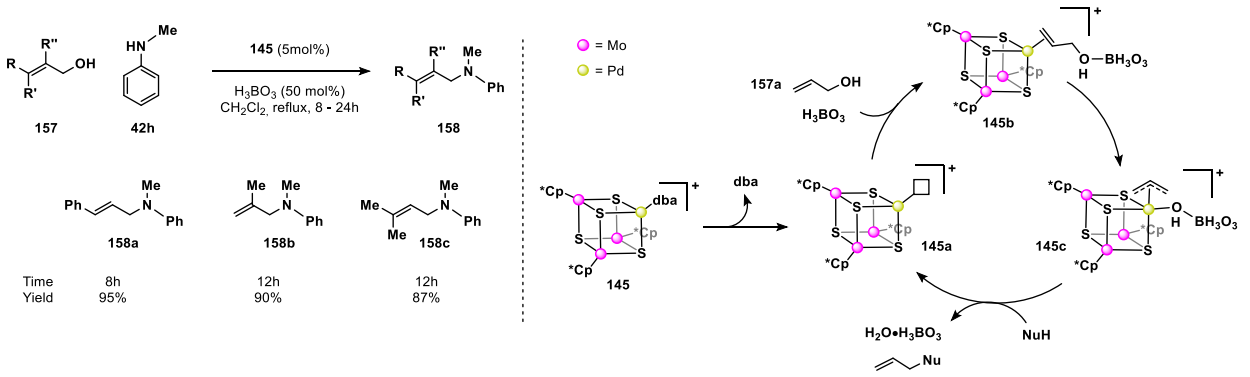

Scheme 42. Left: Allylation of **42h** leading to **158** using **145** as catalyst precursor. Right: Catalytic cycle for allylation of various nucleophiles as proposed by Qu, [171].

Continued studies of **145** was done by Qu, who reported an extended substrate scope for the allyllation reaction, to include additional amines as well as active methylene compounds **159**, such as 2-nitro-acetophenone, leading to **160** (**Scheme 43**, left) [172]. High yields up to 98% were obtained using a 5 mol% catalyst loading. In a later study, they demonstrated that the same cluster is an efficient catalyst precursor for the Friedel-Crafts-type allylation of both anilines and indoles with allylic alcohols, **Scheme 43**, right [173]. In both studies, the lack of catalytic activity of related lower nuclearity species, combined with previous findings by Hidai, led the authors to propose cluster catalysis as shown in the scheme. Nucleophilic attack to **145e** is directed by the $[(Cp^*Mo)_3S_4]$ unit that acts an extended ligand **145f**, rather than the hindered allylic carbon, resulting. Subsequent ligand substitution with **157** forms **145g** that undergoes protonation of the allylic alcohol moiety (**145d**).

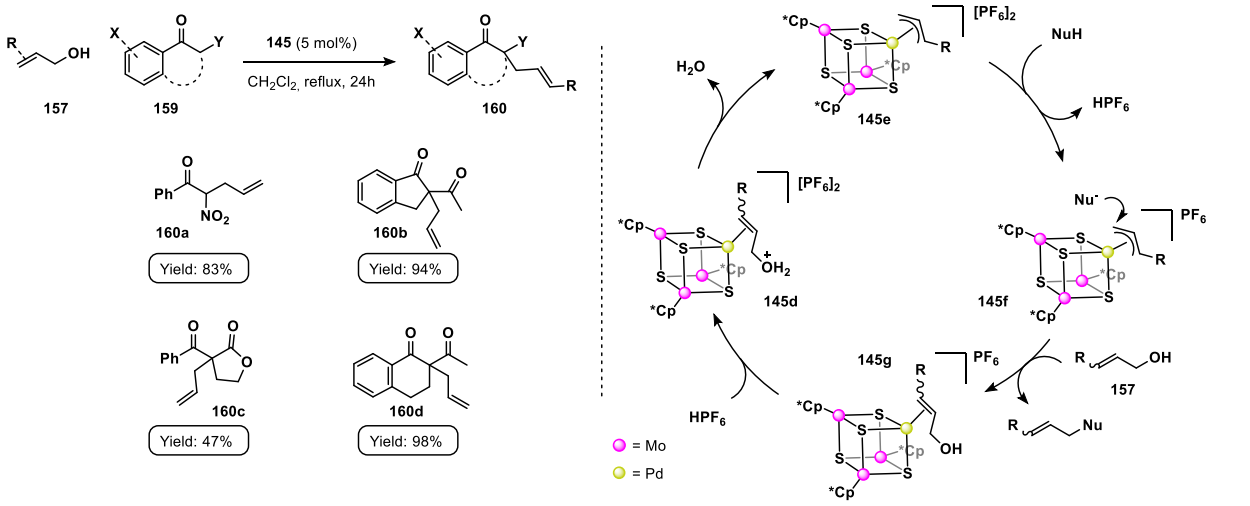

Scheme 43. Left: allylation of **159** to **160** using **145** as catalyst precursor. Right; Catalytic cycle in allylation of amines and Friedel-Crafts-type reaction as proposed by Qu, [172, 173].

Disproportionation

Hidai reported the cubane-cluster **161** containing Ru as an efficient catalyst for cleaving of N-N bonds in hydrazines [174]. Thus, catalytic disproportionation of hydrazine occurs from treatment with **161**, **Table 33**. In addition to the disproportionation products (NH_3 and N_2), an ammonia ligated cluster, **161a**, along with a di-cubane cluster **161b** bridged by both an amido and hydrazido ligand, μ-NH_2 and μ-$NHNH_2$, were observed. Substitution of PPh_3 with PCy_3 resulted in a catalytically more active cluster in the disproportionation reaction whilst suppressing the formation of **161a**. The authors conclude a low reactivity of the clusters compared to a mononuclear molybdenum [175], and a dinuclear ruthenium thiolate-complex [176].

Table 33. [$RuMo_3S_4$] **161** in disproportionation of hydrazine and the corresponding adducts, [174].

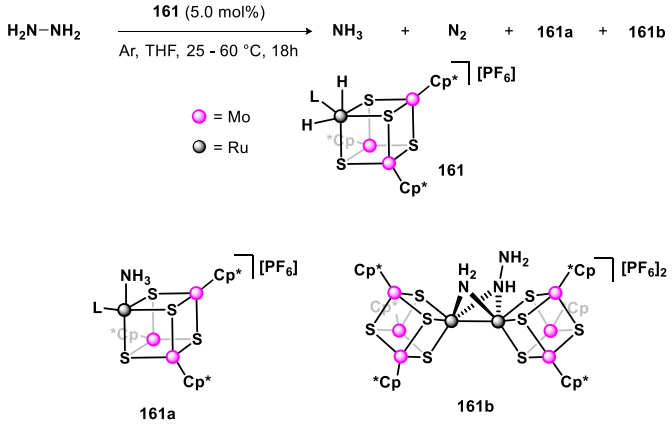

L	Temperature [°C]	TON	Equiv. Of			
			NH_3	N_2	**161a**	**161b**
PPh_3	25	3.4	3.1	0.9	0.56	0.07
PCy_3		3.6	4.0	1.2	-	0.19
PPh_3	60	5.9	6.6	1.6	0.38	0.15
PCy_3		15.2	20	4.7	-	0.23

Cross-alkylation

Blum reported the triangulated mixed-metal clusters **106a** and **106b** as an efficient catalyst precursors for the cross-alkylation of (pseudo)-halide arenes by group thirteen-stabilized alkylation agents, **Table 34** [177]. The authors provide evidence in support of cluster catalysis. Thus, the use of either catalyst precursor **106a** or **106b**, exclusively afford methylation products, whereas mononuclear Pd-compounds promote both homocoupling and hydrogenolysis. Moreover, the authors note that whereas conventional Pd-catalysts do not activate chloroarenes, both clusters demonstrated 99% yields when using **41g** as substrate. The authors further suggest that side-reactions are suppressed based on a synergistic interaction between Pd and Mo or W.

Table 34. Methylation of aryl arenes using either **106a** or **106b**, [177].

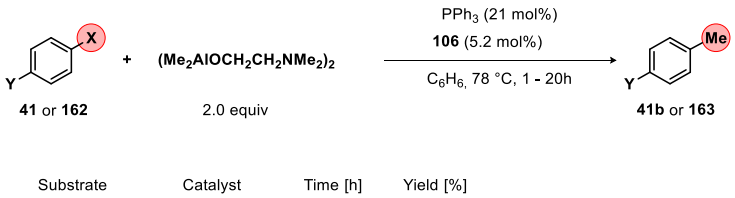

Substrate	Catalyst	Time [h]	Yield [%]
41g	**106a**	20	99
	106b	20	99
41h	**106a**	1	25
	106b	1	11
162a	**106a**	2	100
	106b	2	65
162b	**106a**	1	89
	106b	1	63

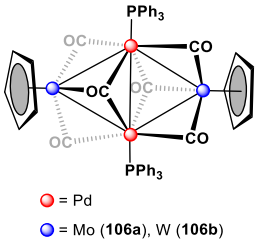

Aryl homocoupling

Shieh investigated three *N*-heterocyclic (NHC) functionalized mixed-metal pentanuclear clusters **164**-**166**, which provided catalytic activity under Suzuki–Miyaura conditions for the homocoupling of *p*-bromoboronic acid **167** to biphenyl product **168** [178]. Comparing the reactivity the three clusters **164**, **165**, and **166**, the authors conclude that the steric encumbering at the Cu center affords a greater activity in **166** (18.2 h^{-1} in **164** *vs.* 36.8 h^{-1} **166**), **Table 35**. Furthermore, based on DFT and spectroscopical data (^{13}C NMR), the authors suggest a facile oxidation of Cu(I), with the NHC groups stabilizing a Cu(III) intermediate during the catalytic cycle.

Table 35. Mixed-metal clusters **164**-**166** stabilized by Te in Suzuki-Miyaura homocross-copuling of **167** leading to **168**, [178]. Terminal CO molecules have been omitted for clarity.

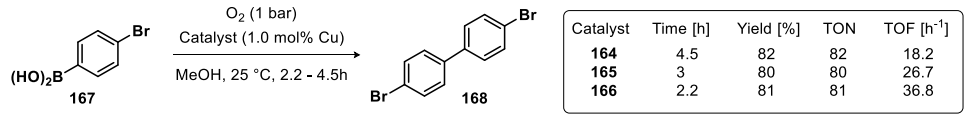

Catalyst	Time [h]	Yield [%]	TON	TOF [h^{-1}]
164	4.5	82	82	18.2
165	3	80	80	26.7
166	2.2	81	81	36.8

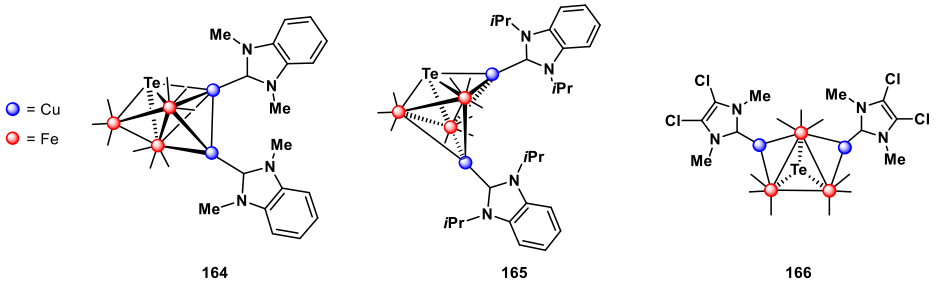

4 CONCLUSION

During the past decades, the homogeneous catalytic research community has witnessed an impressive development within the use of polynuclear clusters as catalysts for a plethora of organic transformations. Interestingly, is has been demonstrated on numerous occasions that these clusters bear the potential to provide unique product selectivities, and thus represent a highly exciting rising methodology.

In this review, we have presented multiple examples of successes in homogeneous cluster catalysis. We have shown how the use of either homonuclear or heteronuclear clusters, respectively, may provide increased catalyst activity as well as different chemo-, regio-, and stereoselectivities than those seen with traditional mononuclear organometallic catalysts. Furthermore, several accounts shed light on the effect on catalysis when substituting among the members of a transitional metal triad of a single metal center in a heteronuclear cluster. Finally, throughout the review we have presented the Laine criteria for cluster catalysis and highlighted how the structures of the true catalysts have been addressed by use of a multitude of analytical tools. These investigations have led to several mechanistic proposals, which have been discussed here as well.

Many of the examples shown in this review demonstrate a fundamental challenge relating to cluster catalysis, namely the lack of framework stability, resulting from fluxional ligands, such as carbonyls and hydrides, often leading to cluster fragmentation. On the other hand, considerable evidence already supports that polynucleating ligands provide the necessary rigidity to retain cluster integrity while accommodating the essential geometric rearrangements during catalysis.

Cluster catalyzed reactions have the potential to open new avenues in chemical transformations stemming from the synergistic interaction between several vicinal metal centers, and their ability to mediate multiple electron transfers. Despite a wide range of cluster structures found in literature, their provision has largely relied on (serendipitous) self-assembly of appropriate metal and strong-field ligand combinations. Moreover, the majority of catalytic transformations are dictated by the parent cluster structure, thus limiting the scope. Consequently, the development of cluster catalyst that are structurally dictated by their polynucleating ligands are of high interest.

5 REFERENCES

1. Shriver DF, Sailor MJ (1988). *Acc. Chem. Res.* **21**, 374–379
2. Giordano R, Sappa E, Knox SAR (1996). *J. Clust. Sci.* **7**, 179–190
3. Sappa E, Tiripicchio A, Braunstein P (1983). *Chem. Rev.* **83**, 203–239
4. Keister JB, Shapley JR (1975). *J. Organomet. Chem.* **85**, C29–C31
5. Muetterties EL, Stein J (1979). *Chem. Rev.* **79**, 479–490
6. Nagashima H, Fukahori T, Aoki K, Itoh K (1993). *J. Am. Chem. Soc.* **115**, 10430–10431
7. Nagashima H, Suzuki A, Nobata M, Itoh K (1996). *J. Am. Chem. Soc.* **118**, 687–688
8. Yi CS, Zeczycki TN, Lindeman S V (2008). *Organometallics* **27**, 2030–2035
9. Buchwalter P, Rosé J, Braunstein P (2015). *Chem. Rev.* **115**, 28–126
10. Powers IG, Uyeda C (2017). *ACS Catal.* **7**, 936–958
11. Cotton FA (1964). *Inorg. Chem.* **3**, 1217–1220
12. Cotton FA (1966). *Q. Rev. Chem. Soc.* **20**, 389
13. E. Rosenberg, R., M. Laine, in Catalysis by Di- and Polynuclear Metal Cluster Complexes ed. By R. D. Adams and F. A. Cotton, (Wiley-VCH, Weinheim, 1998), p. 4.
14. Adams RD, Captain B, Zhu L (2004). *J. Am. Chem. Soc.* **126**, 3042–3043
15. Sculfort S, Braunstein P (2011). *Chem. Soc. Rev.* **40**, 2741–2760
16. Gray TG (2003). *Coord. Chem. Rev.* **243**, 213–235
17. Walton RA (2004). *J. Clust. Sci.* **15**, 559–588
18. Muetterties EL, Krause MJ (1983). *Angew. Chem. Int. Ed.* **22**, 135–148
19. Kuiper JL, Shapley PA, Rayner CM (2004). *Organometallics* **23**, 3814–3818
20. Laine RM (1982). *J. Mol. Catal.* **14**, 137–169
21. Anton DR, Crabtree RH (1983). *Organometallics* **2**, 855–859
22. Hagen CM, Vieille-Petit L, Laurenczy G, Süss-Fink G, Finke RG (2005). *Organometallics* **24**, 1819–1831
23. Lausarot PM, Vaglio GA, Valle M (1982). *J. Organomet. Chem.* **240**, 441–445
24. Lausarot PM, Vaglio GA, Valle M (1984). *J. Organomet. Chem.* **275**, 233–237
25. Moura FCC, Lago RM, dos Santos EN, Helena Araujo M (2002). *Catal. Commun.* **3**, 541–545
26. Joh T, Doyama K, Onitsuka K, Shiohara T, Takahashi S (1991). *Organometallics* **10**, 2493–2498
27. Alvila L, Pakkanen TA, Pakkanen TT, Krause O (1992). *J. Mol. Catal.* **73**, 325–334
28. Chatani N, Kamitani A, Oshita M, Fukumoto Y, Murai S (2001). *J. Am. Chem. Soc.* **123**, 12686–12687
29. Inoue S, Yokota K, Tatamidani H, Fukumoto Y, Chatani N (2006). *Org. Lett.* **8**, 2519–2522
30. Driller KM, Klein H, Jackstell R, Beller M (2009). *Angew. Chem. Int. Ed.* **48**, 6041–6044
31. Morimoto T, Chatani N, Fukumoto Y, Murai S (1997). *J. Org. Chem.* **62**, 3762–3765
32. Kondo T, Suzuki N, Okada T, Mitsudo T (1997). *J. Am. Chem. Soc.* **119**, 6187–6188
33. Kondo T, Nakamura A, Okada T, Suzuki N, Wada K, Mitsudo T (2000). *J. Am. Chem. Soc.* **122**, 6319–6320

34. Kondo T, Kaneko Y, Taguchi Y, Nakamura A, Okada T, Shiotsuki M, Ura Y, Wada K, Mitsudo T (2002). *J. Am. Chem. Soc.* **124**, 6824–6825

35. Yamazaki H, Hong P (1983). *J. Mol. Catal.* **21**, 133–150

36. Chatani N, Ie Y, Kakiuchi F, Murai S (1997). *J. Org. Chem.* **62**, 2604–2610

37. Ishii Y, Chatani N, Kakiuchi F, Murai S (1997). *Organometallics* **16**, 3615–3622

38. Chatani N, Asaumi T, Yorimitsu S, Ikeda T, Kakiuchi F, Murai S (2001). *J. Am. Chem. Soc.* **123**, 10935–10941

39. Koelliker R, Bor G (1991). *J. Organomet. Chem.* **417**, 439–451

40. Ragaini F, Ghitti A, Cenini S (1999). *Organometallics* **18**, 4925–4933

41. Han SH, Geoffroy GL, Dombek BD, Rheingold AL (1988). *Inorg. Chem.* **27**, 4355–4361

42. Sanchez-Delgado RA, Bradley JS, Wilkinson G (1976). *J. Chem. Soc., Dalton Trans.* 399–404

43. Blazina D, Duckett SB, Dyson PJ, Lohman JAB (2001). *Angew. Chem. Int. Ed.* **40**, 3874–3877

44. Blazina D, Duckett SB, Dyson PJ, Lohman JAB (2003). *Chem. Eur. J.* **9**, 1045–1061

45. Park BY, Montgomery TP, Garza VJ, Krische MJ (2013). *J. Am. Chem. Soc.* **135**, 16320–16323

46. Hasegawa N, Charra V, Inoue S, Fukumoto Y, Chatani N (2011). *J. Am. Chem. Soc.* **133**, 8070–8073

47. Shibata K, Hasegawa N, Fukumoto Y, Chatani N (2012). *ChemCatChem* **4**, 1733–1736

48. Hasegawa N, Shibata K, Charra V, Inoue S, Fukumoto Y, Chatani N (2013). *Tetrahedron* **69**, 4466–4472

49. Fleischer I, Wu L, Profir I, Jackstell R, Franke R, Beller M (2013). *Chem. Eur. J.* **19**, 10589–10594

50. Fleischer I, Dyballa KM, Jennerjahn R, Jackstell R, Franke R, Spannenberg A, Beller M (2013). *Angew. Chem. Int. Ed.* **52**, 2949–2953

51. Liu J, Kubis C, Franke R, Jackstell R, Beller M (2016). *ACS Catal.* **6**, 907–912

52. Rameshkumar C, Periasamy M (2000). *Tetrahedron Lett.* **41**, 2719–2722

53. Periasamy M, Mukkanti A, Raj DS (2004). *Organometallics* **23**, 619–621

54. Periasamy M, Mukkanti A, Raj DS (2004). *Organometallics* **23**, 6323–6326

55. Chini P, Martinengo S (1969). *Inorg. Chim. Acta* **3**, 315–318

56. Martinengo S, Fumagalli A, Chini P, Albano VG, Clani G (1976). *J. Organomet. Chem.* **116**, 333–342

57. Martinengo S, Fumagalli A, Chini P (1985). *J. Organomet. Chem.* **284**, 275–279

58. Matsuda I, Fukuta Y, Tsuchihashi T, Nagashima H, Itoh K (1997). *Organometallics* **16**, 4327–4345

59. Longoni G, Campanella S, Ceriotti A, Chini P, Albano VG, Braga D (1980). *J. Chem. Soc., Dalton Trans.* 1816–1819

60. Kondo T, Akazome M, Tsuji Y, Watanabe Y (1990). *J. Org. Chem.* **55**, 1286–1291

61. Moore EJ, Pretzer WR, O'Connell TJ, Harris J, LaBounty L, Chou L, Grimmer SS (1992). *J. Am. Chem. Soc.* **114**, 5888–5890

62. Chatani N, Fukuyama T, Kakiuchi F, Murai S (1996). *J. Am. Chem. Soc.* **118**, 493–494

63. Agarwala R, Azam KA, Dilshad R, Kabir SE, Miah R, Shahiduzzaman M, Hardcastle KI, Rosenberg E, Hursthouse MB, Abdul Malik KM (1995). *J. Organomet. Chem.* **492**, 135–144

64. Bruce MI, Goodall BL, Gordon F, Stone A (1973). *J. Organomet. Chem.* **60**, 343–349

65. Chatani N, Morimoto T, Fukumoto Y, Murai S (1998). *J. Am. Chem. Soc.* **120**, 5335–5336

66. Chatani N, Ishii Y, Ie Y, Kakiuchi F, Murai S (1998). *J. Org. Chem.* **63**, 5129–5136

67. Burgess K, Holden HD, Johnson BFG, Lewis J, Hursthouse MB, Walker NPC, Deeming AJ, Manning PJ, Peters R (1985). *J. Chem. Soc., Dalton Trans.* 85–90

68. Chatani N, Fukuyama T, Tatamidani H, Kakiuchi F, Murai S (2000). *J. Org. Chem.* **65**, 4039–4047

69. Fukuyama T, Chatani N, Tatsumi J, Kakiuchi F, Murai S (1998). *J. Am. Chem. Soc.* **120**, 11522–11523

70. Inoue S, Shiota H, Fukumoto Y, Chatani N (2009). *J. Am. Chem. Soc.* **131**, 6898–6899

71. Kakiuchi F, Sato T, Tsujimoto T, Yamauchi M, Chatani N, Murai S (1998). *Chem. Lett.* **27**, 1053–1054

72. Cabeza JA, Fernandez-Colinas JM, Llamazares A, Riera V, Garcia-Granda S, Van der Maelen JF (1994). *Organometallics* **13**, 4352–4359

73. Cabeza JA, del Rio I, Fernández-Colinas JM, Llamazares A, Riera V (1995). *J. Organomet. Chem.* **494**, 169–177

74. Cabeza JA, del Río I, Fernández-Colinas JM, Riera V (1996). *Organometallics* **15**, 449–451

75. Castiglioni M, Giordano R, Sappa E (1991). *J. Organomet. Chem.* **407**, 377–389

76. Algarra AG, Guillamón E, Andrés J, Fernández-Trujillo MJ, Pedrajas E, Pino-Chamorro JÁ, Llusar R, Basallote MG (2018). *ACS Catal.* **8**, 7346–7350

77. Bergounhou C, Fompeyrine P, Commenges G, Bonnet JJ (1988). *J. Mol. Catal.* **48**, 285–312

78. Haupt H-J, Wittbecker R, Flörke U (1996). *J. Organomet. Chem.* **518**, 213–219

79. Gieshoff TN, Chakraborty U, Villa M, Jacobi von Wangelin A (2017). *Angew. Chem. Int. Ed.* **56**, 3585–3589

80. Chakraborty U, Reyes-Rodriguez E, Demeshko S, Meyer F, Jacobi von Wangelin A (2018). *Angew. Chem. Int. Ed.* **57**, 4970–4975

81. Matteoli U, Beghetto V, Scrivanti A (1996). *J. Mol. Catal. A. Chem.* **109**, 45–50

82. Homanen P, Persson R, Haukka M, Pakkanen TA, Nordlander E (2000). *Organometallics* **19**, 5568–5574

83. Moberg V, Haukka M, Koshevoy IO, Ortiz R, Nordlander E (2007). *Organometallics* **26**, 4090–4093

84. Moberg V, Duquesne R, Contaldi S, Röhrs O, Nachtigall J, Damoense L, Hutton AT, Green M, Monari M, Santelia D, Haukka M, Nordlander E (2012). *Chem. Eur. J.* **18**, 12458–12478

85. Moberg V, Homanen P, Selva S, Persson R, Haukka M, Pakkanen TA, Monari M, Nordlander E (2006). *Dalton Trans.* 279–288

86. Abdel-Magied AF, Patil MS, Singh AK, Haukka M, Monari M, Nordlander E (2015). *J. Clust. Sci.* **26**, 1231–1252

87. Abdel-Magied AF, Singh AK, Haukka M, Richmond MG, Nordlander E (2014). *Chem. Commun.* **50**, 7705–7708

88. Abdel-Magied AF, Majeed MH, Abelairas-Edesa MF, Ficks A, Ashour RM, Rahaman A, Clegg W, Haukka M, Higham LJ, Nordlander E (2017). *J. Organomet. Chem.* **849**–**850**, 71–79

89. Zhang H, Yang C-B, Li Y-Y, Donga Z-R, Gao J-X, Nakamura H, Murata K, Ikariya T (2003). *Chem. Commun.* 142–143

90. Cabeza JA, da Silva I, del Río I, Gossage RA, Miguel D, Suárez M (2006). *Dalton Trans.* 2450–2455

91. Sorribes I, Wienhöfer G, Vicent C, Junge K, Llusar R, Beller M (2012). *Angew. Chem. Int. Ed.* **51**, 7794–7798

92. Pedrajas E, Sorribes I, Junge K, Beller M, Llusar R (2015). *ChemCatChem* **7**, 2675–2681

93. Pedrajas E, Sorribes I, Gushchin AL, Laricheva YA, Junge K, Beller M, Llusar R (2017). *ChemCatChem* **9**, 1128–1134

94. Pedrajas E, Sorribes I, Junge K, Beller M, Llusar R (2017). *Green Chem.* **19**, 3764–3768

95. Nakajima Y, Suzuki H (2005). *Organometallics* **24**, 1860–1866

96. Takao T, Horikoshi S, Kawashima T, Asano S, Takahashi Y, Sawano A, Suzuki H (2018). *Organometallics* **37**, 1598–1614

97. Federsel C, Boddien A, Jackstell R, Jennerjahn R, Dyson PJ, Scopelliti R, Laurenczy G, Beller M (2010). *Angew. Chem. Int. Ed.* **49**, 9777–9780

98. Federsel C, Ziebart C, Jackstell R, Baumann W, Beller M (2012). *Chem. Eur. J.* **18**, 72–75

99. Wesselbaum S, vom Stein T, Klankermayer J, Leitner W (2012). *Angew. Chem. Int. Ed.* **51**, 7499–7502

100. Hull JF, Himeda Y, Wang W-H, Hashiguchi B, Periana R, Szalda DJ, Muckerman JT, Fujita E (2012). *Nat. Chem.* **4**, 383

101. Shitaya S, Nomura K, Inagaki A (2019). *Chem. Commun.* **55**, 5087–5090

102. Guzman-Jimenez IY, Van Hal JW, Whitmire KH (2003). *Organometallics* **22**, 1914–1922

103. Bachman RE, Whitmire KH (1994). *Inorg. Chem.* **33**, 2527–2533

104. Suzuki N, Kondo T, Mitsudo T (1998). *Organometallics* **17**, 766–769

105. Süss-Fink G, Herrmann G (1985). *J. Chem. Soc., Chem. Commun.* 735–737

106. Süss-Fink G, Schmidt GF (1987). *J. Mol. Catal.* **42**, 361–366

107. Diz EL, Neels A, Stoeckli-Evans H, Süss-Fink G (2001). *Polyhedron* **20**, 2771–2780

108. Ryan RC, Pittman CU, O'Connor JP (1977). *J. Am. Chem. Soc*. **99**, 1986–1988

109. Pitmann CU, Ryan RC (1978). *Chemtech* **8**, 170–175

110. Pittman CU, Wilemon GM, Wilson WD, Ryan RC (1980). *Angew. Chem. Int. Ed.* **19**, 478–479

111. Nombel P, Lugan N, Mulla F, Lavigne G (1994). *Organometallics* **13**, 4673–4675

112. Nombel P, Lugan N, Donnadieu B, Lavigne G (1999). *Organometallics* **18**, 187–196

113. Kim D-S, Park W-J, Lee C-H, Jun C-H (2014). *J. Org. Chem.* **79**, 12191–12196

114. Ko S, Na Y, Chang S (2002). *J. Am. Chem. Soc.* **124**, 750–751

115. Na Y, Ko S, Hwang LK, Chang S (2003). *Tetrahedron Lett.* **44**, 4475–4478

116. Ko S, Lee C, Choi M-G, Na Y, Chang S (2003). *J. Org. Chem.* **68**, 1607–1610

117. Ko S, Han H, Chang S (2003). *Org. Lett.* **5**, 2687–2690

118. Park EJ, Lee JM, Han H, Chang S (2006). *Org. Lett.* **8**, 4355–4358

119. Kondo T, Okada T, Mitsudo T (1999). *Organometallics* **18**, 4123–4127

120. Yoneda E, Kaneko T, Zhang S-W, Onitsuka K, Takahashi S (2000). *Org. Lett.* **2**, 441–443

121. Yoneda E, Zhang S-W, Zhou D-Y, Onitsuka K, Takahashi S (2003). *J. Org. Chem.* **68**, 8571–8576

122. Tsubuki M, Takahashi K, Honda T (2009). *J. Org. Chem.* **74**, 1422–1425

123. Nagashima H, Suzuki A, Iura T, Ryu K, Matsubara K (2000). *Organometallics* **19**, 3579–3590

124. Sasakuma H, Motoyama Y, Nagashima H (2007). *Chem. Commun.* 4916–4918

125. Yumino S, Hashimoto T, Tahara A, Nagashima H (2014). *Chem. Lett.* **43**, 1829–1831

126. Hanada S, Yuasa A, Kuroiwa H, Motoyama Y, Nagashima H (2010). *Eur. J. Org. Chem.* **2010**, 1021–1025

127. Miyamoto K, Motoyama Y, Nagashima H (2012). *Chem. Lett.* **41**, 229–231

128. Hanada S, Motoyama Y, Nagashima H (2008). *Eur. J. Org. Chem.* **2008**, 4097–4100

129. Nagashima H, Itonaga C, Yasuhara J, Motoyama Y, Matsubara K (2004). *Organometallics* **23**, 5779–5786

130. Harada N, Nishikata T, Nagashima H (2012). *Tetrahedron* **68**, 3243–3252

131. Beltrán TF, Feliz M, Llusar R, Mata JA, Safont. VS (2011). *Organometallics* **30**, 290–297

132. Alfonso C, Beltrán TF, Feliz M, Llusar R (2015). *J. Clust. Sci.* **26**, 199–209

133. Yi CS, Zeczycki TN, Guzei IA (2006). *Organometallics* **25**, 1047–1051

134. Yi CS, Lee DW (2009). *Organometallics* **28**, 947–949

135. Kim J, Pannilawithana N, Yi CS (2016). *ACS Catal.* **6**, 8395–8398

136. Takao T, Kawashima T, Kanda H, Okamura R, Suzuki H (2012). *Organometallics* **31**, 4817–4831

137. Haak RM, Decortes A, Escudero-Adán EC, Belmonte MM, Martin E, Benet-Buchholz J, Kleij AW (2011). *Inorg. Chem.* **50**, 7934–7936

138. Kielland N, Escudero-Adán EC, Martínez Belmonte M, Kleij AW (2013). *Dalton Trans.* **42**, 1427–1436

139. Li B, Park Y, Chang S (2014). *J. Am. Chem. Soc.* **136**, 1125–1131

140. Chakraborty U, Demeshko S, Meyer F, Jacobi von Wangelin A (2019). *Angew. Chem. Int. Ed.* **58**, 3466–3470

141. Pittman CU, Honnick W, Absi-Halabi M, Richmond MG, Bender R, Braunstein P (1985). *J. Mol. Catal.* **32**, 177–190

142. Castiglioni M, Giordano R, Sappa E, Tiripicchio A, Camellini MT (1986). *J. Chem. Soc., Dalton Trans.* 23–30

143. Castiglioni M, Giordano R, Sappa E (1987). *J. Organomet. Chem.* **319**, 167–181

144. Castiglioni M, Giordano R, Sappa E (1988). *J. Organomet. Chem.* **342**, 111–127

145. Adams RD, Li Z, Swepston P, Wu W, Yamamoto J (1992). *J. Am. Chem. Soc.* **114**, 10657–10658

146. Adams RD, Barnard TS, Li Z, Wu W, Yamamoto JH (1994). *J. Am. Chem. Soc.* **116**, 9103–9113

147. Adams RD, Barnard TS (1998). *Organometallics* **17**, 2567–2573

148. Adams RD, Barnard TS (1998). *Organometallics* **17**, 2885–2890

149. Smirnova ES, Muñoz Molina JM, Johnson A, Bandeira NAG, Bo C, Echavarren AM (2016). *Angew. Chem. Int. Ed.* **55**, 7487–7491

150. Richmond MG, Absi-Halbi M, Pittman CU (1984). *J. Mol. Catal.* **22**, 367–371

151. Senocq F, Randrianalimanana C, Thorez A, Kalck P, Choukroun R, Gervais D (1984). *J. Chem. Soc., Chem. Commun.* 1376–1377

152. Gervais D, Jaud J, Kalck P, ChoUKroun R, Senocq F (1986). *Organometallics* **5**, 67–71

153. Choukroun R, Gervais D, Rifaï C (1989). *Polyhedron* **8**, 1760–1761

154. Choukroun R, Dahan F, Gervais D, Rifai C (1990). *Organometallics* **9**, 1982–1987

155. Casado MA, Pérez-Torrente JJ, Ciriano MA, Oro LA, Orejón A, Claver C (1999). *Organometallics* **18**, 3035–3044

156. Casado MA, Ciriano MA, Edwards AJ, Lahoz FJ, Oro LA, Pérez-Torrente JJ (1999). *Organometallics* **18**, 3025–3034

157. Haupt HJ, Wittbecker R, Florke U (2001). *Z. Anorg. Allg. Chem.* **627**, 472–484

158. Pittman Jr. CU, Richmond MG, Absi-Halabi M, Beurich H, Richter F, Vahrenkamp H (1982). *Angew. Chem. Int. Ed.* **21**, 786–787

159. Shapley PA, Liang H-C, Dopke NC (2001). *Organometallics* **20**, 4700–4704

160. Nagaoka M, Kawashima T, Suzuki H, Takao T (2016). *Organometallics* **35**, 2348–2360

161. Li Y, Pan W-X, Wong W-T (2002). *J. Clust. Sci.* **13**, 223–233

162. Murata T, Mizobe Y, Gao H, Ishii Y, Wakabayashi T, Nakano F, Tanase T, Yano S, Hidai M (1994). *J. Am. Chem. Soc.* **116**, 3389–3398

163. Wakabayashi T, Ishii Y, Murata T, Mizobe Y, Hidai M (1995). *Tetrahedron Lett.* **36**, 5585

164. Masui D, Ishii Y, Hidai M (1998). *Chem. Lett.* **27**, 717–718

165. Masui D, Kochi T, Tang Z, Ishii Y, Mizobe Y, Hidai M (2001). *J. Organomet. Chem.* **620**, 69–79

166. Wakabayashi T, Ishii Y, Ishikawa K, Hidai M (1996). *Angew. Chem. Int. Ed.* **35**, 2123–2124

167. Takei I, Enta Y, Wakebe Y, Suzuki T, Hidai M (2006). *Chem. Lett.* **35**, 590–591

168. Takei I, Wakebe Y, Suzuki K, Enta Y, Suzuki T, Mizobe Y, Hidai M (2003). *Organometallics* **22**, 4639–4641

169. Feliz M, Guillamón E, Llusar R, Vicent C, Stiriba S-E, Pérez-Prieto J, Barberis M (2006). *Chem. Eur. J.* **12**, 1486–1492

170. Guillamón E, Llusar R, Pérez-Prieto J, Stiriba S-E (2008). *J. Organomet. Chem.* **693**, 1723–1727

171. Tao Y, Zhou Y, Qu J, Hidai M (2010). *Tetrahedron Lett.* **51**, 1982–1984

172. Tao Y, Wang B, Wang B, Qu L, Qu J (2010). *Org. Lett.* **12**, 2726–2729

173. Tao Y, Wang B, Zhao J, Song Y, Qu L, Qu J (2012). *J. Org. Chem.* **77**, 2942–2946

174. Takei I, Dohki K, Kobayashi K, Suzuki T, Hidai M (2005). *Inorg. Chem.* **44**, 3768–3770

175. B. Hitchcock P, L. Hughes D, J. Maguire M, Marjani K, L. Richards R (1997). *J. Chem. Soc., Dalton Trans.* 4747–4752

176. Kuwata S, Mizobe Y, Hidai M (1994). *Inorg. Chem.* **33**, 3619–3620

177. Shenglof M, Molander GA, Blum J (2006). *Synthesis (Stuttg)* **2006**, 111–114

178. Shieh M, Liu YH, Li YH, Lin CN, Wang CC (2018). *J. Organomet. Chem.* **867**, 161–169